MODELS AND THERAPEUTICS FOR ENGINEERING THE OCULAR SURFACE

by
Qiaozhi Lu

A dissertation submitted to Johns Hopkins University in conformity with the requirements for the degree of Doctor of Philosophy

Baltimore, Maryland

January, 2017

ABSTRACT

The ocular surface is the outermost part of the eye that protects the refractive surface and enables sharp vision. The primary components of the ocular surface are corneal and conjunctival epithelia, lacrimal glands, and meibomian glands that are functionally linked as one system. Because of its location, the ocular surface is subject to traumatic injuries and diseases. Dry eye, due to inadequate tear production or excessive evaporation, is one of the most complicated diseases of the ocular surface, whose exact pathogenesis is not yet fully understood, and more effective treatments need to be investigated.

This dissertation will address the development of an *in vitro* ocular surface system and its application in therapeutic discovery. We first investigated a vitrified collagen membrane and its ability to support ocular surface epithelium, which also promoted the repopulation of goblet cells, a key component in mucin production. Afterwards a more complex ocular surface system was established with both conjunctival epithelium and lacrimal glands, the essential parts in tear film secretion. The three-dimensional coculture system highly resembles the structure and tear-secretion function of the native environment. This was further evaluated as a model for dry eye disease and a platform for therapeutic evaluation. One potential therapeutic we had studied is decellularized extracellular matrices (ECM). The particulate form was used as an immunomodulator to reduce inflammation and fibrosis on the ocular surface and to accelerate tissue regeneration. Model systems built based on engineering principle provide a new approach for drug discovery. This *in vitro* ocular surface system is proved to recapitulate the physiology of both healthy and diseased ocular surface. Its potential as a therapeutic screening device is promising and could be further investigated.

Thesis committee:

Prof. Jennifer H. Elisseeff (BME & TTEC, advisor)

Prof. Michael P. Grant (Ophthalmology, co-advisor)

Prof. Hai-Quan Mao (MSE & TTEC)

Prof. Margarita Herrera-Alonso (MSE)

Prof. Samuel C. Yiu (Ophthalmology)

For my parents, Hong Lu and Liya Sun

ACKNOWLEDGEMENTS

I would like to thank many people for their support during my pursuit of the PhD degree in the last few years. First, I truly want to thank my parents, who are always there for me. Although they do not work in academia, their life experience and insights are the most valuable for me. Their persistence and optimism has deeply influenced me and set up a perfect example for me ever since I was a child. I also want to thank my husband Daniel for the incredible support he offered during my PhD, without whom I could not have enjoyed life so much.

I want to sincerely thank my advisor, Prof. Jennifer H. Elisseeff, for her guidance through my time working in her lab. I have learned so much from her on conducting research and solving problems. She has inspired me countless times and helped me go though many obstacles. As a scientist and professor, she is a great role model to me. I also want to thank Prof. Michael P. Grant and Prof. Hai-Quan Mao for their support and encouragement on my research projects and PhD study.

I have worked with so many amazing people during my time in the JHE lab: Dr. Jeannine Coburn, Dr. Iossif Strehin, Dr. Jacob A. Simson, Dr. Qiongyu Guo, Dr. Jeremy J. Chae, Okhee Jeon, Dr. Huifang Zhou, Dr. Hongbo Yin, Dr. Anirudha Singh, David Lee and many more. I really appreciated the opportunities working with them and have benefited a lot from these experiences. I want to thank many former and present members of the lab for helping me with trouble-shooting and protocols.

Finally, I want to thank all friends that have supported me during all these years. My life-changing journey at Johns Hopkins opens a new era ahead of me, and I am forever grateful for everything and every moment of it.

TABLE OF CONTENTS

LIST OF TABLES

LIST OF FIGURES

Chapter 1. Objectives and Significance

The ocular surface is the outermost frontier of our eyes, and it is crucial for the vision system. It includes corneal and conjunctival epithelia, lacrimal glands, and meibomian glands. All components are functionally linked together as one system, and its homeostasis is regulated by the nervous, immune and endocrine system as well. Tear film is the secretory product of the ocular surface and is composed of three layers, which are mucin, aqueous and lipid layers. Ocular surface and tear film protect the vision system against foreign pathogens, provide lubrication to the refractory surface, and also play an important role in the immunity of anterior eye during inflammation.

Because of its location, the ocular surface system is subject to traumatic injuries and multiple diseases. In case of severe injuries, tissue engineering strategies are necessary for optimal wound healing. Dry eye is an immunopathogenic disease, in which one or more layers of the tear film are altered, and it is affecting the life quality of millions of people in the United States. It is a complicated ocular surface disease, and its exact pathogenesis is not yet fully understood. Typical treatments for dry eye are either artificial tear supplement for symptom relief or anti-inflammatory reagents for immuno-regulation.

This dissertation addressed the development of biomaterials and *in vitro* model systems for the ocular surface. In Chapter 2, we reviewed the current available biomaterials for ocular

surface wound healing and their features, with an emphasis on vitrified collagen membrane. It also included an overview of organ model systems, for the pathogenesis study of diseases and for the discovery of new therapeutics.

Chapter 3 is the investigation of using vitrified collagen membrane for conjunctival reconstruction. Vitrigel was able to support the growth of conjunctival epithelial and goblet cells *in vitro*. Vitrigel was transplanted on a rabbit model with conjunctival defects, and its ability in supporting wound healing and preventing fibrosis was evaluated.

We developed a coculture model for the ocular surface *in vitro* in Chapter 4. The 3-dimentional model was composed of conjunctival epithelium and lacrimal gland spheroids. Culture conditions for both type of cells were studied first for phenotypic development and protein secretion. Different designs of coculture were compared for optimal performance as well. At last, the coculture system was validated as an *in vitro* dry eye model for therapeutic evaluation.

Extracellular matrix (ECM) scaffolds have been widely used on tissue engineering and regenerative medicine. In Chapter 5, particulate ECM particles were used for corneal wound healing after lamellar keratectomy. Results from experiments *in vitro* and *in vivo* have proven that ECM particles have anti-inflammatory properties and could effectively reduce scar size and fibrosis. Therefore, ECM materials are promising therapeutics for corneal wound healing, and the immunoregulation of the ocular surface system.

In summary, this dissertation addressed multiple approaches in the strategic development for ocular surface tissue engineering. Novel biomaterials such as vitrigel and ECM were explored and optimized for ocular surface application. Animal experiments were conducted

throughout different studies as preparation for clinical translations in the future. *In vitro* model system for the ocular surface and tear film was investigated as an alternative to animal testing for new therapeutic discovery and screening. The relationship between corneal wound healing and the immunomodulation of the ocular surface was also studied. In Chapter 6, we also discussed several possible future research directions, to further improve the current therapies for ocular surface diseases. Overall, we successfully developed and applied unique tissue engineering strategies on the ocular surface and tear film system, involving both novel biomaterials scaffolds and organ model system. They enabled us to keep moving forward in the study of disease pathology and to accelerate the evaluation of potential therapeutics.

Chapter 2. Introduction and Background[1]

2.1. THE OCULAR SURFACE

The eye is the organ that enables us to perceive the world around us. The ocular surface is an essential component of the visual system, as it protects the vital parts of the eye and provides the appropriate refracting surface for light rays to enter. Ocular surface is composed of the cornea, conjunctiva, lacrimal glands, meibomian glands and other accessory glands (*1*). The eye and the ocular surface are closely related to other organ systems. The nervous and endocrine systems control and affect the secretion of multiple glands on the ocular surface; immune cells migrate to the conjunctiva during infection and inflammation; the vascular system provides the necessary nutrients for the ocular surface, and is responsible for tear fluid metabolism.

2.1.1. The structure and transparency of cornea

Corneal diseases and injuries account for about 80% of blindness worldwide. Besides mechanical supports, the cornea also provides about two thirds of the eye's refraction power (*2*), and this function is guaranteed by the highly organized structure within all layers of

[1] This chapter contains material modified from the following article, previously published as:
Q Lu, O Al-Sheikh, JH Elisseeff and MP Grant (2015). Biomaterials and tissue engineering strategies for conjunctival reconstruction and dry eye treatment. *Middle East African journal of ophthalmology* 22 (4), 428

the cornea. There are five distinct layers in the human cornea: the epithelium, Bowman's layer, the stroma, Descemet's membrane and the endothelium.

The collagen-rich stroma comprises about 90% of the thickness of the whole cornea. At microscopic level, the collagen fibrils are strictly aligned within each lamella, and there are about 200 lamellae across the human cornea, stacked together in alternating orthogonal directions (*3*). Corneal transparency mainly depends on two important factors: the uniformity of fibril diameter and the distance between adjacent collagen fibrils, and the latter is controlled by small leucine-rich proteoglycans, such as decorin, lumicana and keratocan. Other layers of the cornea are relatively thin compared to the stroma, but they also affect the overall transparency. The epithelium and endothelium serve as barriers for the stroma and they play an important role in maintaining the homeostasis of the whole cornea.

2.1.2. The conjunctiva and goblet cells

The conjunctiva starts at the corneoscleral limbus, and it covers the sclera and lines the inside of eyelids (bulbar and palpebral conjunctiva, respectively), and is connected by the fornix. The conjunctiva is composed of a layer of epithelium lying on top of a basement membrane, and is the main source of mucins in the tear film. It enables the free movement of the eye, provides immune surveillance and secretes mucins into the tear fluid (*1*).

The conjunctiva contains a stratified, squamous and non-keratinized epithelium, similar to corneal epithelium. Goblet cells are glandular cells residing on conjunctival epithelium, that synthesize and secrete the majority of large gel-forming mucins (mucin 5AC) to the

ocular surface. Many membrane-bond mucins have been identified on conjunctival epithelium as well, including mucin 1, 4 and 16, and together with the corneal membrane-bond mucins, they comprise the glycocalyx on the ocular surface (*4*).

2.1.3. The structure of lacrimal gland and its function

Human lacrimal glands contain both the main glands and the accessory glands. The main lacrimal glands contain the palpebral and orbital lobes about 3-5 mm in size. The lacrimal gland is an exocrine gland, similar to mammary and salivary glands, and it is comprised of many lobules separated from one another by loose connective tissue. The connective tissue contains interlobular ducts, vessels, nerve fibers, fibroblasts, many plasma cells, and a few lymphocytes (*5, 6*).

The interlobular ducts are open to the fornix of conjunctiva, and can be blocked by damaged epithelia during diseased states, thus healthy ocular surface epithelia are crucial for maintaining a normal of lacrimal secretion (*6*). Meanwhile, lacrimal glands secrete the aqueous tear fluid containing many ingradients to the ocular surface, and keep the ocular surface hydrated and unsusceptible to the infection of pathogens, including antibodies, cytotoxic agents, and growth factors and electrolytes (*5*).

2.2. BIOMATERIALS FOR OCULAR SURFACE RECONSTRUCTION

2.2.1. Injuries and diseases of the ocular surface

As the front cover for the eye, the ocular surface supports several of the eye's major functions, as it is composed of highly specialized cells and matrices. At the same time, the ocular surface is susceptible to many injuries and diseases. It can spontaneously begin wound healing upon injury, however, severe injuries to the ocular surface, such as chemical or thermal burns, Stevens-Johnson syndrome (SJS), and cicatricial pemphigoid post a great clinical challenge, especially when the stem cell populations in the cornea are affected. Therefore, tissue engineering strategies are necessary for optimal reconstruction of a healthy ocular surface without complications, such as fibrosis and wound contracture (*7, 8*). The ideal material for ocular surface reconstruction should be a stable, thin and elastic membrane, biocompatible with the human body (*9*). Here we summarize the major materials that have shown significant promise in either animal models or clinical trials.

2.2.2. Autologous Tissue Grafts

An autograft is a piece of tissue harvested from a healthy site in the same patient and transplanted to the damaged site to promote healing. As it is from the same individual, an autograft is the safest tissue product that can be used. In conjunctival reconstruction, autologous tissues are either conjunctival or non-conjunctival mucous membranes. A conjunctival graft from the same or contralateral eye is often applied following the excision of a pterygium, tumor, scar tissue or other lesions. As the graft is usually small, the donor site is often left to heal spontaneously, or can be closed with a local flap (*8-10*). Studies have shown that conjunctival defects replaced with healthy conjunctival autografts have less

wound contracture and lower risk of disease recurrence. An early study by Tan *et al.* found that donor conjunctival grafting reduced the recurrence rate of pterygium to less than 5%, compared to tissue excision alone, which had a recurrence rate of 60% (*11*). Although this procedure is effective, there are several drawbacks. First, autograft transplantation is limited to unilateral injury, as normal conjunctiva should exist in at least one eye to serve as the donor site. Therefore, autologous conjunctival transplantation is impossible in bilateral chemical/thermal burns or systemic ocular surface diseases. Other concerns with this procedure include postoperative discomfort and donor site morbidity, such as fibrosis (*10*).

To overcome the limitations of autologous conjunctival grafts, mucous membranes from other areas in the patient have been developed as replacements. Oral and nasal mucosas are common alternatives when healthy conjunctiva is not available. Oral mucosas harvested from different places in the mouth have variable properties. Grafts from the hard palate are the thickest and, thus, contract the least, but they are difficult to obtain compared to grafts from the buccal or labial regions (*12*). Researchers have also expanded mucosal epithelial cells on oral mucosal graft for treatment of complete limbal stem cell deficiency. This procedure is called, "cultured oral mucosal epithelial transplantation (COMET)" (*9, 13, 14*). However, unlike nasal mucosa, an oral mucosal graft does not contain goblet cells; therefore, it is less satisfactory in situations of extreme dry eye with mucous and goblet cell deficiency, such as Sjögren's syndrome (*9*).

2.2.3. Amniotic Membrane

Human amniotic membrane (AM) is a tissue product harvested from the inner layer of the placenta. It is composed of a single layer of epithelium, a thick basement membrane and

the underlying avascular stroma (*15*). Currently, AM is the most widely accepted conjunctival substitute (*8*). In the 1940s, a fetal membrane containing both amnion and chorion was transplanted for conjunctival reconstruction, but the success rate was low as a result of live cell inclusion (*16*). In 1997, the U.S. Food and Drug Administration (FDA) produced guidelines and surgical standards on the procurement, processing and distribution of a tissue product, such as AM. Subsequently, various applications of AM have been reported in the literature yearly. Similar to autologous grafts, allogeneic AM can be used as a replacement for damaged conjunctival stromal tissue. For example, Acelagraft™ (Celgene Corp., Summit, NJ, USA) is a denuded AM that has been lyophilized and sterilized with γ-irradiation. Moreover, AM can also be used as a preventive patch/dressing for the ocular surface to reduce inflammation, scarring and neovascularization, such as Prokera® (Bio-Tissue®, Doral, FL, USA), where AM is attached to a soft contact lens-sized conformer. The beneficial effect of AM could also be utilized as an extracellular matrix (ECM) extract. The product, AMX (Amniotic Membrane eXtract, Dr. Emiliano Ghinelli, Verona, Italy), is available in Europe for topical applications (*17*).

The resemblance between AM and conjunctiva in the composition of basement membranes makes AM a successful substitute for the treatment of various ocular surface conditions, including chemical or thermal burns, conjunctival tumors or recurrent pterygia (*9, 18*). When processed properly and preserved, AM could promote rapid epithelialization, reduce inflammation and vascularization, and suppress fibrosis and pain (*15*). An analysis of the composition of AM ECM extract indicated that the anti-inflammatory action of AM is due to the presence of interleukin-10 (IL-10). Additionally, AM supports nerve growth, which explains the near scarless healing after AM transplantation (*19*).

Although AM and related products hold great potential in ophthalmic applications, the availability, cost and standardization of AM preparation remain problematic. In general, the variable composition and properties of AM, reflecting donor differences and non-standardized preparation, could influence transplantation and result in inconsistent outcomes. Additionally, the mechanism of AM's beneficial actions and its precise molecular composition require extensive studies (*20*). Most importantly, as AM is an allogeneic tissue product, donor-associated risk of infectious transmission cannot be completely eliminated because only limited disease screening tests are performed prior to harvesting AM (*21*). The optimal method for processing AM without compromising the therapeutic value is the topic of intense research (*17*).

Table 2.1. Comparison of different tissue graft materials for conjunctival reconstruction.

(Adapted and modified from Mai and Bertelmann (*12*)with permission from Karger Publishers)

Graft material	Oral mucosa	Nasal mucosa	Amniotic membrane
Stability	high	high	low
Thickness	thick	thick	thin
Color	pink	pink	colorless
Transparency	opaque	opaque	transparent
Goblet cell replacement	no	yes	no
Easy accessibility	yes	no	yes
Has epithelial stem cells	yes	yes	no

Numerous characteristics require evaluation for the selection of the type of tissue grafts for conjunctival reconstruction. For example, injuries in the fornix require the graft to contract less than a graft in the bulbar conjunctiva. In extreme dry eye, nasal mucosa is superior to

oral mucosa and AM, because it contains goblet cells (*12*). The features of each tissue graft material are summarized in Table 2.1.

2.2.4. Biomacromolecular Materials

Since autologous/allogeneic graft transplantations have numerous limitations, advances in ophthalmic tissue engineering techniques have led scientists to develop new biomaterial matrices. Biomaterials engineered in a laboratory based on macromolecules, such as synthetic polymers and proteins, could have better properties for healing ocular diseases and injuries than traditional autologous/allogeneic tissue grafts. First, bioengineered macromolecular materials are tunable, in that their properties can be designed precisely to accommodate different requirements. For example, the degradation rate of poly(lactide-co-glycolide) (PLGA) can be changed by varying the ratio of lactide to glycolide. Furthermore, these biomaterials have much more consistent qualities, and their compositions have been extensively studied. Hence these biomaterials present a lower risk for translational use. Some biomaterials can be modified to have different functional groups or motifs to selectively promote the growth of a certain type of cells, and drug-loaded particles can be embedded in the materials for controlled release. Due to these advantages, biomacromolecular materials are a very promising alternative to tissue grafts for ocular surface reconstruction.

Although there is a significant body of literature on many biomaterials for conjunctival reconstruction, with some positive and promising results, none of the existing materials meet all criteria for an optimal substrate for conjunctival repair. The degradable polymer matrices PLGA (*22*) and poly(ε-caprolactone) (PCL) (*23*) were tested *in vitro* and on animal models as candidates for conjunctival reconstruction. Lee *et al.* developed a porous

PLGA matrix using a solvent-casting particulate-leaching method that was also modified with collagen, hyaluronic acid (HA) and human AM components. The modified PLGA matrix showed increased cell adhesion and growth *in vitro*. In a rabbit model of conjunctival injury, a PLGA graft significantly prevented conjunctival contracture and stromal scarring (*22*). However, due to the preparation process, the PLGA matrix was neither elastic nor transparent. Ang *et al*. prepared ultrathin PCL membranes by solvent-casting and biaxial stretching. The material formed was highly flexible and promoted the attachment and proliferation of conjunctival epithelial cells *in vitro* (*23*). However, it has not been tested on an animal model of ocular injury, and it may be difficult to integrate into the host tissue, and there may be induced scar formation due to its aligned fibrillar structure.

Natural protein molecules, such as collagen (*24*) and keratin (*25*), were also tested in animal models for conjunctival regeneration. Similar to the PLGA graft, the porous collagen-glycosaminoglycan matrix prevented scar formation in a rabbit conjunctival injury model (*24*). The disadvantage of this matrix is that it not elastic or transparent. Keratin film has good mechanical properties including elasticity and transparency, and it is very tunable depending on the preparation process (*25*). However, it may still be too stiff for ocular surface use, and the phenotypic development of epithelial cells on a keratin substrate remains unknown, as keratin is not a natural component of conjunctiva.

2.2.5. Collagen Vitrigel

Type I collagen is the most abundant component in the ECM of the conjunctival stroma; therefore, it is one of the top choices for biomaterial engineers when designing substrates for the ocular surface. However, the applications are limited, because collagen hydrogels

are opaque and composed of loosely packed collagen fibrils, while the collagen fibrils in native conjunctival stroma are highly condensed and well organized (*14*). To improve the properties of collagen hydrogels, Takezawa *et al.* developed a type I collagen hydrogel membrane using a three-step processing method: gelation, vitrification and rehydration (*26, 27*). Vitrification is a unique step that allows water in a hydrogel to evaporate in a controlled manner, during which, collagen fibrils reorganize and form crosslinks between each other (Figure 2.1A, B). Hence, a normal opaque collagen hydrogel is transformed into a thin, elastic and transparent membrane, and, most importantly, its fibril density increases tremendously. This material is called "vitrigel" (Figure 2.1C). Beginning with the original recipe, our group has studied collagen vitrigel extensively for optimization in ocular surface applications.

Electron microscopy revealed that the nanoscale structure of vitrigel is a network of randomly aligned collagen fibrils (Figure 2.1D). There are three variables in the vitrification process: temperature, relative humidity (RH) and time. Calderón-Colón *et al.* systematically varied these variables and studied the properties of vitrigel under each condition to optimize the manufacturing process. Optical, mechanical and thermal properties were measured and compared, as they are most relevant for ocular surface application. Conclusively, vitrification occurring at 40 °C and 40% RH for a week yields the optimal vitrigel that is highly transparent, mechanically strong and elastic, and denatures at a temperature well above the core body temperature of humans (*28, 29*). As cell proliferation and differentiation largely depend upon the surrounding environment, Guo *et al.* studied the influence of nanostructure on cell morphology and phenotype by making vitrigels from different

vitrification conditions (*30*). Although fibrillar density increased with increasing temperature and time, fibrillar diameter remained constant in all mature vitrigels. The biological effect was investigated by growing corneal keratocytes on different vitrigels. Due to the difference in nanoarchitecture (fibrillar density, bending, etc.), keratocytes developed distinct morphologies (*30*). The optimal vitrigel was able to maintain the native characteristics of keratocytes under *in vitro* conditions (*30*). Vitrigel is an effective substrate for corneal keratocytes, it was successfully used in the reconstruction of corneal epithelium and endothelium, and it could preserve the stemness of limbal stem cells *in vitro* (*31*).

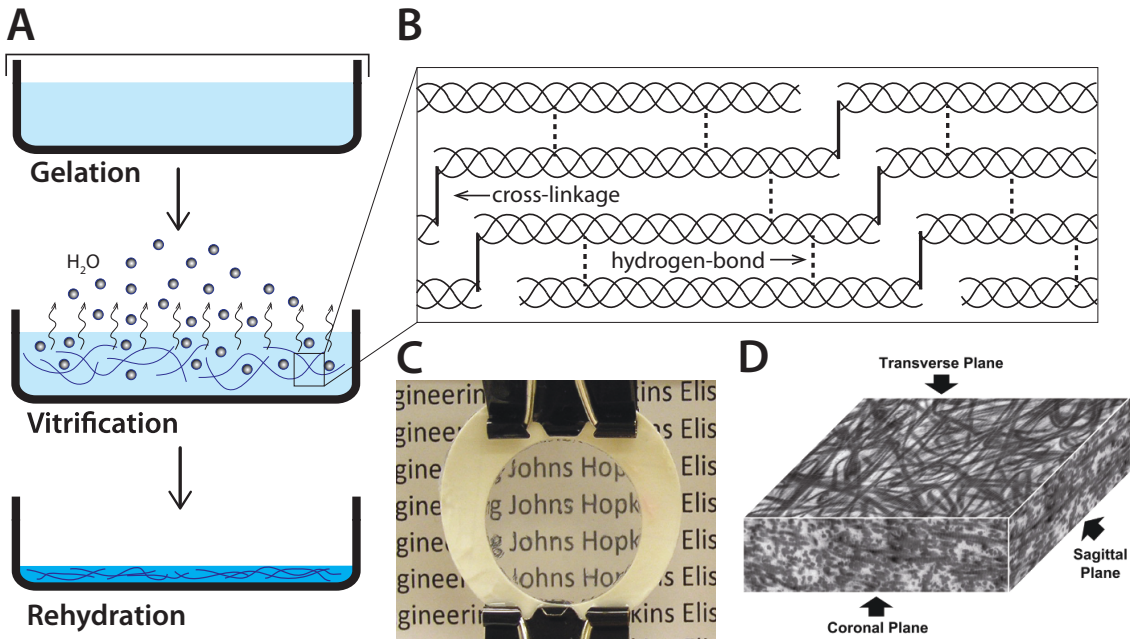

Figure 2.1. The preparation of collagen vitrigel and its appearance and structure.

(A) Three-step preparation. (B) Crosslinking between collagen fibrils occurs during the vitrification process. (C) The final vitrigel is a transparent and thin membrane. (D) Transmission electron microscopy reveals the nanostructure of the vitrigel – the presence of densely and randomly packed collagen fibrils (adapted and modified from Guo et al. (*30*) and Calderón-Colón et al. (*28*) with permission from Elsevier).

2.3. TEAR FILM AND DRY EYE DISEASE

2.3.1. Tear film structure and components

The tear film, secretion products of the ocular surface, is fundamental for maintaining the smoothness and homeostasis of the ocular surface. The components of the tear film include a lipid layer and an aqueous layer with soluble mucins, which are mainly secreted by the meibomian glands, lacrimal gland and conjunctival goblet cells, respectively.

2.3.2. Dry eye disease and treatment

Dry eye represents a major ocular surface disease. According to the 2007 report of the International Dry Eye WorkShop (DEWS), dry eye is a multifactorial disease and the symptoms include eye discomfort, visual disturbance, tear instability and, potentially, ocular surface damage (*32*). Based on data from previous studies of dry eye epidemiology, about 4.91 million Americans above 50 years of age suffer from dry eye disease. Additionally there are tens of millions more people with less severe symptoms that can be triggered through contact with adverse factors, such as contact lens wear or extended use of visual display terminals (*33*). In general, dry eye may have a substantial impact on a patient's quality of life. In patients with severe dry eye, the disease affects even common activities, such as driving and reading. Dry eye can be either aqueous-deficient or evaporative, which results from problems with the aqueous or lipid layer of the tear film, respectively. Dry eye is further categorized into different subtypes, depending on the primary cause (*32*). Although goblet cell dysfunction is not a major cause, most dry eye patients have a significantly decreased number of goblet cells. Lack of mucin will further disturb the already sub-

optimal tear film and ocular surface, increasing the severity of dry eye. Hence, while developing treatment for dry eye, goblet cell repopulation should also be considered.

The most common management for mild-to-moderate dry eye is tear supplementation. Artificial tears, ointments and gels are examples of lubricants that protect the ocular surface and treat dry eye. However, some ingredients, especially the preservatives in these products, may damage the ocular surface epithelium if used long term. In patients with severe dry eye, surgical procedures, such as gland transplantation is necessary to restore a healthy ocular surface and tear film. Over the past two decades, research has focused on evaluating the pathology of dry eye and developing models for *in vitro* and animal studies (*34*). Instead of simply hydrating the eye, future therapies will shift to strategies stimulating natural tear secretion to maintain ocular surface homeostasis, reducing inflammation and inhibiting adverse effects (*32*). A robust *in vitro* model for normal human ocular surface and dry eye is also needed for drug screening purposes and pathophysiology studies.

2.4. IN VITRO MODEL SYSTEMS

2.4.1. Biomimetic “organ-on-a-chip” models

An organ-on-a-chip is a bioengineered microdevice with living cells, and it usually employs microfabrication and microfluidics technologies. It mimics the vital functions of the living organ and recapitulates organ-level pathophysiology *in vitro* (*35*). Organs-on-chips have great potential for studying the physiology of normal or diseased organs (*36*). The organ-on-a-chip technique emerged as a cell culture model to replace some costly and time-

consuming animal studies in the pharmaceutical industry. Regular two- or three-dimensional cell culture was not completely successful because tissue development depends on both the architecture of the ECM and its mechanical/structural features (*37*). Due to the small size, the chip system can be used as a high-throughput drug-screening device, and it also has therapeutic potential. Theoretically, it could be engineered from dissected tissue, primary cells or induced pluripotent stem cells (*38*). Over the past few years, several organ systems have been created on a chip device. A "lung on a chip" was created by apposing two poly(dimethylsiloxane) (PDMS) channels separated by a thin, porous and flexible membrane. Human alveolar epithelial cells and pulmonary microvascular endothelial cells were cultured on opposite sides of the membrane. In the final product, air was introduced into the epithelial compartment to create an air-liquid interface and, together with the two vacuum chambers on each side, the microdevice was able to manipulate fluid flow and membrane stretching, as well as nutrient delivery (*37*). Liver, gut and spleen organs-on-chips systems have also been developed (*39-41*). Recently, bone marrow-on-a-chip, composed of artificial bone and living marrow, was first generated in mice and then maintained *in vitro* within a microfluidic device (*42*).

2.4.2. Current ocular model systems

Thus, such organs-on-chips may have specific use in treating complex ocular diseases. For example, dry eye is a complicated disease affecting all parts in the ocular surface. Currently dry eye therapeutics is tested in animal models before proceeding to clinical trials. However, the pathophysiology of dry eye has very different mechanisms in humans and in other species. The normal composition of tear fluid also varies among different species. Ophthalmic pharmaceutical companies are developing *in vitro* corneal epithelial models to

evaluate the safety and efficacy of novel tear substitutes/lubricants. *In vitro* models of conjunctival epithelium and artificial lacrimal glands have also been investigated in the laboratory (*43, 44*). However, these models contained only a single cell type, and they could not be maintained for an adequate duration *in vitro* for physiological study. Hence, for future dry eye studies and drug development, it is critical to have an *in vitro* model that recapitulates the normal or diseased state of the human ocular surface. The combination of multiple cell types, such as conjunctival epithelium and lacrimal gland acinar cells, and microfluidic channels, will create a model of an aqueous tear-secreting unit. Although some difficulties exist, such as the necessary biological and mechanical cues for the construction of chips, advances in gene regulation and protein expression of the ocular surface have shed light on a potential design for "ocular surface-on-a-chip" for the study of dry eye. For example, these chips can be constructed with genetically modified cells to recreate a disease-state organ. Marko *et al.* discovered that a single gene knockout in a mouse model ($SPDEF^{-/-}$) resulted in complete goblet cell loss and moderate dry eye, which is very similar to Sjögren's syndrome (*45*). Therefore, it would appear that ocular chips made from $SPDEF^{-/-}$ cells could serve as a comprehensive *in vitro* model for Sjögren's syndrome. Furthermore, linking a dry eye disease chip with a multi-organ microfluidic device that connects more than one single organ chip, such as chips reproducing the immune and vascular systems, would allow a greater understanding of the overall pathophysiology of dry eye.

2.5. SUMMARY

The ocular surface is the external protective component of the eye, and the conjunctiva plays an important role in this protective system. Researchers have been successful in developing tissue- and biomolecule-based grafts to reconstruct conjunctiva. However, improvement is required to render the available biomaterials more consistent, available and biocompatible. Dry eye, which can be a serious ocular surface disease, affects tens of millions of people worldwide. While traditional treatment has major obstacles, breakthroughs in organ-on-a-chip technology offer new directions in establishing *in vitro* models of the ocular surface for dry eye disease research.

Chapter 3. Vitrified Collagen-Based Conjunctival Equivalent for Ocular Surface Reconstruction[2]

3.1. INTRODUCTION

The primary function of the ocular surface system is to protect the refractive surface on the eye. It is composed of continuous epithelia, including the cornea and conjunctiva, and injury to one part may result in system-wide secondary dysfunction (*34*). The conjunctiva, starting from the corneoscleral limbus and lining the inner surface of the eyelids, is a very important component of the ocular surface. It is a natural mechanical barrier against pathogens, and its main functions include maintaining the equilibrium of the tear film by secreting mucins (*8, 9*). Therefore, conjunctival repair is the prerequisite for successful ocular surface reconstruction. The conjunctiva consists of a stratified non-keratinized epithelium with goblet cells resting on a basement membrane, and has the capacity to spontaneously re-epithelialize upon injury (*10*). However this is usually accompanied with a certain amount of fibrosis and wound contracture, especially in extensive disorders, such as cicatricial pemphigoid, Stevens-Johnson syndrome and chemical/thermal burns (*9*). In these

[2] This chapter contains material modified from the following article, previously published as:
H Zhou*, Q Lu*, Q Guo, J Chae, X Fan, JH Elisseeff and MP Grant (2014). Vitrified collagen-based conjunctival equivalent for ocular surface reconstruction. *Biomaterials* 35 (26), 7398-7406. (*equal contribution)

cases, an appropriate tissue substitute needs to be applied for optimal wound healing after the excision of diseased tissue.

The general principle of tissue engineering is to replace tissue lost from disease or trauma using biomaterial scaffolds, in combination with cells and/or biological cues to accelerate the regeneration (*46*). The ideal conjunctival substitute should be a stable, thin and elastic matrix that is not rejected by the patient's immune system (*9*). Although use of autologous tissue substitutes (conjunctiva and oral/nasal mucosa) have made progress in clinical studies (*8*), and synthetic matrices based on fibrin (*47, 48*), keratin (*25*), collagen (*24*) and poly (lactide-co-glycolide) (PLGA) (*22*) were also tested in animal models, they are limited for numerous reasons. For example, available donor grafts are very limited in patients suffering from systemic autoimmune diseases. Donor site morbidity could be a concern if large grafts are required. Furthermore, none of the synthetic matrices is sufficiently elastic for ideal conjunctival reconstruction. So far, the most widely accepted substitute is human amniotic membrane (AM) (*8*). AM is epithelium harvested from the inner layer of human placenta and contains a basement membrane with underlying stroma. Clinically, AM-based conjunctival equivalents have been transplanted to treat ocular diseases with promising results. However, the availability, cost and standardization in the preparation of AM still remain issues. Therefore, there is a need for a biomaterial scaffold with well-defined composition and tunable structure that has excellent mechanical and biological properties for ocular surface application.

Type I collagen is the most abundant component in the extracellular matrix (ECM) of conjunctival stroma, where collagen fibrils synthesized by fibroblasts form a random network. Vitrified collagen (collagen vitrigel, CV) is a vitrified type I collagen membrane and has

densely packed and randomly aligned collagen fibrils (*26*). It is transformed from a normal collagen gel (CG) through a vitrification process to become a thin, elastic and transparent membrane, and, most importantly, its fibril density is tremendously increased, which has been proven to be a significant factor in maintaining cell phenotypes (*30*). The vitrification process has been optimized by systematically varying the conditions (temperature, humidity and time) to yield the best CV that is highly transparent, mechanically strong and elastic, and also has a denaturing temperature well above body temperature (*28*). *In vitro*, CV has been used for the cultivation of various ocular cells, including corneal epithelial cells, without the use of a feeder layer or other substrates (*31*). In summary, CV was designed for ocular surface application with well-defined composition and controllable structure, and it closely imitates the architecture and properties of native conjunctival stroma. Therefore, we considered utilizing CV as a tissue substitute for cell transplantation in conjunctival reconstruction.

In this study, we attempted to employ the optimized CV to engineer a conjunctival equivalent containing goblet cells, a distinctive phenotype of conjunctival epithelium responsible for the secretion of large gel-forming mucins in the tear film. The presence of goblet cells is an essential indication of a functional conjunctival epithelium, as destruction to the conjunctiva could result in decreased numbers of goblet cells. If left uncorrected, this defect may cause severe dysfunction of the ocular surface or even blindness (*8*). Rabbit conjunctival epithelial cells (rCjECs) were isolated and grown on optimized CV, normal CG (without the vitrification process) or tissue culture plates (TCP) (control) to determine the best culture substrate. Cell morphology, proliferation and phenotypes were inspected and compared among them. Furthermore, CV-based conjunctival equivalents were transplanted to

repair conjunctival defects in a rabbit model. The outcomes were evaluated both anatomically and physiologically. Conjunctival scarring and contraction were assessed and inspected histologically; re-epithelialization, cell integration and goblet cell re-population in the defect sites were detected by gene expression and immunohistochemistry studies. Overall, the feasibility of CV transplantation as a strategy for treating conjunctival defects and restoring a balanced, healthy ocular surface post-damage was demonstrated.

3.2. MATERIALS AND METHODS

At all times in this study, the animals involved were housed and treated in accordance with the guidelines in the ARVO Statement for the Use of Animals in Ophthalmic and Visual Research and also with the approval of the Animal Care and Use Committee at Johns Hopkins University.

3.2.1. Collagen vitrigel preparation

The CV membrane was prepared as previously described (*26, 28, 31*). Briefly, the procedure includes three main stages: gelation, vitrification and rehydration. Preceding these steps, acid collagen solution (0.25% v/v, Cosmo Bio, Tokyo, Japan) was prepared in Dulbecco's Modified Eagle Medium (DMEM, Life Technologies, Grand Island, NY) with 10% fetal bovine serum (FBS, Thermo Scientific, Rockford, IL) and 20 nM 4-(2-hydroxyethyl)-1-piperazineethanesulfonic acid buffer (HEPES, Life Technologies) on ice. Collagen solution was then incubated at 37 °C for 2 hours. After complete gelation, the opaque collagen gel was vitrified under 40% relative humidity (RH) at 40 °C, resulting in its conversion

into a glassy material. After 1 week, the gel membrane was rinsed with phosphate buffered saline solution (PBS, Life Technologies) to remove the phenol red pH indicator in DMEM solution. Finally, the vitrigel was rehydrated to obtain a regenerated and stable membrane. Normal CG was prepared similarly to CV except that it was only kept in the humidifier for one day (40% RH, 40 °C) before rehydration.

3.2.2. Transmission electron microscopy (TEM)

The fibrillar structures of CV and CG were revealed by TEM, according to our previous study (*30*). In short, samples were fixed in 3% paraformaldehyde (PFA), 1.5% glutaraldehyde, 5 mM $MgCl_2$, 5 mM $CaCl_2$, 2.5% sucrose and 0.1% tannic acid in 0.1 M sodium cacodylate buffer at pH 7.2 overnight at 4 °C, followed with post-fixation on ice in the dark in 1% osmium tetroxide for 1 hour after buffer rinse. The collagen samples were stained with 2% aqueous uranyl acetate for 1 hour in the dark and dehydrated in a graded series of ethanol before embedding in Eponate 12™ resin (Ted Pella, Inc., Redding, CA), and allowed to polymerize for two to three days at 37 °C before being transferred to 60 °C overnight. Thin sections (60-90 nm) were cut on the Reichert-Jung Ultracut E ultramicrotome (Reichert, Austria) and then placed on naked copper grids, which were again stained with 2% uranyl acetate in 50% methanol. Images were taken on a Hitachi 7600 TEM (Hitachi, Ltd., Tokyo, Japan) at 80 kV. The top view (surface) of the collagen samples was obtained and all chemicals were purchased from Sigma-Aldrich (St. Louis, MO), unless otherwise mentioned.

3.2.3. Isolation and in vitro culture of rabbit conjunctival epithelial cells (rCjECs)

Cell isolation and culture were performed as previously described (*49*). Briefly, after sacrifice, the conjunctiva was carefully dissected from New Zealand white rabbits, with underlying connective tissue removed. Conjunctiva tissue was finely minced into 1 mm^3 pieces and cultured as explants on tissue culture dishes in serum-free medium, with epithelium side facing up (Figure 3.2A). Sufficient medium was added to cover the bottom of the dish so that the tissue would receive nutrients through surface tension. The cells were cultured in keratinocyte-serum-free medium (K-SFM, Life Technologies) supplemented with human recombinant epidermal growth factor (EGF, 5 ng/mL) and bovine pituitary extract (50 μg/mL) at 37 °C in a 5% CO_2 incubator. When reaching confluence, rCjECs were passaged with 0.05% trypsin/EDTA (Life Technologies). For *in vitro* study, passage one rCjECs were seeded on three substrates at a density of 2×10^3 cells/cm^2: CV (Figure 3.2D), CG (Figure 3.2E) and TCP. Histology and immunostaining were carried out as described below when cells reached confluence (about 5 days).

3.2.4. Cell proliferation, viability and morphology

The effects of the three substrates on cell attachment and proliferation were determined through use of the alamarBlue® test (Life Technologies), which tests for cellular viability quantitatively through the presence of cellular respiration. At days 1, 4, 7 and 9 after the initial seeding, alamarBlue® was added directly to the culture medium at 10% v/v and incubated for 4 hours. Absorbance was measured spectrophotometrically at 570 and 600 nm

using a microplate reader (SpectraMax, Molecular Devices, LLC, Sunnyvale, CA). Proliferation rate (cell number) was calculated as percent reduction of the alamarBlue® dye, per manufacturer's instructions.

Cell viability on the three substrates was also examined using the LIVE/DEAD Viability Kit (Life Technologies), a two-color fluorescent assay based on differential permeability of live and dead cells. Live cells (when monolayer cells reached confluence, in about 5 days) were stained with green fluorescent calcein AM, a cytoplasm stain, and dead cells with compromised cell membranes were stained with red fluorescent ethidium homodimer-2 (EthD-2). A Nikon Eclipse TE200 fluorescent microscope (Nikon Inc., Melville, NY) was used to capture the images of the cell staining patterns.

Morphology of rCjECs grown on the three substrates was viewed by F-actin staining with phalloidin. When cells reached confluence, they were fixed with 4% (w/v) PFA, permeabilized with 0.5% Triton X-100 (Sigma-Aldrich) and stained with Alexa Fluor-546 phalloidin (Life Technologies) for 30 min. Nuclei were counterstained with 1 μg/mL DAPI (4',6-diamidino-2-phenylindole dihydrochloride, Life Technologies) for 30 min. The cells were imaged using the Nikon Eclipse TE200 fluorescent microscope.

3.2.5. Reverse transcription and real-time quantitative polymerase chain reaction (RT-qPCR)

RT-qPCR analysis was used to quantify the level of mRNA transcripts of two representative genes (*ck4* and *muc5ac*) expressed in rCjECs on the three substrates. Total RNA was isolated from conjunctival cells using the MagMAX™ Total RNA Isolation Kits (Life Technologies) and cDNA was synthesized using a high capacity reverse transcription kit

for RT-PCR (Life Technologies) according to the manufacturer's protocol. Real-time PCR was carried out on the StepOnePlus™ Real-Time PCR System (Life Technologies) using SYBR® Green PCR Master Mix (Life Technologies) with designed primers (Table 3.1). The relative expression level of all targets was calculated by the $\Delta\Delta C_T$ method (*50*) and normalized against the control sample (TCP) with *gapdh* (glyceraldehyde-3-phosphate dehydrogenase) as the reference.

Table 3.1. Primers used in PCR studies.

Genes		Primers
ck4	F	5'-CAACCTGAAGACCACCAAGA-3'
	R	5'-CAGAGTCTGGCACTGCTTT-3'
muc5ac	F	5'-TGATGACCAACCAGGTCATTT-3'
	R	5'-GGGATGGTCACGTACATCTTG-3'
sry	F (A1)	5'-ATGTATGCCCTTATGTTCG-3'
	R (B1)	5'- CGAAACTCAGACATCAGCA-3'
	F (A2)	5'-GAGCACTGTACAGCGATGCT-3'
	R (B2)	5'- CAACATCAGAGACGCCAGGT-3'
gapdh	F	5'-GGTCGGAGTGAACGGATTT-3'
	R	5'-TGTAGTGGAGGTCAATGAATGG-3'

3.2.6. In vivo rabbit conjunctival defect model

The conjunctival defect model was designed similarly to that used in previous studies (*22, 24*). Six female New Zealand white rabbits weighing between 3 and 4 kg were anesthetized by intramuscular injection of ketamine (15 mg/kg) and xylazine (5 mg/kg). The eyelids were held open during surgery by a speculum, and a surgical microscope was used during all procedures. Round conjunctival defects were produced at the 10 o'clock (superior lateral) position at least 2 mm from the limbus on both eyes of each rabbit. A 7.5-mm diameter

vacuum trephine (JEDMED Instrument Co., St. Louis, MO) was used to completely remove the conjunctival epithelium, substantia propria and Tenon's capsule down to the level of bare sclera (Figure 3.4A). The process was carried out carefully without damaging the underlying sclera. Iris scissors were used to remove the remaining tissue if the trephine did not completely sever Tenon's capsule. Slight retraction of the wound edges resulted in a final wound diameter of approximately 9-9.5 mm.

3.2.7. Collagen vitrigel transplantation

Six female rabbits were divided into 3 groups (4 eyes/group): treated groups – grafted with CV only or CV + cells; untreated group – negative control. Passage 1 rCjECs obtained from a male rabbit were seeded on CV at a density of 2×10^3 cells/cm^2 and allowed to grow for 5 days *in vitro* before transplantation. In the treated groups, the wound was grafted with a 10-mm diameter membrane of CV (with or without cells) using uninterrupted sutures with 9-0 Vicryl violet monofilament suture on a BV100-3 needle (taper point, Ethicon, Somerville, NJ). Defects in the negative control group were left open without grafting. Neomycin and polymyxin B sulfates and dexamethasone ophthalmic ointment (Fera Pharmaceuticals, LLC, Locust Valley, NY) were applied to all groups immediately after surgery and then once daily for 2 weeks post-surgery. The depth of the conjunctival fornix above each wound (Figure 3.4A) was measured immediately post-surgery and at post-operative days 14 and 28 using a blunt probe with a scale for measurement. The percentage of fornix shortening was calculated as the percent decrease in fornix depth compared to the original value (before surgery). Gross images of the defect were taken every week. At the end of 4 weeks, animals were euthanized and conjunctival tissues containing the original

defect area from treated and untreated groups were dissected for further analysis. Conjunctiva without defect was also taken and used as the positive control. Half of each tissue obtained was fixed in 4% PFA and embedded in optimum cutting temperature compound (OCT, Sakura Finetek U.S.A., Inc., Torrance, CA) for sectioning (10 μm) on a cryostat (Leica Microsystems Inc., Buffalo Grove, IL). The other half of the tissue was homogenized by ultrasound and the total DNA was extracted for further analysis.

3.2.8. Histology and immunostaining

Periodic acid-Schiff (PAS) staining was performed on both *in vitro* and *in vivo* samples for the detection and distribution of mucosubstances. After fixation with 4% PFA, samples were stained with a PAS staining kit (Sigma-Aldrich) according to the manufacturer's manual. Hematoxylin & eosin (H&E) and Masson's trichrome (MT) staining were performed, as previously described (*51*), on tissue sections to visualize the morphology of the epithelium and collagen fibril alignment. Samples were imaged as above and at least three randomly selected visual fields were viewed.

Specific antigen expression was visualized in immunostaining experiments. Primary antibodies of cytokeratin 4 (CK4, clone 6B10, Sigma-Aldrich) and MUCIN 5AC (MUC5AC, clone 45M1, Abcam, Cambridge, MA) were used to stain both cell and tissue samples. Fluorophore conjugated secondary antibodies (Jackson ImmunoResearch, West Grove, PA) were used to visualized the specific antigens. Briefly, after fixation with 4% PFA, samples were first permeabilized with 0.5% v/v Triton X-100 in PBS (PBST) for half an hour and then blocked with 4% normal goat serum in PBST for another hour at room temperature. After washing, primary antibodies were added at a dilution of 1:200 for both CK4 and

MUC5AC and incubated at 4 °C overnight. The next day, after extensive washing, secondary antibody was added and incubated for 1 hour at room temperature in the dark. Nuclei were stained with DAPI for 30 min afterwards. Images were taken either under a fluorescent light microscope (Nikon Eclipse TE200) or a confocal microscope (Zeiss LSM 510, Carl Zeiss Microscopy, LLC, Thornwood, NY). The percent of positively stained cells for each marker was calculated using ImageJ software (US National Institutes of Health, Bethesda, MD) and at least 6 random fields per sample were analyzed.

3.2.9. Statistical Analysis

Data are shown as mean ± standard deviation (SD). All experiments were performed with at least three repeats. Data were analyzed using the two-sample equal variance student's *t*-test. A probability (*P*) value less than 0.05 was considered statistically significant.

3.3. RESULTS

3.3.1. Morphology and proliferation of conjunctival epithelial cells

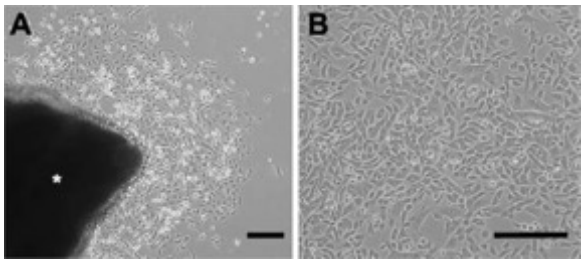

Figure 3.1. rCjEC isolation and culture in vitro.

(A) Cells started to migrate out of the explant (asterisk) within a day. (B) rCjECs displayed a squamous morphology when reaching confluence after proliferating for 3-5 days. Scale bar: 200 μm.

Epithelial cells were isolated and subcultured on three different substrates: CV, CG and TCP. The differences in the fibrillar organization and density of CV and CG were shown by TEM (Figure 3.2D, E). After the 1-week vitrification, CV showed random fibrillar organization with a high density of collagen fibrils. In comparison, CG had a much lower density of collagen fibrils, which also appeared to be bent (Figure 3.2D, arrowhead). In primary explant culture, rCjECs that had migrated from the explant displayed nonkeratinized squamous epithelial morphology and reached confluence within 5 days (Figure 3.1). After being passaged, the cells attached and proliferated on the three different substrates. As shown by live/dead staining (Figure 3.3A-C), attached cells exhibited very high viability (over 95%) regardless of the substrate type. The majority of the cells appeared to be nongoblet epithelial cells with a small squamous morphology (Figure 3.3D), while the larger cells contained an extensive accumulation of secretory vesicles in the cytoplasm and had the typical shape of goblet cells, as seen in F-actin staining (Figure 3.3E).

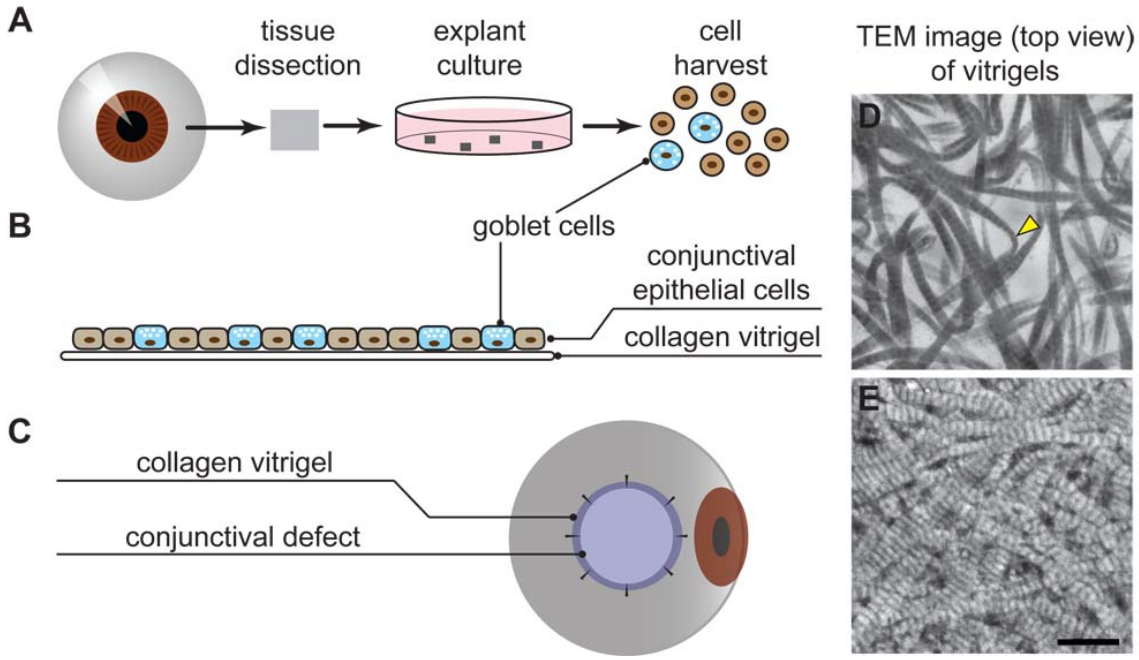

Figure 3.2. Schematic view of experimental design.

(A) Rabbit conjunctival epithelial cells (rCjECs) isolation and harvest. (B) Cultivation of rCjECs on CV with the specific goblet cell phenotype. (C) Reconstruction of conjunctival defect using CV based conjunctival equivalent. (D, E) TEM images showing the fibrillar density and organization of normal CG and optimal CV, respectively. Arrowhead showing the bending of collagen fibril. Scale bar: 500 nm.

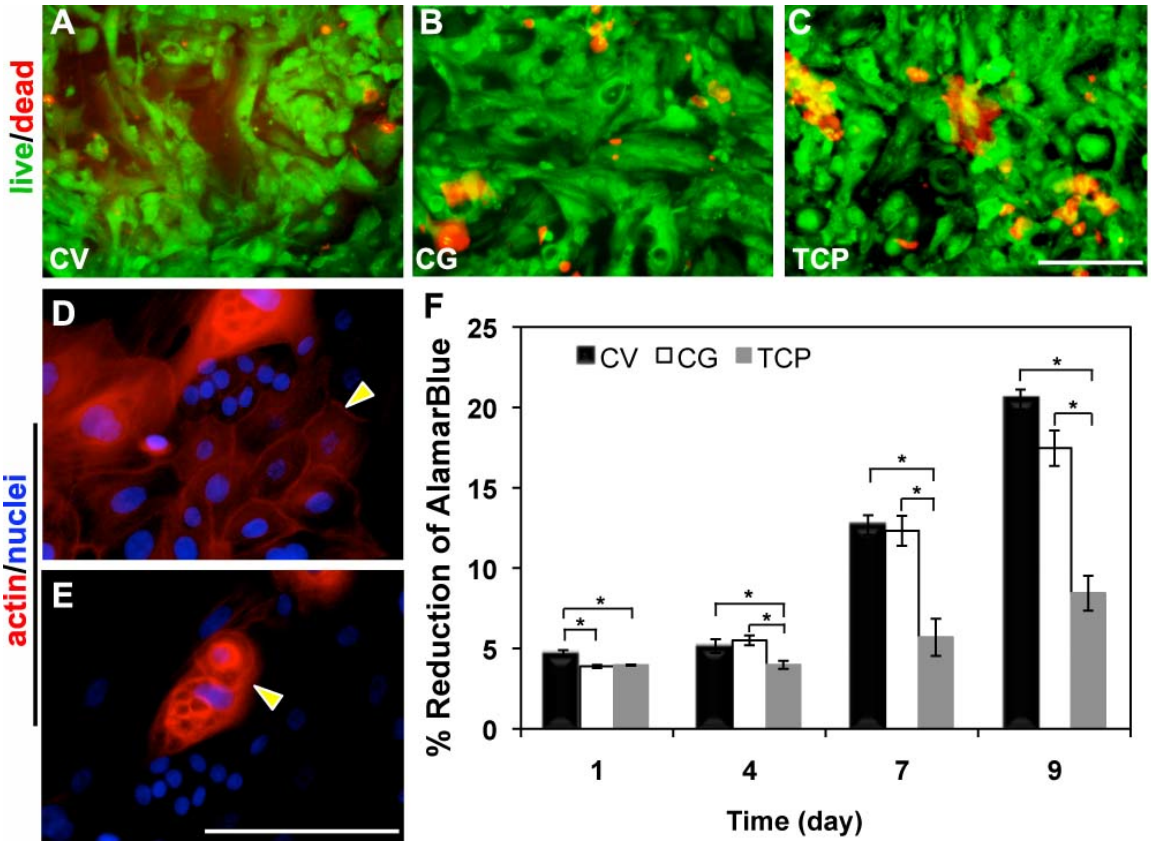

Figure 3.3. rCjEC morphology and proliferation in vitro.

(A-C) Live (green)/dead (red) staining of rCjECs grown on different substrates (CV, CG and TCP). (D, E) Phalloidin 546 (red, for actin) and DAPI (blue, for nuclei) staining for visualization of rCjEC morphology in culture; arrowheads indicated typical squamous epithelial cells (D) and goblet cells (E). (F) Proliferation assay of rCjECs cultivated on different substrates; cell number was directly proportional to the percent reduction of alamarBlue® dye. Scale bar: 100 μm.

The alamarBlue® assay was used to quantify cell proliferation on different growth substrates. The data were plotted as percent reduction of the alamarBlue® dye, which is proportional to cell number (Figure 3.3F). Starting from the same seeding density, one day after cell seeding, CV had a greater number of cells grown on it than either CG or TCP, indicating rCjECs preferentially attached to CV compared to the other substrates. By day 9, there were more than twice as many cells grown on the CV substrate than on the TCP substrate. The difference between the number of cells grown on CG and TCP substrates was also statistically significant.

3.3.2. Collagen vitrigel maintained the phenotypes of rCjECs in vitro

Rabbit CjECs grown on the three substrates were tested to determine their conjunctival epithelial phenotypes. PAS staining is used to detect mucosubstances (magenta) in cells and tissues, and strong staining indicates the presence of mucin-secreting goblet cells. More mucins and stronger staining were observed on the CV and CG substrates compared to the TCP substrate (Figure 3.4A-C). Non-goblet epithelial cells and goblet cells can be identified by the presence of CK4 (Figure 3.4G-I) and MUC5AC (Figure 3.4D-F) respectively. Approximately 13% of the rCjECs grown on CV stained positive for MUC5AC and 41% stained positive for CK4. The percentages for CG were 8% and 26%, respectively. Only 2% (MUC5AC) and 17% (CK4, Figure 3.4J) of cells grown on TCP stained positive, significantly lower than those on CV.

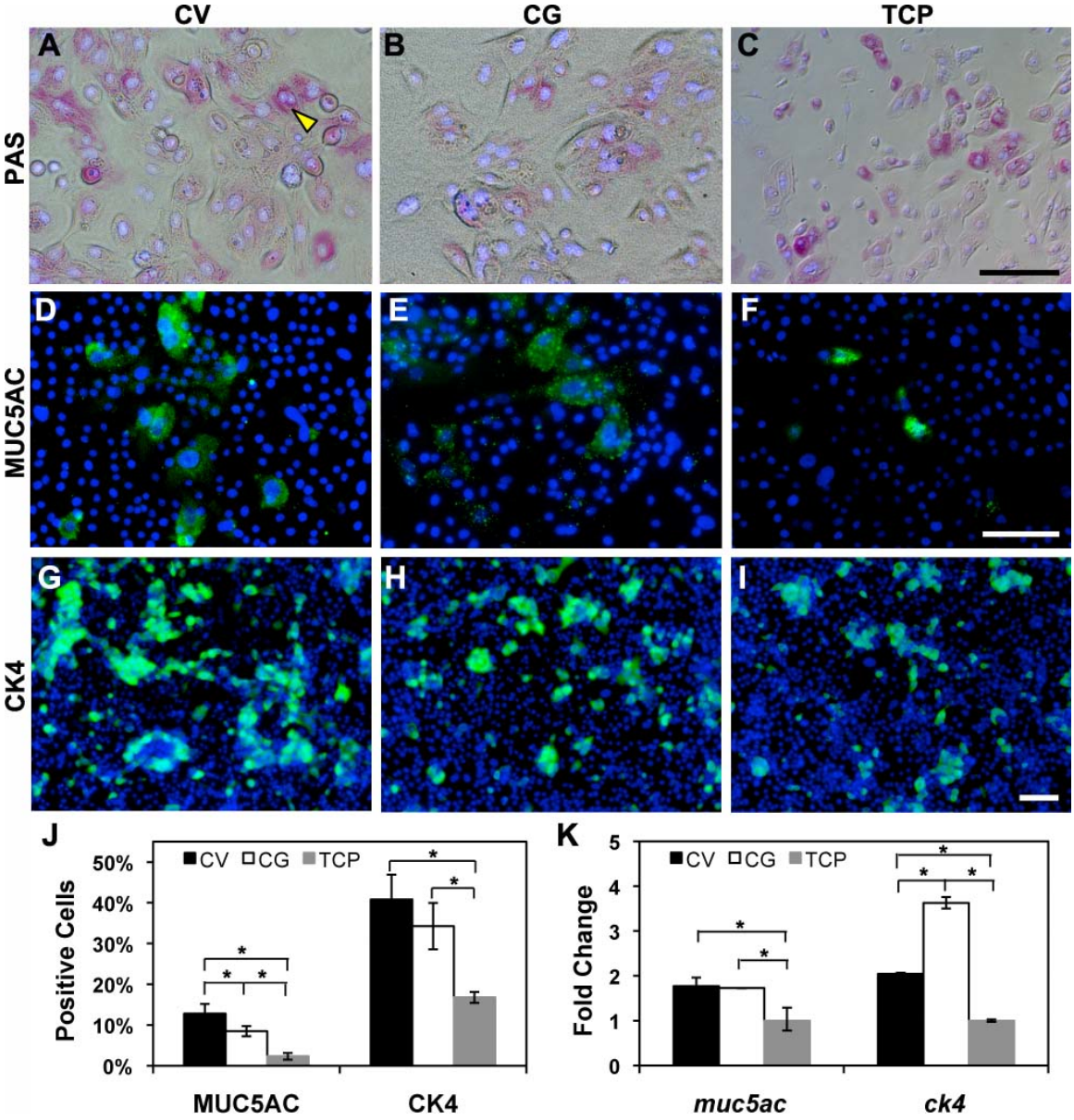

Figure 3.4. rCjEC phenotypic analysis in vitro.

rCjECs were cultured on 3 substrates, CV, CG and TCP. (A-C) Mucins were detected by PAS staining (goblet cells were indicated by the arrowhead). (D-I) Immunocytochemistry was performed to visualize conjunctival epithelial specific markers: (D-F) MUC5AC for goblet cells; (G-I) CK4 for non-goblet epithelium. (J) Percent of positively stained cells in MUC5AC and CK4 immunostaining, analyzed by ImageJ software. (K) RT-qPCR analysis of the expression of conjunctival epithelial specific genes. Scale bar: 100 μm.

RT-qPCR was also conducted to characterize gene expression of rCjEC cultured on the three substrates (Figure 3.4K). Cells grown on CV exhibited a 2.0- and 1.8-fold increase in *ck4* and *muc5ac* transcripts in comparison to TCP, respectively. There was no significant difference in *muc5ac* expression of cells grown on CV and CG. However, *ck4* expression was higher in cells grown on CG than those on CV.

3.3.3. Reconstruction of conjunctival defect using CV

We attempted to reconstruct conjunctival defects by transplanting the CV conjunctival equivalent in a rabbit model. The 7.5-mm wound involved injury to all three parts (bulbar, tarsal and forniceal) of the conjunctiva (Figure 3.5A). The defect was grafted with CV (with or without cells, Figure 3.5B) by sutures. Re-epithelialization started at 1 week in all groups, including the negative control (Figure 3.5C, F and I). After 2 weeks, the CV membranes turned opaque and began to degrade, but still remained intact on the defects (Figure 3.5D, G); while there was early sign of wound contracture in the negative control (Figure 3.5I, J), it was not observed in the two treated groups. By the end of 4 weeks, healing was finished in all three groups and the CV membranes were completely degraded in the treated groups. The negative control showed obvious conjunctival shortening in the defect area (Figure 3.5E, H and K). Furthermore, forniceal length was measured and compared between groups as a quantitative indication of wound contracture (Figure 3.5L, M). The negative control group showed significant conjunctival contraction with fornix shortening of 21.1% at 2 weeks and 35.5% at 4 weeks, respectively. By contrast, neither of the CV treatments exhibited significant change in forniceal depth when comparing pre-surgery and post-transplantation values.

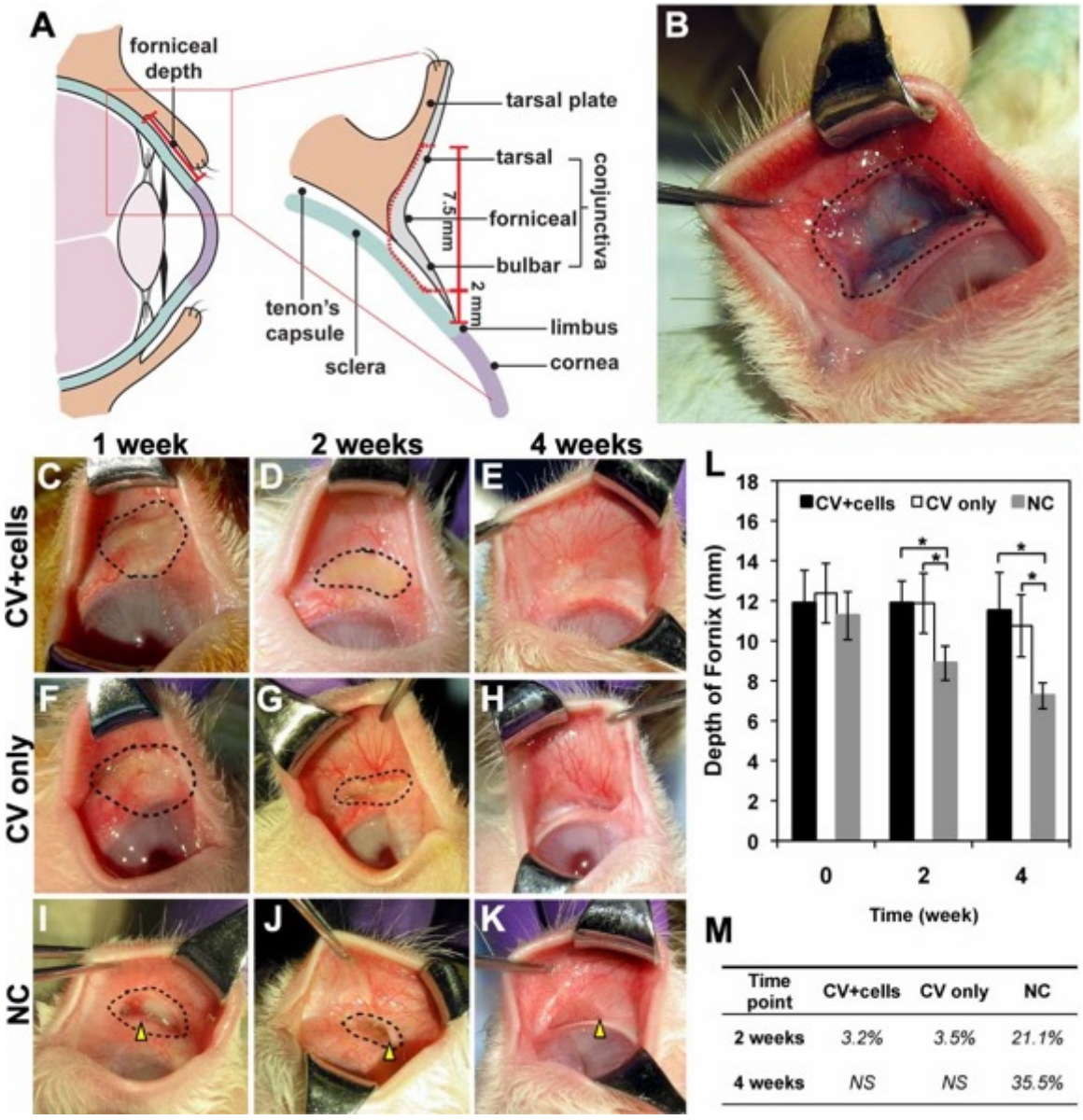

Time point	CV+cells	CV only	NC
2 weeks	*3.2%*	*3.5%*	*21.1%*
4 weeks	*NS*	*NS*	*35.5%*

Figure 3.5. Macro-inspection of conjunctival reconstruction using CV in a rabbit model.

(A) Illustration of the defect model: the superior forniceal depth was measured starting from the fornix to the limbus; a close-up look of the defect model with the upper eyelid extended. The defect was 7.5 mm in diameter and at least 2 mm from the limbus; all layers above the red dashed line were removed. (B) A photo taken right after grafting CV (with alamarBlue® dye) on the conjunctival defect with sutures. (C-K) Gross images showing the progress of conjunctival repair in the two treatment groups plus control at various time points. (L) Depth of fornices after surgery at various time points in the two treatment groups plus control. (M) Shortening of the fornix (%) after introducing the defect. The edges of the defect were outlined by the black dashed line; wound contracture in the NC group was indicated by yellow arrowheads (NC, negative control; NS, not significant).

3.3.4. Assessment of the repaired conjunctival tissue

The outcomes of conjunctival defects repaired by CV were evaluated by histological staining and compared to both positive (no defect) and negative (defect without repairs) controls. H&E staining after 4 weeks shows complete re-epithelization (continuous epithelia) in all groups (Figure 3.6A-D). The two groups treated with transplanted CV membranes (with and without epithelial cells) both showed three-to-seven stratified epithelial layers with distinct cuboidal basal cells, very similar to normal conjunctival epithelium. PAS staining was used to visualize mucin distribution (Figure 3.6E-H). Strong PAS-positive staining, representing conjunctival goblet cells, was found in these stratified epithelial layers, and the amount of stained mucins was also comparable to that present in the positive control. There were fewer epithelial layers in the negative control and the cells had a flattened morphology with very few of them stained strongly with PAS.

To further visualize the conjunctival stroma fibrillar organization, MT staining was performed (Figure 3.6I-L). In both treated groups, collagen networks composed of random aligned fibrils and loosely packed fibroblasts were found in the reconstructed substantia propria, resembling the uninjured normal tissue. In contrast, mature subepithelial fibrous scar tissue was identified in the untreated wound by the high density of aligned collagen fibrils (stained blue, Figure 3.6L, asterisk).

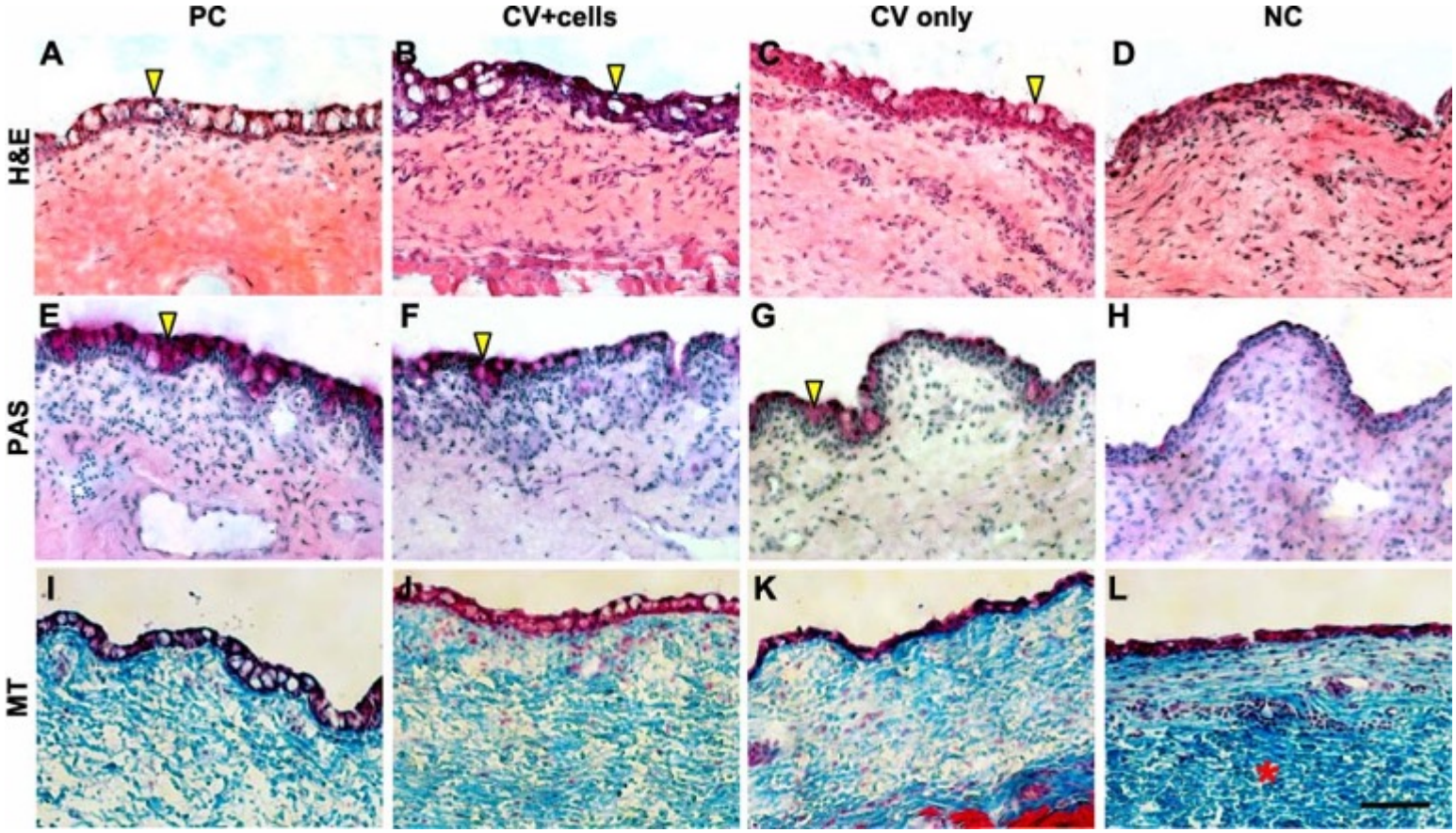

Figure 3.6. Histological analysis of conjunctival defect reconstruction.

(A-D) H&E staining. (E-H) PAS staining, showing the mucin distribution in the repaired epithelium. Goblet cells are shown by arrowhead. (I-L) Masson's trichrome staining for the visualization of collagen fibrils; scar tissue (asterisk) was observed only in the negative control (NC; PC, positive control). Scale bar: 100 μm.

The presence of goblet cells and the phenotypes of reconstructed epithelium were further proven by immunohistochemistry. The staining of CK4, a conjunctival specific cytokeratin, suggested a continuous epithelium in all groups (Figure 3.7A-D). MUC5AC staining recognized the specific secretory conjunctival mucin (5AC subtype), and selectively stained goblet cells. Examination of MUC5AC staining in the defect site after transplantation revealed a significant difference in goblet cell percentages (Figure 3.7E-H) among the groups. The defect site grafted with CV+cells was densely repopulated by MUC5AC-positive goblet cells (23%), comparable to uninjured tissue (30%), and some mucins might have even been secreted outside the epithelium. On the contrary, goblet cells were nearly absent (less than 5%) in the defect site of the CV only treated group and the negative control (4%).

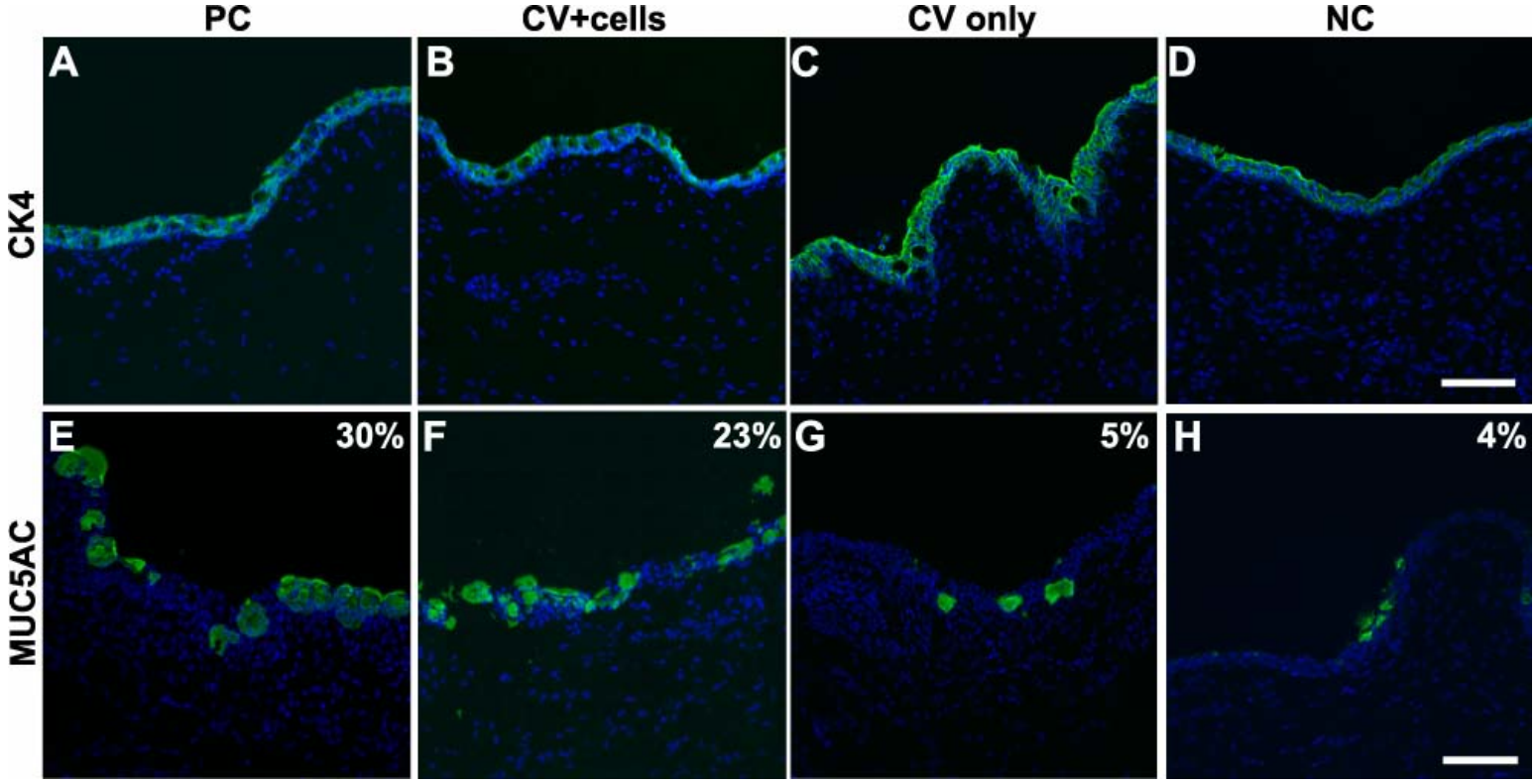

Figure 3.7. Immunohistochemistry analysis of reconstructed conjunctiva.

(A-D) CK4 staining showing the thickness and continuity of the epithelium. (E-H) MUC5AC staining for goblet cells; the numbers in upper right corners are the percent of positively stained cells (MUC5AC positive cells divided by total number of cells in the epithelium). Scale bar: 100 μm.

3.3.5. Survival and integration of transplanted cells in the defect

In our *in vivo* study, male rabbit cells were intentionally delivered to female hosts, enabling us to monitor the transplanted cells with PCR by detecting the *sry* gene, specific to the Y chromosome. Four weeks post-transplantation, the reconstructed conjunctival tissue in the CV + cells treated group was dissected and subject to conventional PCR for the detection of *sry*. Nested PCR primers were later designed to further amplify the product and ensure specificity (Figure 3.8A). As confirmed by Figure S3.8B, the treated group (CV+cells) was positive for the *sry* gene, as compared to the positive (DNA from male rabbit tissue) and negative (DNA from female rabbit tissue) controls.

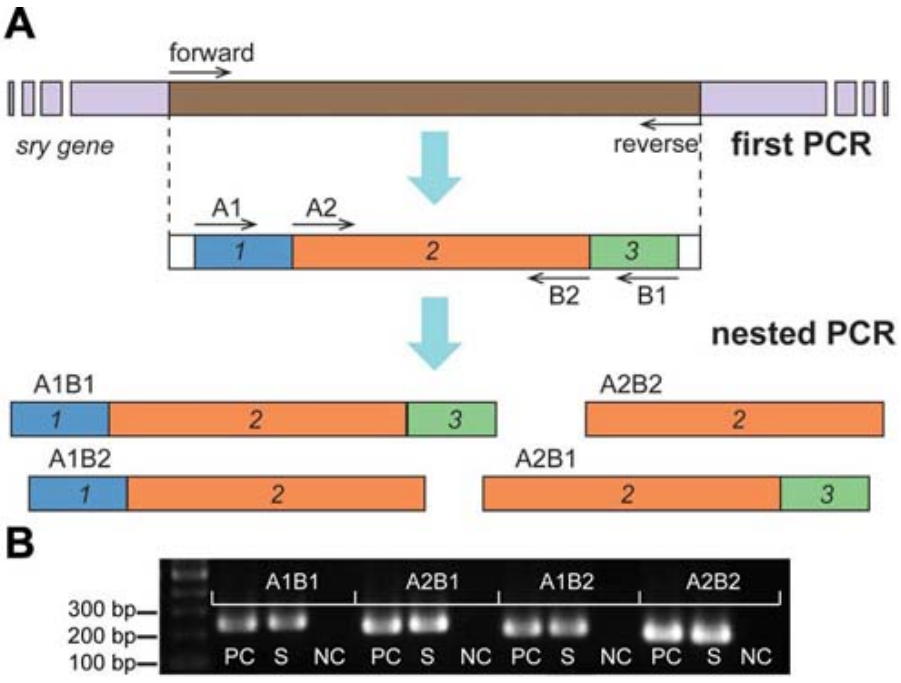

Figure 3.8. Post-transplantation cell integration in the conjunctival defect, detected by nested PCR.

(A) Design of nested PCR for the detection of the sry gene (male cells): conventional PCR was first performed, followed by nested PCR, using 4 primers (A1, A2, B1 and B2). (B) Agarose DNA gel confirmed the presence of the sry gene in the CV+cells treated sample (PC – positive control; S – sample; NC – negative control).

3.4. DISCUSSION

The conjunctiva is an important functional and structural component of the ocular surface. Conjunctiva-related diseases and injuries will compromise the homeostasis and functionality of the ocular surface, and, in severe conditions, tissue-engineering strategies must be applied for optimal reconstruction to prevent severe morbidities or even blindness. An ideal conjunctival equivalent should meet several criteria: sufficiently elastic and well tolerated without causing inflammation or stimulating rejection; it should carry an epithelium with the distinctive goblet cell phenotype for better mucin production and secretion, as many ocular surface disorders are associated with mucin-deficient dry eye diseases (*9*). Here, we reported the development of a conjunctival equivalent composed of CV and an epithelial layer for the treatment of ocular surface disorders involving conjunctival defects.

Cell differentiation and tissue development largely depend on the surrounding niche. To achieve optimal outcomes in the tissue engineering process, the applied biomaterials should imitate the properties of the native tissue (*46*). CV is a type I collagen membrane, formed through a three-step procedure (gelation, vitrification and rehydration). Its mechanical and optical properties can be easily controlled by changing the vitrification parameters (time, temperature and humidity). Considering ocular surface application, Calderón-Colón et al. (2012) found that CV synthesized at 40 °C and 40% RH for one week had the best properties, i.e., transmittance of up to 90%, tensile strength up to 12 MPa and a denaturing temperature significantly higher than 37 °C (*28*). On the nanoscale, the vitrification process results in a dramatic increase in fibrillar density and stiffness. As a cell culture substrate, it

has been shown that the unique nanoarchitecture of CV could maintain the characteristics of corneal keratocytes even in serum-based medium (*30*). In our study, two types of collagen materials were compared: the optimized CV and normal CG to investigate the effect of the materials' nanoarchitecture on the cultivation of conjunctival epithelium. TEM images (Figure 3.2D, E) revealed significant differences in the organization of collagen fibrils between the two materials. With the optimized vitrification process, the collagen fibrils in CV were much more densely packed and organized compared to those in CG, although the fibrillar diameter and D-periodicity remain unaltered for the two collagen materials (*30*).

One of the most important functions of the conjunctiva is mucin production and secretion, mainly fulfilled by goblet cells. Therefore, the number and secretory level of goblet cells are crucial indications of the epithelium's functionality. Previously, it was commonly accepted that conjunctival epithelium cultivated *in vitro* cannot develop the unique goblet cell phenotype, even when cultured on a supporting substrate. For example, when AM was used, the epithelium could proliferate, but without goblet cells, despite adding retinoic acid, lifting the culture to the air-medium interface or co-culturing with fibroblasts on the stromal side of AM (*52, 53*). However, our results proved that CV membrane successfully supported the growth and phenotypic development of rCjECs, as shown in Figures 2 and 3, including goblet cells. The epithelium formed on top of CV could express markers of both non-goblet epithelial (CK4) and goblet (MUC5AC) cells detected by gene expression and immunocytochemical analyses. The CG group also showed an improvement in supporting rCjECs over TCP, but except the transient increase in *ck4* mRNA level, the effect was not as profound as CV. The beneficial effect of CV in supporting cell culture could be attributed to its highly organized and dense fibrillar structure, which closely mimics the

extracellular matrix (ECM) in native connective tissue. Our *in vitro* model justifies the feasibility of utilizing CV as a carrier for conjunctival epithelium transplantation.

Different types of tissue substitutes have been developed and studied as conjunctival equivalents for transplantation. These include autografts from healthy conjunctiva, oral mucous membrane and nasal turbinate mucosa, human AM and synthetic materials. The application of an autograft is restricted to the regeneration of a small, unilateral conjunctival defect, as the size of an available donor site could be very limited and insufficient. Human AM, initially used to promote wound healing, is the most widely accepted substrate for the repair of ocular surface defects and has been reported to be used for reconstruction following different conditions, including chemical or thermal burns, conjunctival tumors or recurrent pterygia (*9, 18*). It could promote rapid epithelialization, reduce inflammation and vascularization, and also suppress fibrosis (*15*). However, certain drawbacks still exist for AM transplantation. Generally speaking, the composition of AM may vary because of donor differences, which influence clinical results after transplantation; furthermore, the mechanism of its beneficial effect is not extensively studied and well understood (*20*). In addition, there is a donor-associated risk of transmitting infections because only limited disease screening tests are performed before AM is harvested. Specifically, although numerous AM products are now available for ocular surface application, the preparation procedure is not standardized. Researchers are still looking for the optimal processing method for AM without affecting its physical and biological properties (*17*).

The limitation of AM transplantation and advancements in tissue engineering techniques have inspired scientists to develop synthetic and biomaterial matrices for ocular surface repair. Synthetic substrates, such as PLGA (*22*) and poly(ε-caprolactone) (PCL) (*23*), and

natural biomolecules, such as collagen (*24*) and keratin (*25*), were investigated and tested in animal models for conjunctival regeneration. Although positive outcomes were reported, none of the existing biomaterials could meet all the criteria of an optimal substrate for ocular surface reconstruction. The PLGA and collagen sponges have a randomly porous structure favored for cell infiltration and regeneration, but they are neither elastic nor transparent and are not suitable for carrying an epithelial layer. Keratin film has good mechanical properties, but it is too stiff for ocular surface use and the phenotypic development of epithelial cells on a keratin substrate remains unknown. PCL membrane was shown to be thin and elastic, and a conjunctival equivalent was created *in vitro*; however, it may be difficult to integrate into the host tissue and its aligned fibrillar structure may induce scar formation. CV, however, exhibits superior properties over other available biomaterials for ocular surface application because of its mature fibrillar structure resulting from controlled vitrification. Transparent and elastic CV membrane can be made with customizable dimensions, and is easy to manipulate and fixate with forceps and sutures. In our animal study, CV manufactured under optimized conditions was grafted onto the conjunctival defect either on its own or as a carrier for epithelial cells. In both cases, CV showed good biocompatibility and it was completely degraded at the end of the healing process.

Many ocular surface diseases involving conjunctiva are accompanied by decreased goblet cell number and/or lowered MUC5AC secretion level (*8*). After severe injuries or surgical trauma to the conjunctiva, although re-epithelization usually starts spontaneously, the repopulation of goblet cells cannot happen effectively unless an appropriate graft is applied to aid the healing process (*22*). Our present study shows that there is no significant difference between CV and CV with cells in promoting wound healing and re-epithelization;

both treated groups resulted in intact and stratified conjunctival epithelium within the area of the wound. However, evidence from histology and immunohistochemistry assays (Figures 5 and 6) confirmed that the graft of CV with cells led to the best result and the greatest number of re-populated goblet cells. Strong PAS and MUC5AC staining could be observed in the reconstructed area only when cells were transplanted together with CV, and the level of staining for both was comparable to that of uninjured conjunctiva.

Furthermore, by detecting the expression of the *sry* gene (Figure 3.8), we proved that transplanted male donor cells survived and integrated into the female host. The absence of goblet cells at the defect site in the CV only and negative control groups suggests that in the cell treatment group the re-populated goblet cells were primarily derived from transplanted cells rather than being of endogenous origin. The CV carrier has protected transplanted goblet cells within a hostile defect environment for better survival. Previous attempts at reconstruction in different models utilized AM as the epithelium carrier in treating limbal stem cell deficiency (*54*) or conjunctival defect (*55*); however, neither epithelial equivalent could confirm the presence of goblet cells. Thus, here, we demonstrate that CV membrane seeded with epithelial cells can help the phenotypic development of goblet cells *in vivo* during conjunctival regeneration.

Anatomically, the surface area of conjunctiva exceeds the area of contact with the eyeball and eyelids. This excess tissue folds in the fornix, the junction of bulbar and tarsal conjunctiva, ensuring the restriction-free excursion of the eye (*10*). Biopsy studies also pointed out that the fornix has the greatest density of goblet cells (*56*). During spontaneous wound healing, re-epithelialization is followed by formation of a subconjunctival fibrous scar, wound contracture and eventually fornix shortening. The fibrous scar occurs as a result of

the uniaxial arrangement of newly synthesized collagen fibers by fibroblasts in the wound bed, which differs from the random alignment in normal subconjunctival stromal tissue (*22*). The amount of scarring that the conjunctiva undergoes can have severe consequences on the movement and function of the eye and may ultimately cause visual impairment (*10*). Grafting of a matrix with randomly aligned fibrils could effectively prevent the formation of both aligned ECM fibrils and myofibroblast differentiation, helping to re-establish the normal fornix (*22, 24*). Similarly, transplantation of CV resulted in significant inhibition of forniceal shortening (less than 4% shortening for both treated groups). Histologically, a loose network of collagen fibrils and fibroblasts in the reconstructed subconjunctival stroma resembles that in normal tissue, while the untreated wound has severe sign of fibrous tissue, indicated by the condensed, aligned collagen fibrils (Figure 3.6L).

This study has extended the application of CV further to parts of the ocular surface other than the cornea. Previous studies have already demonstrated that CV could be used to expand numerous types of corneal cells. Therefore, with our results, we can hypothesize that CV tissue equivalent could be applied when injuries involve more than one part on the ocular surface. Except for the re-population of goblet cells, the difference between CV only and CV with cells are not quite significant. The reason could be due to the design of the conjunctival defect model, which involves only surgical injury. In this case, re-epithelization occurs very rapidly in rabbits. However, in clinical cases, ocular surface injuries often are not restricted to one region and are usually associated with other complications, such as limbal stem cell deficiency and dry eye diseases. In the latter cases, expansion of harvested cells is necessary before transplantation. Therefore, CV with an expanded epithelial

cell layer may be more promising in these complex clinical injuries. In the future, the application of CV on ocular surface defect models involving more complicated conditions should be investigated before clinical studies are carried out.

3.5. CONCLUSIONS

Our work proves the efficacy of utilizing CV to create a transplantable conjunctival equivalent to repair defects resulting from surgical trauma, severe burns or other injuries or diseases. Unlike previous attempts using other materials, because of the unique collagen fibrillar structure of CV, considerable numbers of goblet cells were present on the membrane before transplantation and in the reconstructed defect area, as well. We were able to limit the amount of contraction and fibrosis scarring to the minimum without compromising the re-epithelization process. Therefore, CV holds great potential clinically as a carrier for epithelial cell transplantation for the reconstruction of ocular surface injuries.

Chapter 4. An *In Vitro* Model for the Ocular Surface and Tear Film System[3]

4.1. INTRODUCTION

The ocular surface is the outermost layer of the eye. Together with the tear film, it protects the refractive surface and enables sharp vision (*57*). This ocular surface and tear film system is comprised of corneal and conjunctival epithelia, as well as many tear-secreting glands, such as lacrimal and meibomian glands (*58*). They are functionally linked as one system by continuous epithelia, innervation, and the immune system (*1*). The tear film is divided into three layers: mucin, aqueous, and lipids. It lubricates the eye surface, protects it against foreign pathogens and infections, and closely interacts with ocular surface epithelial cells through the mucin-aqueous layers (*59*). The ocular surface and tear film system is a highly dynamic structure. The maintenance of its stability is essential to healthy vision. Even minor disruptions can result in significant permanent damage to other parts of the visual-sensory system (*57*).

Dry eye is a common ocular surface disease involving dysfunction of the tear film that affects millions of people worldwide, with a significant impact on the quality of life (*58*)

[3] This chapter contains material modified from the following manuscript, previously submitted as:
Q Lu, H Yin, MP Grant and JH Elisseeff (2017). An *In Vitro* Model for the Ocular Surface and Tear Film System. *Scientific Reports* under review.

Although the exact pathogenesis is not completely understood, it is widely believed that the development and progression of dry eye is mediated by cellular inflammatory molecules secreted by the ocular surface immune system (*60*). When the ocular surface is exposed to environmental stress that causes changes in tear composition, an inflammatory cascade is activated in which various cytokines and chemokines are released (*61*). This results in the migration of antigen presenting cells, and subsequently the infiltration of helper T cells (subtypes TH1 and TH17) to the ocular surface. During this time more cytokines and chemokines are secreted, and the epithelia are consequently damaged (*60, 61*). To learn more about the molecular basis of dry eye, disease pathogenesis study and potential therapeutic evaluation have been conducted either in vivo or on simple models *in vitro* (*33, 34*).

Tissue models and organ-on-a-chip strategies combine multiple cell types to create miniaturized versions of physiologically active and functional tissues in the body. Numerous organ systems, such as lung, intestine, and bone marrow, have been successfully fabricated and utilized in various disease conditions (*37, 39, 42*). Specifically, a complex disease system was induced in a lung-on-a-chip microdevice, leading to the discovery of a potential new drug for pulmonary edema (*62*). Numerous in vitro models have been established in the past few years to mimic different parts of the ocular system. Mature retina was generated from human induced pluripotent stem cells (hiPSCs) with fully functional photoreceptors to recapitulate retinal development. This system was applied to model retinal dysfunction, including age-related macular degeneration (*63*). Coculture of retinal pigment epithelium (RPE) and photoreceptors has been attempted to further mimic normal differentiation and morphology (*64*). Moreover, Chan KY, et al. manufactured a microfluidic

chip to study the intraocular emulsification of silicone oil (*65*). An in vitro corneal model was developed on a sacrificial collagen film across microfluidic channels, presenting an alternative for the screening of ocular irritants (*66*).

Considering the ocular surface and tear film, researchers have been investigating the *in vitro* modeling of several components individually, including conjunctival epithelium (*43*) and lacrimal glands (*67, 68*). In these models, cell morphology and phenotype resembled the equivalent cells *in vivo*. However, combining these cells types to create a functional tear film has not been studied. To address this gap, we developed a complex three-dimensional (3D) *in vitro* model for the ocular surface. This model contains primary rabbit conjunctival epithelial cells and lacrimal gland cell spheroids, to recapitulate the aqueous and mucin layers of the tear film. We first investigated the culture conditions for both cell types to optimize their secretory functions. Next, we combined the two cell types and compared several coculture systems to optimize tissue structure and tear secretion. Inflammation was induced to mimic dry eye disease in the coculture model system, and its response to therapeutics was compared to monoculture. Overall, we engineered a model system for both a healthy and diseased ocular surface amenable to studying disease pathogenesis and therapeutic screening.

4.2. MATERIALS AND METHODS

4.2.1. Primary cell isolation

Young New Zealand white rabbit tissues (eyes and lacrimal glands) were purchased from Pel-Freez Biologicals (Rogers, AR).

Rabbit conjunctival epithelial cells (CECs) Rabbit eyes with eyelids attached were rinsed with DMEM/F12 (Dulbecco's Modified Eagle Medium/Nutrient Mixture F-12; Thermo Fisher Scientific, Waltham, MA) with 1% antibiotic-antimycotic solution (Thermo). The entire conjunctiva (including bulbar, fornix and palpebral) was dissected 1 mm from the glandular edge of the tarsal plate and 2 mm from the limbus, with excessive Tenon's tissue trimmed off. The tissue was digested with Dispase® II (1.2 U/mL, Roche Diagnostics, Indianapolis, IN) at 4°C overnight. The loosened epithelial aggregates were collected with a cell scraper, followed by centrifugation at 200 *g* for 5 minutes. The cell pellet was treated with Accutase® (Sigma-Aldrich, St Louis, MO) for 10 minutes at 37°C and filtered through a 100 μm cell strainer to obtain a single cell suspension.

In order to increase the density of goblet cells, the primary cell suspension was layered on a Percoll®/PBS (Sigma-Aldrich) density gradients which ranged from 18% to 57% (v/v; Figure 4.1A), and centrifuged for 10 minutes at 100 *g* with zero acceleration and deceleration. Based on the results of gene expression study (Figure 4.1B) of the cells from each layer, 30% Percoll/PBS was chosen for further study. The top, bottom cell layers (Figure 4.1A) and unseparated CECs were collected and seeded on tissue culture plates (TCP) pre-treated with FNC coating mix (AthenaES, Baltimore, MD) respectively, at a density of

2×10^4 cells/cm^2 and cultured at 37°C with 5% CO_2. Bronchial Epithelial Cell Growth Medium (BEGM™, with all supplements added; Lonza, Walkersville, MD) was changed every other day until cells reached confluence, in about 3-5 days.

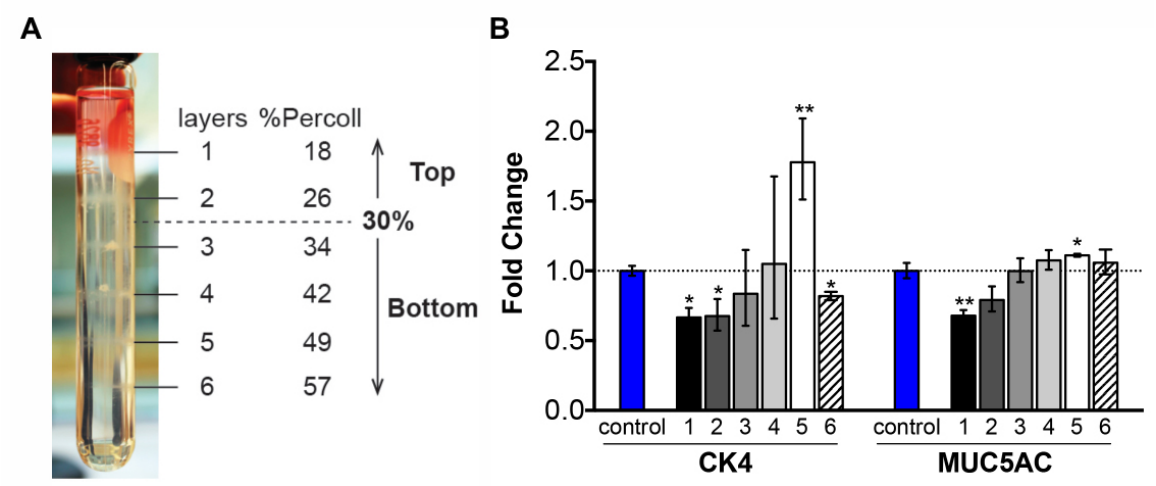

Figure 4.1. Separation of primary conjunctival epithelial cells by Percoll density gradient centrifugation.

(A) Primary conjunctival epithelial cells were subject to a Percoll density gradient and the centrifugation resulted in six cell populations; the percent (v/v) of Percoll in each layer was shown; (B) Phenotypic analysis of each cell population by gene expression (RT-qPCR); *$p < 0.05$; **$p < 0.001$.

Rabbit lacrimal gland acinar cells (LGACs) Primary LGAC isolation was carried out as previous described. Inferior lacrimal glands from young rabbits were rinsed with DMEM/F12 (with 1% antibiotics-antimycotics) and finely minced into small pieces in a petri dish. The procedure was similar as previously described (*69*). The minced tissues were digested with an enzyme cocktail containing collagenase (Worthington Biochemical, Lakewood, NJ), hyaluronidase (Sigma-Aldrich) and DNase I (Roche) for 30 minutes at 37°C with vigorous shaking. The cells were filtered through a 70 μm cell strainer and then subject to a Percoll® gradient to reduce fibroblast contamination.

4.2.2. Submerged and airlifting culture of CECs

Primary CECs were seeded on polyester Transwell® (Corning, Lowell, MA) membranes (0.4 μm pore size) at a density of 2×10^4 cells/cm^2 and cultured at 37°C with 5% CO_2. BEGM was added to both upper and lower compartments, and the inserts were kept at 37°C with 5% CO_2 until the cells reached confluence in about 3-5 days. Afterwards, medium was switched to a 1:1 mixture of BEGM and DMEM/F12 in order to induce stratification. Induction medium was added to both upper and lower compartments of the Transwell insert for submerged culture, while only the lower compartment had medium for airlifting culture, letting the cells on the membrane be exposed to air (Figure 4.2C). The induction was kept 1-2 weeks in the incubator at 37°C with 5% CO_2.

4.2.3. Spheroids formation and three-dimension (3D) culture of LGACs

Primary LGACs were suspended at a density of 1×10^7 cells/mL in HepatoStim Medium (HSM) supplemented with 10 μg/mL epidermal growth factor (EGF) and 10% fetal bovine serum (FBS, Thermo). The suspension was added to a non-treated tissue culture flask

(Thermo) to prevent adhesion, and placed on an orbital shaker at 100 rpm for 24 hours in the incubator (37°C, 5% CO_2). Cell spheroids were collected by centrifugation at 100 *g* for 5 minutes. The spheroids were resuspended with Matrigel® matrix (growth factor reduced; Corning; 10^8 cells/mL of Matrigel). The mixture was added to TCP to form a thin layer of gel (100 μL/cm^2) by incubating at 37°C for half an hour. HSM was changed every other day and images of spheroids encapsulated in Matrigel were taken using Axio Imager 2 inverted fluorescent microscope (Carl Zeiss, Jena, Germany). The number and size of LG cell spheroids were analyzed using ImageJ software (National Institute of Health, NIH, Bethesda, MD). The spheroids were kept encapsulated in Matrigel for 1-2 weeks in the incubator (37°C, 5% CO_2) until being harvested for analyses.

4.2.4. Coculture of CECs and LG cell spheroids

The coculture systems were demonstrated as in Figure 3a and 4a. LG cell spheroids were introduced into the system after CECs had been undergone airlifting culture for 5 days. Three different designs were utilized in this study. No contact model: a thin layer of Matrigel with encapsulated LG cell spheroids was added to the bottom well of the Transwell system. Indirect contact model: the LG cell spheroids was put on the other side of the insert membrane; therefore, the two types of cells were separated by the porous membrane. Direct contact model: Matrigel containing LG cell spheroids were layered on top of CECs on the periphery of the insert. All coculture systems were established in 12-well Transwell system, and 50 μL Matrigel was used in all coculture models. The seeding density for each cell type was the same as it was in monoculture. HSM medium was added to the lower compartment of the Transwell system only, and the cocultures were maintained for one to two weeks before harvest.

4.2.5. Induction of dry eye-like inflammation with interleukin 1 beta (IL-1β)

The direct contact coculture model was subject to IL-1β (Thermo) exposure, at a concentration of 10 ng/mL. The direct contact coculture model was constructed as described above, with the addition of IL-1β in the medium. Dexamethasone (Sigma) was used as a treatment for IL-1β-induced inflammation. The cultures were maintained for one weeks, and the response of the direct contact model to the exposure of IL-1β, dexamethasone and the two substances combined were analyzed. The results were also compared to monocultured samples under the same exposures.

4.2.6. Reverse transcription and real-time quantitative polymerase chain reaction (RT-qPCR)

RT-qPCR analysis was used to quantify the gene expression of CECs, LG cell spheroids and the cocultured cells. Total RNA was extracted and purified using RNeasy Mini Kit (Qiagen, Valencia, CA) and the RNA concentration was measured by NanoDrop 2000 (Thermo). cDNA synthesis was carried out with high capacity reverse transcription kit for RT-PCR (Thermo) according to the manufacturer's protocol. Real-time PCR was performed on the StepOnePlus™ Real-Time PCR System using SYBR® Green PCR Master Mix (Thermo). The relative expression level of all targets was calculated by the $\Delta\Delta C_T$ method (*50*) and normalized against the control samples with β-actin as the endogenous reference. A full list of primer sequences could be found in Table 4.1.

Table 4.1. Primer sequences for RT-qPCR

Gene			Sequence
conjunctiva specific	*CK4*	forward	CAA CCT GAA GAC CAC CAA GA
		reverse	CAG AGT CTG GCA CTG CTT T
	MUC5AC	forward	CGC CTT CTT CAA CAC CTT CA
		reverse	TGG GCA AAC TTC TCG TTC TC
lacrimal gland specific	*AQP5*	forward	CAA CGC GCT CAA CAA CAA
		reverse	GTG AGT CGG TGG AAG AGA AA
	LTF	forward	GAT GCC ATG ACC CTG GAT AG
		reverse	GTC TGT GGC TTC GCT TCT
	CDH1	forward	CAC CAT CGC CAT GAG TCT T
		reverse	GAA TAA CCC AGT CCC TCT TCT G
inflammatory	*IL-6*	forward	GAA TAA TGA GAC CTG CCT GCT
		reverse	TTC TTC GTC ACT CCT GAA CTT G
	IL-8	forward	TGG ACC TCA CTG TGC AAA T
		reverse	GCT CAG CCC TCT TCA AGA AT
	TNFα	forward	GTA GTA GCA AAC CCG CAA GT
		reverse	GGT TGT CCG TGA GCT TCA T
	MMP9	forward	AGT ACC GAG AGA AAG CCT ACT T
		reverse	TGC AGG ATG TCA AAG CTC AC
internal control	*B-actin*	forward	GCT ATT TGG CGC TGG ACT T
		reverse	GCG GCT CGT AGC TCT TCT C

4.2.7. Histology preparation and stainings

Both CECs cultured on TCP and Transwell membranes with cells (removed from the inserts with razor blades) were fixed with 4% paraformaldehyde (PFA; Electron Microscopy Sciences, Hatfield, PA) in PBS for 10 minutes at room temperature and washed three times with PBS. The Transwell samples were further dehydrated through ethanol gradients, cleared in xylenes, and embedded in paraffin. Sections of 5 μm thick were used for histological stainings. The samples were stained with Hematoxylin & eosin (H&E) and Periodic acid-Schiff (PAS) staining kits (Sigma-Aldrich) according to the manufacturer's manuals

to visualize the morphology and detect the distribution of mucosubstances, respectively. Images of stained samples were taken on the Axio Imager 2 fluorescent microscope (Carl Zeiss).

4.2.8. Immunohistochemistry

TCP and Transwell samples were first fixed with 4% PFA at room temperature for 10-20 minutes, followed by PBS rinse. F-actin was stained with alexa fluor® 647 phalloidin (Thermo) per manufacture's instruction and then the nuclei were counterstained with 1 μg/mL DAPI (4',6-diamidino-2-phenylindole dihydrochloride; Thermo) for 15 minutes. Staining with antibodies for the detection of specific antigens was performed as previously described (*21*). Anti-rabbit mucin 5AC, lysozyme and pan-cytokeratin monoclonal antibodies were purchased from Abcam (Cambridge, MA); Anti-rabbit cytokeratin 4 monoclonal antibody was purchased from Sigma-Aldrich. Axio Imager 2 fluorescent microscope (Carl Zeiss) and confocal laser scanning microscope 510 (LSM 510; Carl Zeiss) were used for imaging.

4.2.9. β-Hexosaminidase assay

The secretion ability of LG cell spheroids was assessed by the measurement of β-N-Acetyl-glucosaminidase (NAG), a lysosomal enzyme in the tear fluid secreted by lacrimal glands. The culture medium was replaced with DMEM/F12 and the cells were incubated at 37°C for 2 hours. Carbamylcholine chloride (carbachol, CCH; Sigma-Aldrich) was then added to the medium to a final concentration of 100 μM, and the samples were incubated for another 30 minutes. The media were collected and centrifuged at 200 *g* for 5 minutes. The resulting supernatants were analyzed for NAG catalytic activity with a NAG assay kit

(Sigma-Aldrich) per the protocol. The absorbance at 405 nm was measured using Synergy 2 microplate reader (BioTek, Winooski, VT). The total protein content in the samples was measured by Pierce BCA protein assay kit (Thermo) per the instruction.

4.2.10. Mucin layer visualization by confocal microscopy

The mucins secreted by air-lifted samples were visualized and semi-quantified by loading a small amount (20 μL per 12-well insert) texas red conjugated dextran solution (10 kDa MW, 2 mg/mL in PBS; Thermo) in the upper chamber of Transwell inserts. The Transwell cultures were gently rinsed with warm PBS to remove secreted mucins before the addition of texas red-dextran. The inserts were incubated for 24 hours to allow mucin secretion and then examined using confocal microscopy with Z-stack scanning by LSM 510. The serial images were analyzed and stacked to generate 3D images for the measurement of mucin layer thin film with ZEN imaging software (Carl Zeiss) and ImageJ (NIH).

4.2.11. Permeability tests with Dextran

The function of CEC tight junctions was assessed by dextran permeability test. Texas red-dextran (10 kDa; 10 mg/mL in PBS) was used in the study. Before the test, medium in the lower compartment in the Transwell was switched to serum free DMEM/F12; medium in the insert in submerged cultures was aspirated. Dextran solution was added in the insert and the Transwell cultures were incubated at 37°C, 5% CO_2 for 30 minutes. The concentration of texas red-dextran in both upper and lower compartments was calculated by measuring the fluorescence on Synergy 2 microplate reader (excitation: 520 nm; emission: 590

nm). A serial concentration of texas red-dextran solution was made to construct the standard curve. Data was presented as percentage of dextran molecules that had diffused through the insert membrane.

4.2.12. Statistical analysis

Experiments were run by at least triplets, and results are presented as mean values ± standard deviation (SD). Data analysis was performed by GraphPad Prism, and the variance was analyzed by one-way ANOVA with post-hoc Tukey HSD for multiple comparison. Generally, a *P* value less than 0.05 was considered to be statistically significant.

4.3. RESULTS

4.3.1. Goblet cell enrichment and air-lifting culture of CECs

Primary rabbit CECs were isolated from rabbit conjunctival tissues. Goblet cells were enriched using a Percoll gradient where six different layers were tested (Figure 4.1A). Cells in layers 1 and 2 expressed significantly lower levels of *cytokeratin 4* (*CK4*) and *mucin 5AC* (*MUC5AC*) compared to the cell population before Percoll separation (Figure 4.1B). Therefore, 30% Percoll/PBS solution was selected for goblet cell enrichment for all subsequent studies, and the three cell populations were named as top, bottom (enriched), and control (unseparated) (Figure 4.1A). In general, the enriched CECs expressed significantly more *CK4* and *MUC5AC* mRNAs than the control, while the top layer had much less expression of *CK4* (< 0.3-fold), and expression of *MUC5AC* was undetectable (Figure 4.2A).

Enriched CECs also expressed more epithelial markers in culture and secreted more mucosubstance when compared to unseparated control, as confirmed by CK4, PAS, and MUC5AC stainings, respectively (Figure 4.2B).

Airlifting culture was compared to submerged culture to optimize the mucin secretion by CECs *in vitro* (Figure 4.2C). After one week of airlifting, CECs stratified into 5-6 layers of epithelial cells, while submerged culture had less than two layers of cells (Figure 4.2D). Immunohistochemistry for CK4 and MUC5AC (Figure 4.2F) confirmed improved epithelial and goblet cell differentiation as well. Airlifting also significantly benefited the mucin secretion of CECs. Three-dimensional confocal *z*-scanning of the mucin layer, stained by Texas Red-dextran, confirmed that airlifting resulted in a thicker and more continuous extracellular mucin secretion (Figure 4.2G). The side view of the confocal *z*-scanning indicated an overall thicker mucin layer (50.0 ± 5.0 μm for airlifting culture and 15.0 ± 1.7 μm for submerged culture). Though *CK4* expression was the same in both cultures, airlifting culture significantly increase the mRNA level of *MUC5AC* (Figure 4.2E).

.

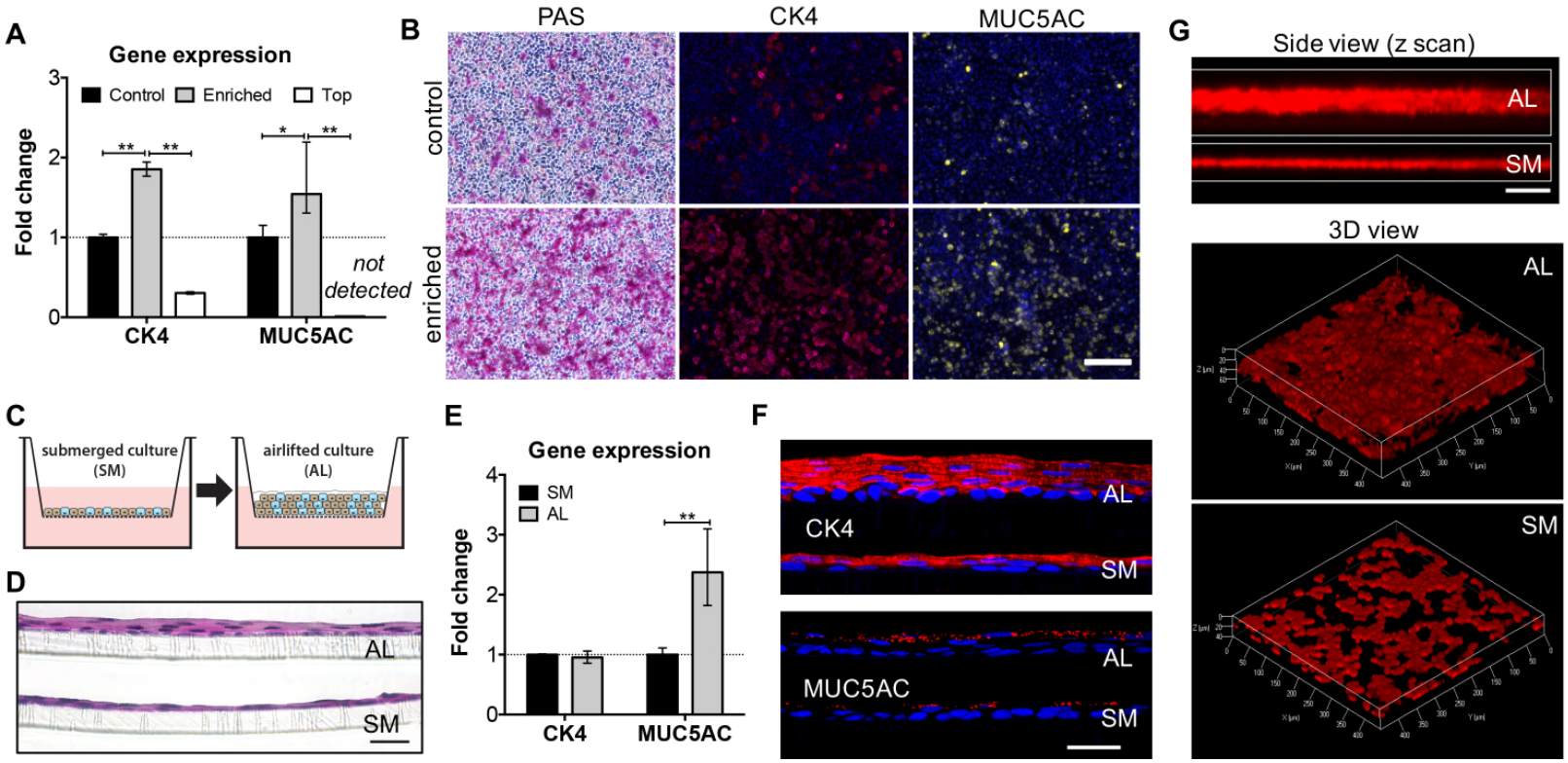

Figure 4.2. Goblet cell enrichment and airlifting culture of conjunctival epithelial cells (CECs).

(A) Gene expression (RT-qPCR; fold change is expressed as $2^{-\Delta\Delta CT}$) of CECs before (control) and after goblet cell enrichment. CECs were separated into two populations after Percoll gradient separation – top and bottom (enriched). (B) Stainings (PAS, CK4 and MUC5AC immunostainings) comparing the phenotypes of CECs with or without goblet cell enrichment. Scale bar 200 μm. (C) The schematics for airlifting (AL) and submerged (SM) cultures of CECs based on Transwell insert. H&E staining (D) and RT-qPCR (E) comparing CECs under AL and SM culture. Scale bar 100 μm. (F) IHC (top: CK4; bottom: MUC5AC) showing the difference in cell phenotypes between AL and SM cultures. Scale bar 50 μm (G) Mucin secretion (stained by Texas red labeled dextran) visualized by confocal microscope (z scan). Both side view and 3D views are shown. Scale bar 100 μm. *$p < 0.05$; **$p < 0.001$.

4.3.2. The formation and development of 3D LG cell spheroids in Matrigel

Primary rabbit LGACs spontaneously formed spheroids after 24 hours on the orbital shaker, and the average diameter of the spheroids was 124 ± 19 μm (Figure 4.3). The spheroids underwent structural development in Matrigel to produce glandular tissue. After encapsulation, the LG cell aggregates formed spheroids at day two (Figure 4.4A), and continued to develop into multi-branched organoids by day five (Figure 4.4B). Phalloidin staining revealed formation of hollow cavities inside the spheroids (Figure 4.4C). By day 5, each spheroid further developed multiple acinus-like compartments (Figure 4.4D). The LG cell spheroids stained positive for both epithelial maker pan-cytokeratin (PCK, Figure 4.4E) and lysozyme (LYZ, Figure 4.4F).

Next, the function of LG cells in 2D monolayer or 3D spheroids in Matrigel matrix was compared (Figure 4.4G). Three-dimensional culture influenced tear film secretion on the transcriptional level. The genes aquaporin 5 (*AQP5*) and lactoferrin (*LTF*) increased 4- and 2.5-fold, respectively, in the 3D culture (Figure 4.4H). Media supernatants and cell lysates were collected to measure the concentration of active lysozyme in the tear film secreted by the lacrimal glands. The cell lysate of LG cells cultured in 2D monolayer had a higher level of active lysozyme, but the lysozyme concentration in the supernatant of 3D spheroid cultures was more than eight times than that of 2D culture (0.0017 vs 0.0002; Figure 4.4I).

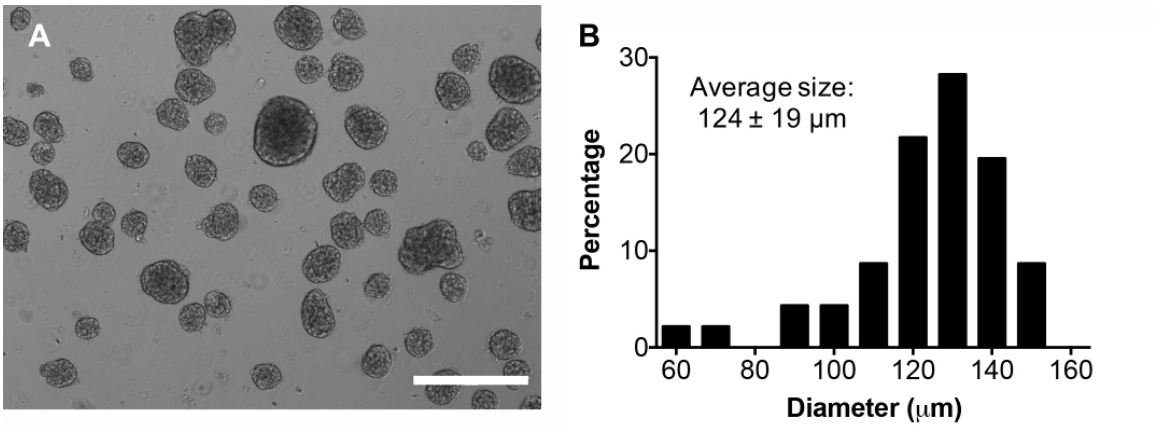

Figure 4.3. Size distribution of lacrimal gland spheroids.

(A) A typical image of lacrimal gland spheroids. Five similar images were used for size analysis by Image J) Scale bar 400 μm. (B) Size distribution histogram of lacrimal gland spheroids. The average size is 124 ± 19 μm.

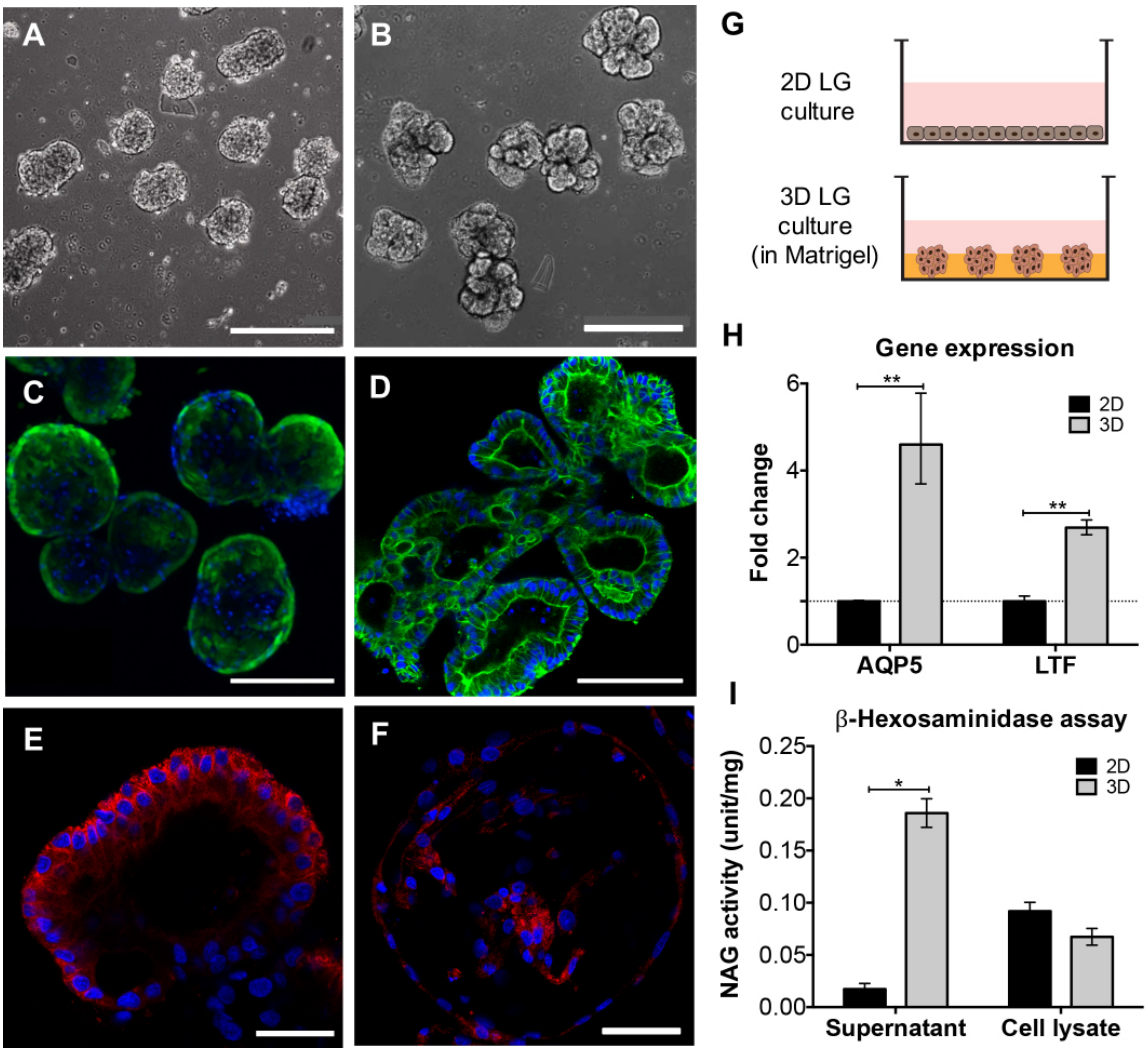

Figure 4.4. 3D lacrimal gland (LG) cell spheroids formation and culture.

(A) Schematics of LG cultured as either 2D monolayer or 3D spheroids embedded in Matrigel. (B) Gene expression (RT-qPCR; fold change is expressed as $2^{-\Delta\Delta CT}$) and (C) β-hexosaminidase assay comparing LG cells culture under 2D and 3D conditions. Both supernatant and cell lysate were collected for hexosaminidase assay and the value (units) was normalized to total protein content (mg). (D-G) Phase contrast and F-actin staining (Phalloidin) images of LG spheroids in Matrigel at different stages. (D,F) day 1; (E,G) day 5. (H,I) IHC showing the expression of LG specific markers. (H) Pan-cytokeratin; (I) lysozyme. Scale bar: 100 μm (D,E); 50 μm (F-I). *$p < 0.05$; **$p < 0.001$.

4.3.3. Coculture of airlifted CECs and LG cell spheroids

Airlifted CECs and LG cell spheroids were cultured together to study the effect of coculture on tear secretion and gene expression. Stratified CECs were on the upper compartment and encapsulated LG cell spheroids were on the lower compartment. The two monoculture groups were composed of either the LG cell spheroids, or air-lifted CECs (Figure 4.5A). By day 10, air-lifted CECs under both coculture and monoculture conditions secreted a continuous layer of extracellular mucins. The average thickness of mucin film secreted by cocultured CECs was 45.8 ± 5.3 μm, as compared to 30.0 ± 5.0 secreted by monocultured CECs (Figure 4.5D). The media supernatants and LG cell lysates were collected for the measurement of lysozyme concentration. At day four, cocultured LG cell spheroids secreted more than 10 times the amount of active lysozyme into the media supernatant compared to monocultured LG cell spheroids; however, this difference decreased at day 10 (Figure 4.5E). Regarding the cell lysates, coculture was beneficial for lysozyme synthesis at day 4; however, monocultured LG cells contained more NAG than cocultured cells at day 10. Regarding gene expression, the cocultured group reported elevated level of *CDH1* and *MUC5AC* at day four, and *LTF* and *CK4* at day 10 (Figure 4.5B,C). Gene expression values are normalized to cells cultured in monolayer.

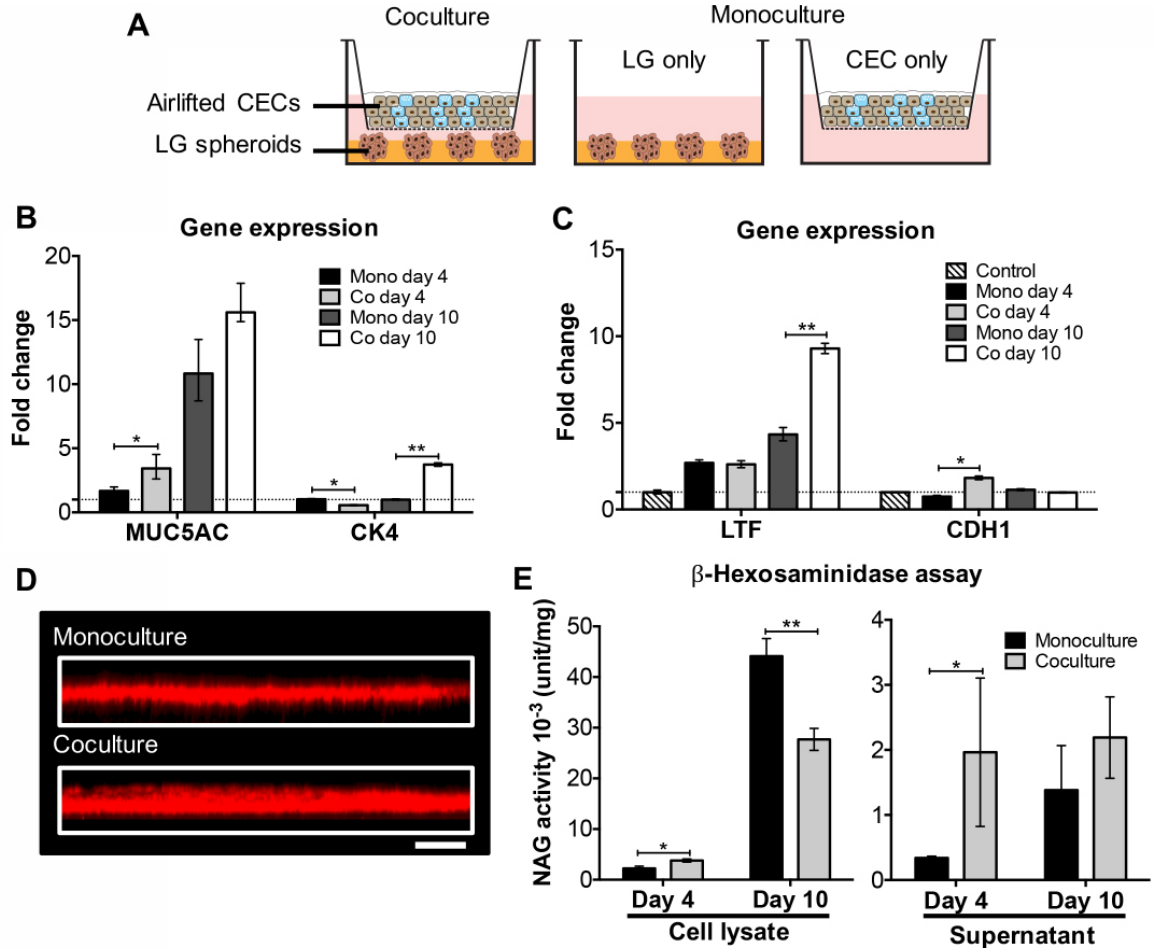

Figure 4.5. Coculture of conjunctival epithelium and lacrimal glands.

(A) Schematics showing the setup of coculture in the Tranwell system. Airlifted CECs cultured on the insert was combined with LG/Matrigel in the lower compartment to achieve coculture. In monocultures, only one cell population was present. (B,C) The difference in gene expression between monocultures and cocultures. (B) Conjunctival epithelium specific markers; (C) lacrimal gland specific markers. Samples at day 4 and 10 were collected and analyzed. Control in (C) was LG cells culture in 2D monolayer. (D) Confocal (z scan) microscopic image of the secreted mucin layer from airlifted CECs cultured in monocultures and cocultures. Scale bar 100 μm. (E) β-hexosaminidase assay of LG cell lysates and supernatants. Samples at day 4 and 10 were collected and analyzed. *$p < 0.05$; **$p < 0.001$.

4.3.4. The influence of cell contact on the secretory function in coculture

Different coculture architectures were developed to investigate the influence of cell contact on the function of the *in vitro* model system. The three designs tested were based on the degree of contact between the two cell types: (I) Bottom: no cell contact, (II) Membrane: indirect cell contact (separated by a porous membrane), and (III) Top: direct cell contact (Figure 4.6A). Permeability test with 10 kD Texas Red-dextran (Figure 4.6B,C) was conducted to assess the tight junctions of CECs in different coculture models. Less than 17% of dextran diffused through during this experiment in all three models. Moreover, when there was indirect or direct cell contact between the two cell populations, the diffusion percentage reduced to about 10%, significantly lower compared to the no cell contact model.

The level of cell contact also impacted the level of gene expression and protein secretion in the coculture models. The amount of *LTF* mRNA in the direct cell contact model was twice as much as those in the other two models (Figure 4.6D). This same trend was observed in the measurement of secreted mucin layer, with average mucin thickness values for models (I)-(III) of 31.5 ± 1.7 μm, 40.3 ± 2.5 μm, and 82.1 ± 4.0 μm, respectively (Figure 4.6E). Specifically, direct cell contact between CECs and LG cell spheroids gave rise to the highest level of MUC5AC staining compared to the other two models (Figure 4.6F).

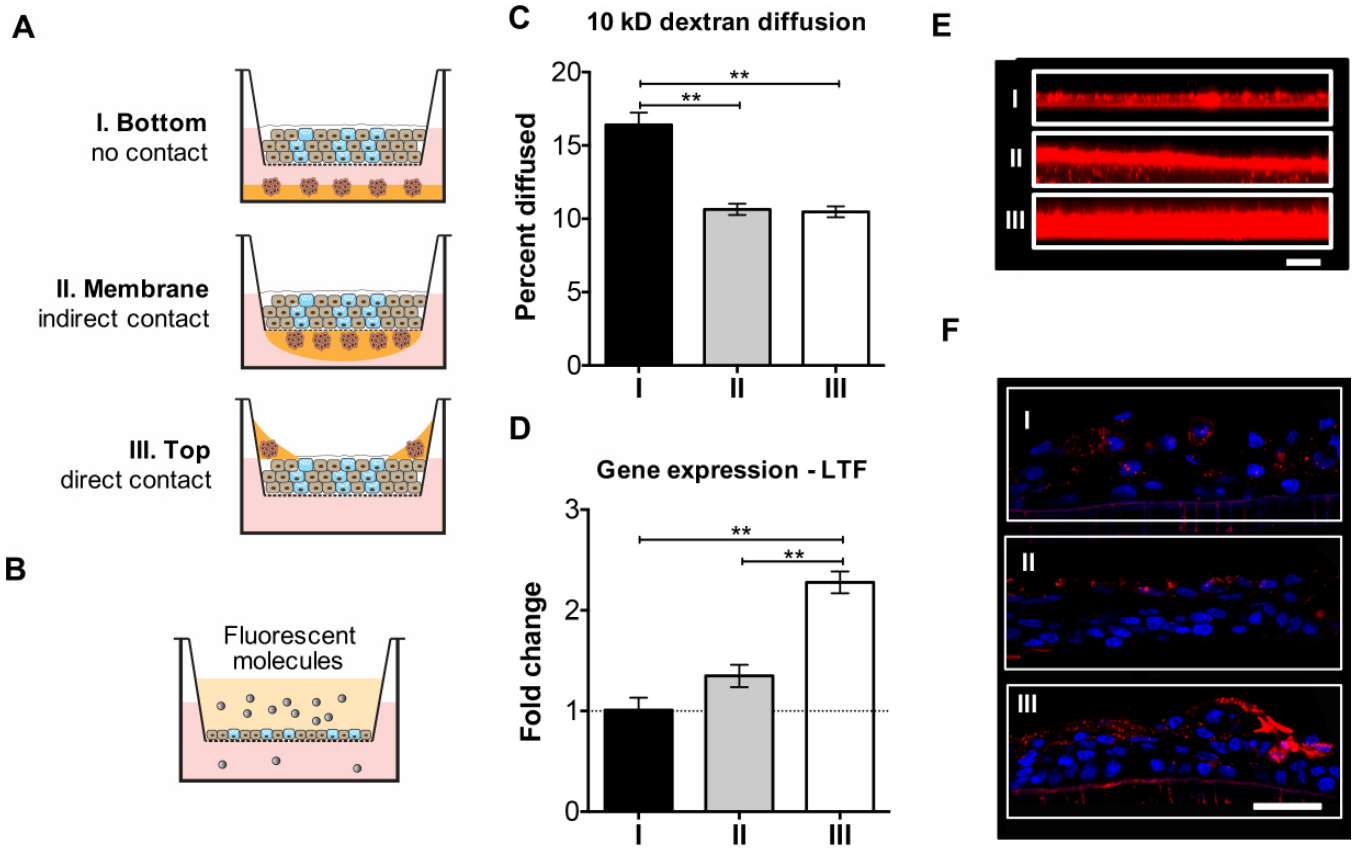

Figure 4.6. Influence of coculture setups on in vitro ocular surface and tear film.

(A) The three different designs of coculture system, which were named after the relative interactions between CECs and LG spheroids. (B,C) Diffusion study (with fluorescent 10 kD dextran). Data in (C) was presented as percent of dextran diffused through. (D) LTF gene expression across the three coculture designs. (E) Secreted mucin layer from airlifted CECs in coculture, visualized by confocal microscopes (z scan). Scale bar 100 μm. (F) MUC5AC IHC staining (red fluorescence; nuclei were counterstained with DAPI) of the airlifted CECs. Scale bar 50 μm. *$p < 0.05$; **$p < 0.001$.

4.3.5. Direct cell contact coculture system as a complex 3D dry eye model *in vitro*

Using the coculture system that provided the best mimic for the ocular surface tear film, response to inflammation-inducing molecules was tested. Specifically, the direct cell contact model system was exposed to the proinflammatory cytokine IL-1β and the commonly used therapeutic dexamethasone. IL-1β exposure upregulated the mRNA level of various cytokines and chemokines, including *IL-6, IL-8, tumor necrosis factor alpha* (*TNFα*), and *matrix metalloproteinase-9 (MMP9)*, at both six- and 24-hour time points (Figure 4.7A and Figure 4.8A). Dexamethasone was effective in downregulating these genes at the 24-hour time point (Figure 4.8A). Cytokine exposure also changed the expression of ocular surface specific genes (Figure 4.7B,C and Figure 4.8B,C). The level of *CK4* and *AQP5* was reduced, while LYZ expression was increased upon the addition of IL-1β. When CECs or LG cell spheroids were cultured alone, IL-1β also induced significant changes in gene expression. However, the addition of dexamethasone was ineffective in restoring the mRNA level of either proinflammatory or tissue-specific genes (Figure 4.9), highlighting the importance of the coculture system in providing a physiologically-relevant screening response.

IL-1β exposure resulted in thinning of the conjunctival epithelial in the ocular surface model. Treatment with dexamethasone restored the thickness of epithelium after IL-1β exposure (Figure 4.8D). A similar trend was observed with MUC5AC staining (Figure 4.8E), in which goblet cells (MUC5AC+) were almost absent with IL-1β culture. IL-1β also significantly decreased the thickness of the tear film secreted by the model system (Figure

4.8F), while the combination of IL-1β and dexamethasone increased lysozyme secretion (Figure 4.8H).

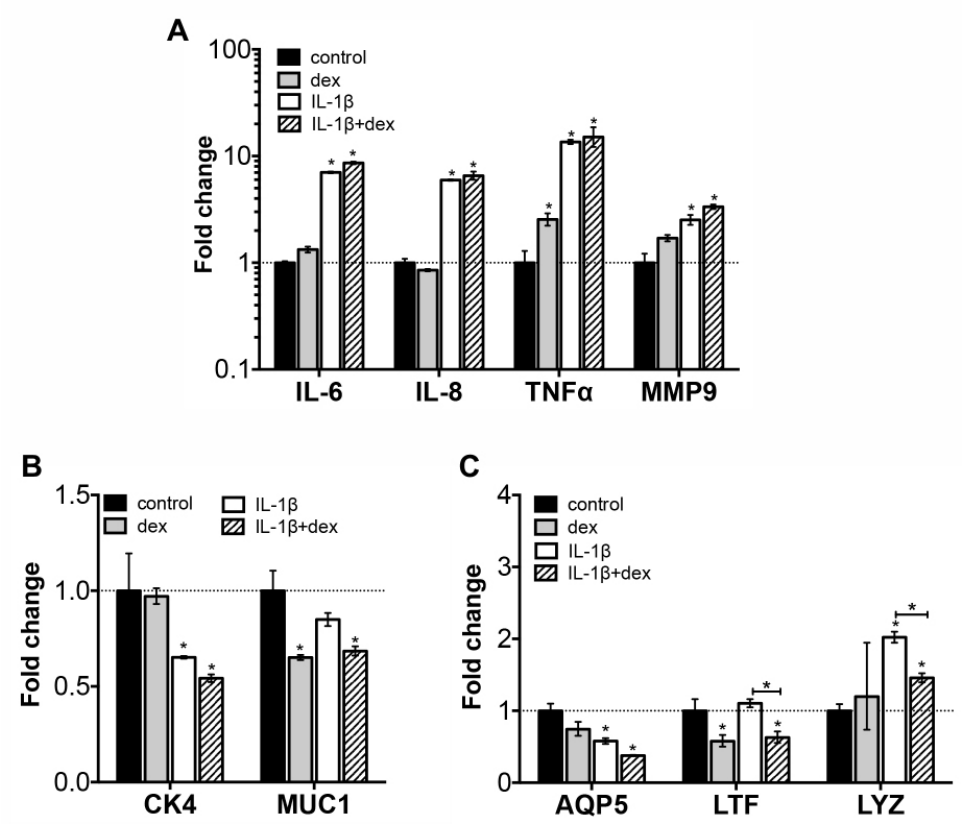

Figure 4.7. Influence of IL-1β addition in the coculture system on gene expression at early time point (six hours).

(A-C) Gene expression of the coculture system after the addition of IL-1β. (A) Inflammatory genes; (B) conjunctival epithelial specific genes; (C) lacrimal gland specific genes. *$p < 0.05$; **$p < 0.001$.

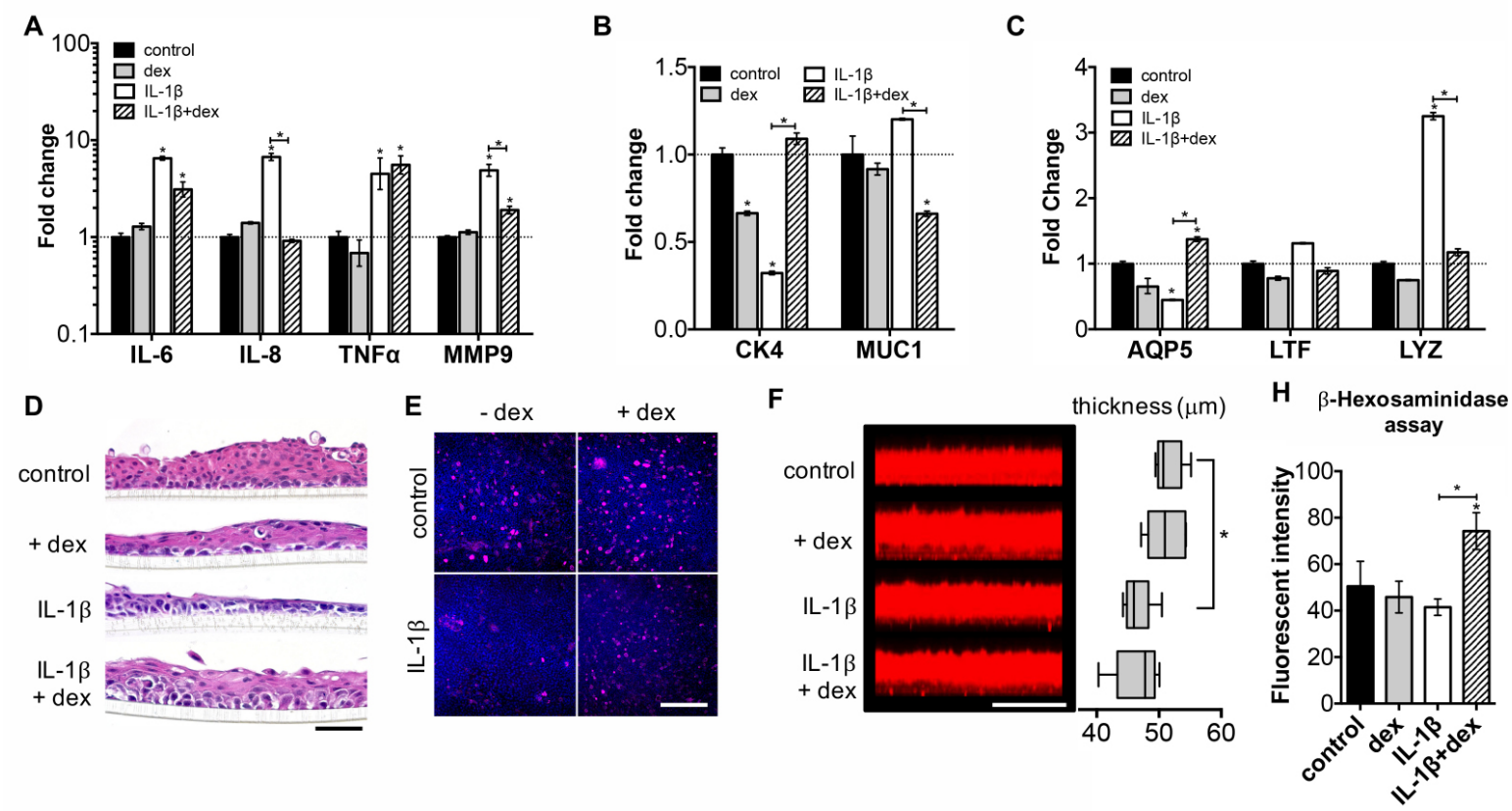

Figure 4.8. Responses of direct contact coculture model after cytokine IL-1β stimulation.

(A-C) Gene expression of the coculture system after the addition of IL-1β. (A) Inflammatory genes; (B) conjunctival epithelial specific genes; (C) lacrimal gland specific genes. (D) The change of epithelial thickness and morphology (H&E staining) after IL-1β exposure. Scale bar 100 μm. (E) MUC5AC staining of the airlifted CECs under various conditions (top view). Scale bar 200 μm. (F) Mucin layer secreted by airlifted CECs imaged by confocal z-scanning. The thickness values were measured using ImageJ. Scale bar 100 μm. (H) β-hexosaminidase assay (supernatant of LG spheroids culture). Dexamethasone: dexamethasone, used as a treatment to inflammatory caused by IL-1β. *$p < 0.05$; **$p < 0.001$.

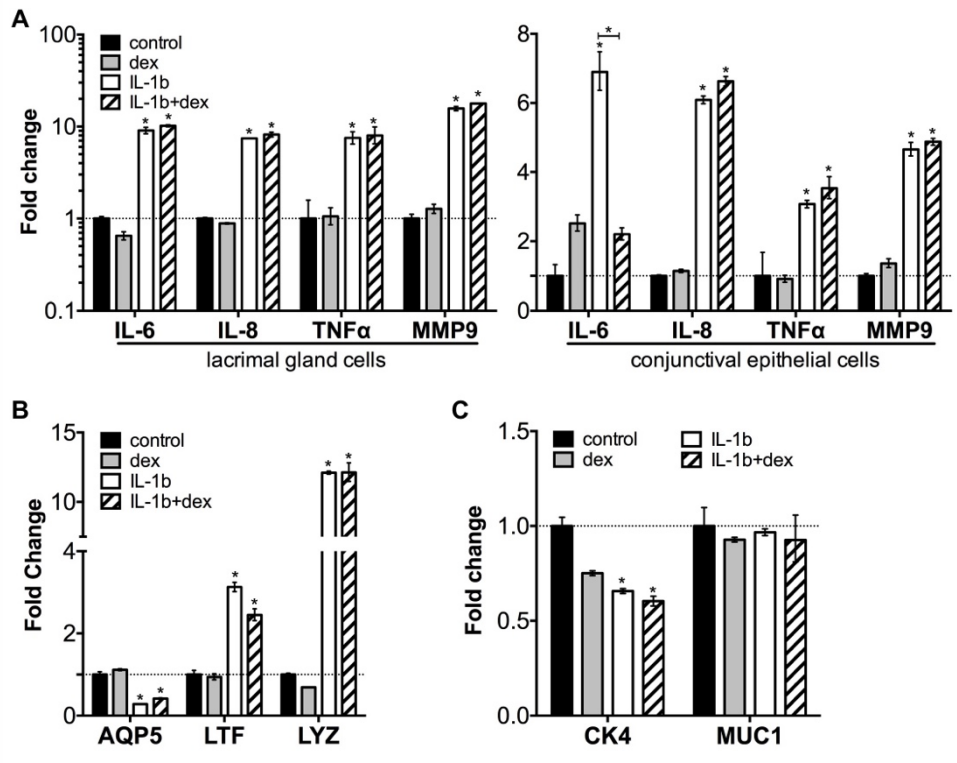

Figure 4.9. Responses of cells under monoculture after cytokine IL-1β stimulation.

Gene expression of monocultured LG spheroids and CECs when exposed to IL-1β. (A) Proinflammatory factors; (B) Lacrimal gland specific genes; (C) Conjunctival epithelial specific genes. Dex: dexamethasone, used as a treatment to inflammatory caused by IL-1β. *$p < 0.05$; **$p < 0.001$.

4.4. DISCUSSION

Conjunctival epithelium, goblet cells, and lacrimal glands are parts of the ocular surface and tear film system. The mucin-aqueous layer in the tear film is of essential importance in protecting the ocular surface epithelium, and is frequently damaged in dry eye disease. Therefore, we constructed a model system for rabbit ocular surface in which the synergistic interactions between conjunctival epithelium and lacrimal glands can be realized and precisely examined.

Coculture is a common technology utilized in tissue engineering to study the natural and/or synthetic interaction between cell populations, and to improve *in vitro* culture time (*70*). In the ocular system, coculture of RPE and photoreceptors was able to provide a better mimic of retinal differentiation and morphology (*64*). Dry eye is an internationally prevalent disease with few efficacious therapies. Besides animal models, robust *in vitro* models of the ocular surface and tear film provide a tool to study pathogenesis and to improve drug screening. Thus, we cocultured conjunctival epithelial and lacrimal gland cells, two important components for tear secretion, in the ocular surface model system. The coculture system was compared to monocultures with respect to the expression of tear secretory markers. Goblet cells in coculture contributed to a thicker mucin layer, and LG cell spheroids had elevated secretion as well. Coculture also helped maintain the morphology and phenotype of the two cell populations (Figure 4.5).

To create functional tissue mimics, we need to consider the effect of cell contact. Different organ/tissue systems require special consideration while designing coculture models. For example, Wallace CS *et al.* developed tissue engineered blood vessel model by coculturing

endothelial (ECs) and smooth muscle cells (SMCs). In this model quiescent SMCs reduced the inflammatory response of ECs mediated by TNFα (*71*). To find the most effective co-culture model and analyze the secreted tear fluid, three different coculture models were compared (Figure 4.6). Results of the permeability test confirmed that the tight junction of conjunctival epithelium is not compromised by the introduction of cell contact in models (II) and (III). The thickness of tear fluid increased significantly with more cell contact (Figure 4.6E), especially in the direct cell contact model (III). Because the stratified CECs remained as a barrier between the LG cell spheroids and the medium reservoir below, the tear fluid secreted by LG cell spheroids accumulated on the top chamber instead of diffusing into the reservoir. This resulted a mixture of both mucin and aqueous layers. This design allows the extraction of the secreted tear fluid for further proteomics and rheological analyses.

Although conjunctival epithelium and lacrimal glands do not have direct contact anatomically, the unique organization of the two cell populations in the direct contact model leads to greatly improved tear secretory function compared to other models. It provides an innovative design for the collection and analysis of secreted tear fluid. Moreover, the unique architecture supported long term culture *in vitro*. We tested this specific model system as a mimic for aqueous dry eye disease, induced by IL-1β, an early molecular mediator in the progression of inflammatory diseases (*72*). After IL-1β exposure, at early time points, we observed changes in the mRNA level of various proinflammatory factors as well as tear-secretory markers. At later time points, the number of goblet cells was reduced significantly, and tear secretion from both cell populations decreased when IL-1β was present. Epithelial damage and thinning were also observed, possibly due to the release of MMPs (Figure 4.8).

Dexamethasone is an anti-inflammatory corticosteroid, known to be beneficial in treating dry eye disease (*73*), and it was able to counteract the effect of IL-1β on our model system. The outcomes we observed in the direct cell contact model system mimic moderate dry eye symptoms in animal models (*74*). Monocultured CECs and LG cell spheroids both showed altered gene expression in response to IL-1β. However, treatment with dexamethasone could not alleviate these symptoms (Figure 4.9). Therefore, the complex 3D coculture system is a more reliable dry eye model *in vitro* compared to monocultured models because it provides a physiologically-relevant response to treatment, and is necessary for the accurate evaluation of therapeutic effects. For further analyses and improvement of the model, humidity and air flow rate could be controlled for more accurate mimicking of dry eye disease, and rabbit primary cells could be substituted with human cells as well.

The mucin layer of the tear film is critical in maintaining homeostasis of the ocular surface. Low goblet cell density and a disrupted mucin layer could accelerate the vicious cycle in the development of dry eye (*75*). Previously established conjunctival epithelial models have lower percentages of goblet cells than their corresponding native tissue (*54*). To ensure adequate goblet cell number and mucin secretion, CECs were subject to Percoll density separation and airlifting culture. After Percoll separation, the gene expression results indicated that the bottom cell population was enriched with *MUC5AC* positive goblet cells, as well as *CK4* positive epithelial cells. With the Percoll gradient enrichment, primary CECs were able to give rise to more goblet and epithelial cells in culture, confirmed by immunocytochemistry (Figure 4.2A,B). Airlifting culture is essential for goblet cell maturation and mucin secretion, and the development of a normal mucin layer in the tear film (*76*). After one week of airlifting culture, cells stratified into four to five layers of CK4

positive epithelial cells and MUC5AC producing goblet cells (Figure 4.2C-F). Airlifted CECs also secreted a thicker and more homogenous mucin-aqueous thin film, labeled by fluorescent dextran (Figure 4.2G).

Lacrimal glands are the main secretory source of the aqueous tear components. Aqueous deficient dry eye usually involves decreased secretion and inflammation in the lacrimal glands (*58*). A 3D environment is required for the successful mimicking of this condition. To investigate the mechanism of lacrimal gland secretion and dry eye disease, various methods have been attempted to recapitulate the 3D environment *in vitro*, including rotary cell culture system (*77*) and gel encapsulation (*78*). We employed a simple yet effective method to form homogenous LG cell spheroids by self-assembly, which were later harvested and encapsulated in Matrigel. The spheroids underwent organoids development, formed hollow cavities first, and then were interconnected together with ductal structure into multi-branched lobules with lumens. These lacrimal organoids were functionally active, confirmed by lysozyme staining (Figure 4.4).

4.5. CONCLUSIONS

In summary, we engineered a synthetic coculture model system, composed of conjunctiva epithelium and LG cell spheroids, as a recapitulation for the ocular surface and aqueous tear system. We demonstrated the efficacy of this model system as a mimic for both the healthy ocular surface and aqueous dry eye disease induced by inflammation. Our model

system provides a novel platform for the pathophysiological study of the ocular surface, as well as for the discovery of new therapeutics for dry eye disease.

Chapter 5. Anti-Inflammatory and Anti-Fibrotic Tissue Matrix Particles Enhanced Corneal Wound Healing

5.1. INTRODUCTION

Extracellular matrices (ECMs) are the molecular networks synthesized and secreted by nearby cells. They offer structural support for tissues and organs, serve as reservoirs for growth factors and provide binding sites for cell migration. ECM plays an important role in the physiological development of both regular tissue and many diseases, including cancer (*79*). It offers mechanical support and provides biologically functional molecules during tissue remodeling and wound healing (*80*). Therefore, ECMs have been widely employed as natural biomaterials in regenerative medicine, and the most widely used and studied ECMs are derived from small intestine submucosa and urinary bladder (*81, 82*). To increase the biocompatibility, tissue ECMs can be decellularized mechanically and/or chemically to remove cellular contents (*83*). Decellularized ECM still preserves the functional and structural features of the original tissue, and it also exhibits immunoregulatory effect by inhibiting rejection and driving the macrophage response towards the M2 (anti-inflammatory) lineage during xenotransplantation (*84*). ECM materials lost load-bearing ability after pulverization and become micron-sized powders, however, they can provide more advantages by serving as reservoirs for signaling molecules. Furthermore, the degradation rate of particularized ECM materials could be fine-tuned to match the remodeling rate of target host tissue (*85*).

On the ocular surface, cornea, conjunctiva, lacrimal glands and meibomian glands work together as one integrated unit to protect the homeostasis and function of the anterior part of the visual system (*1*). Ocular surface environment is largely affected by intrinsic and extrinsic immunological factors in case of injuries and diseases (*86*), which involves interaction of cells, ECM and the tear film, and is mediated by a cascade of cytokines and chemokines (*87, 88*). Although cornea is an immune-privileged organ (*89*), and wound healing is relatively simple in the ocular surface comparing to other organs, inappropriate healing of the cornea leads to fibrosis that severely impacts vision and quality of life (*88*).

ECM remodeling during corneal wound healing is regulated by the crosstalk between different parts of the cornea, the binding of ECM and cell surface molecules, and many molecular mediators, including the key players during this process, tumor growth factor-β (TGF-β) (*90*). Tear film is secreted by various parts on the ocular surface, and its components and secretion are also altered when cornea is injured. Higher concentration of growth factors and proinflammatory cytokines, epithelial damage and reduced tear production are signs of dry eye disease observed after corneal refractive surgeries (*88, 91*). Corneal injuries in the context of pre-existing dry eye conditions are more prone to exacerbated immune response and corneal perforation (*92*). Therefore, while developing new therapies for corneal wound healing, we need to investigate their regulatory effect on the whole ocular surface system, instead of focusing only on the cornea.

Several approaches have been applied to reduce scar formation during corneal wound healing, such as transplantation with stem cells from various sources (*93-95*). There cells are shown to have anti-inflammatory effect as they suppressed the infiltration of immune cells

after corneal injuries. Decellularized ECMs from various tissues and organs have been investigated as biomaterial scaffolds for cell culture *in vitro* or implantations *in vivo* (*83*). In general, they promote regeneration and inhibit inflammatory response and fibrosis in many clinical applications, including the repair of skeletal muscle, cartilage and urinary tract (*80*). Since ECM derived scaffolds have yet to be studied thoroughly in the ocular surface system, we utilized them as new therapeutics to regulate the homeostasis of the ocular surface and to achieve optimal corneal wound healing. Therefore, we studied ECM biomaterials derived from several tissue sources, including porcine lymph nodes (LN), cornea (CO) and cartilage (CA). The tissues were decellularized and pulverized into micro-particles. We first investigated their anti-inflammatory effect on ocular surface cells *in vitro*. ECM particles, especially LN-ECM, ameliorated the inflammation of ocular surface cells induced by cytokines. LN-ECM was applied on a rabbit lamellar keratectomy model to promote corneal stromal reconstruction and decline scar formation. Overall, LN-ECM regulated the wound healing process by decreasing the expression of inflammatory mediators, and successfully reduced immune cell infiltration in the wounded area, and prevented corneal fibrosis.

5.2. MATERIALS AND METHODS

5.2.1. Preparation of particulate ECM

ECM particles were prepared as previously described (*96*). Briefly, fresh porcine lymph nodes, corneas and cartilage were purchased from an US certified butcher (Wagner's Meats,

Mt. Airy, MD) and frozen at -20 °C. The thawed tissue was grounded manually and decellularized in 3% peracetic acid (Sigma-Aldrich, St. Louis, MO) at 37 °C for 4 hours and then in 1% Triton-X100 (Sigma-Aldrich) with 2 mM ethylenediaminetetraacetic acid (EDTA; Sigma-Aldrich) at room temperature for 48 hours under continuous agitation. After cellular components were removed, 0.03% DNase I (Roche Diagnostics Corp, Indianapolis, IN) treatment was performed at 37°C for 24 hours. The decellularized ECM was lyophilized, pulverized using cryomill (SPEX 6770, SPEX SamplePrep, Metuchen, NJ) and stored at -20 °C until use.

5.2.2. Morphology and size distribution of particulate ECM

The morphology of ECM particles was characterized by field-emission scanning electron microscopy (SEM; Carl Zeiss, Jena, Germany). Lyophilized ECM particles were taped on the SEM sample stage with carbon tape, and sputter coated at 20 mA, 5 cm working distance with 0.1 mbar, for 120 seconds, to achieve a 10-nm coating. Images were taken under 1.0 kV, 2 mm working distance.

Average particle size and particle size distribution of each type of particulate ECM were determined by a dynamic light scattering method using Zetasizer Nano ZS90 (Malvern Instruments, Malvern, UK) at 25 °C. Samples were diluted with distilled water before measurement.

5.2.3. Ocular surface cell isolation and culture

Cells on the ocular surface were isolated from Young New Zealand white rabbit tissue (eyes and lacrimal glands), purchased from Pel-Freez Biologicals (Rogers, AR).

Rabbit lacrimal gland acinar cells (LGACs)

Inferior lacrimal glands were removed aseptically and finely minced and cell isolation was carried out as previously described (*97*). Briefly, the tissue was enzymatically digested by collagenase (350 U/ml; Worthington Biochemical Corp, Lakewood, NJ), DNase I (40 U/ml; Roche) and hyaluronidase (300 U/ml; Sigma-Aldrich) for 45 minutes at 37°C, and the digests were filtered through a 100 μm cell strainer and then centrifuged at 200 *g* for 5 minutes. Cells were resuspended in HepatoStim culture medium supplemented with epidermal growth factor (EGF; 5 ng/mL; Corning, Tewksbury, MA). The LGACs were seeded on Matrigel® (growth factor reduced, Corning) coated wells at a density of 5×10^5 cells/cm^2 at 37°C with 5% CO_2.

Rabbit conjunctival epithelial cells (CECs)

Conjunctival tissue was removed from rabbit eyes, with excessive Tenon's tissue trimmed off. The tissue was digested with Dispase®II (1.2 U/ml; Roche) at 4 °C overnight. The loosened epithelial aggregates were dispersed from the surface with a cell scraper, and then collected by centrifugation at 200 *g* for 5 minutes. The CECs were separated into single cells by a secondary digestion with Accutase® (Sigma-Aldrich) for 10 minutes at 37°C and filtered through a 100 μm cell strainer. The final cell pellet was resuspended in supplemented bronchial epithelial cell growth medium (BEGM; Lonza Inc, Walkersville, MD). Isolated cells were seeded at a density of 5×10^4 cells/cm^2 on tissue culture plates at 37 °C with 5% CO_2.

The air-lifting culture of CECs was performed according to previous study (*43*). CECs began to stratify into multiple layers in air-lifting condition and the air-lifting culture was maintained for 7 days at 37 °C with 5% CO_2 for downstream experiments.

Rabbit corneal keratocytes

Keratocytes were isolated using a sequential collagenase (3.3 mg/mL; Worthington) digestion (*31*). Briefly, corneas were diced into quarters and digested in 3.3 mg/mL collagenase solution on an orbital shaker at 37 °C. The digests were collected and filtered through 70 μm cell strainer after 30, 60 and 180 minutes of digestion, and each time fresh collagenase solution was added. Keratocytes were pelleted by centrifugation at 200 *g* for 10 min, and seeded at a density of 2×10^4 cells/cm^2 on tissue culture plates with EpiLife® medium (Thermo Fisher Scientific, Waltham, MA) at 37 °C with 5% CO_2.

5.2.4. Interleukin-1 beta (IL-1β) stimulation and particulate ECM treatment *in vitro*

Inflammation of ocular surface cells was induced with IL-1β (20 ng/ml, Thermo Fisher Scientific) after the cells reached confluence. To compare their anti-inflammatory and secretion stimulatory effects, various types of ECM particles (lymph nodes, cornea and cartilage) were added to the media at a concentration of 1 mg/mL. Cells were maintained for 48 hours and then harvested for gene and protein expression analyses. Cells cultured under standard conditions without IL-1β stimulation or ECM particles were used as the controls.

5.2.5. F-actin staining of keratocytes

Alexa Fluor 488 Phalloidin (Thermo Fisher Scientific) was used to visualized the morphology of keratocytes. The cells were rinsed with phosphate buffered saline (PBS; Thermo Fisher Scientific) and fixed with 4% paraformaldehyde (PFA; Sigma-Aldrich) solution for 10 min, followed by permeabilization with 0.1% Triton X-100 for 20 min at room temperature. After thorough rinse with PBS, the keratocytes were stained with Phalloidin for 20 min in the dark, followed by counterstaining with DAPI (4',6-diamidino-2-phenylindole dihydrochloride; Thermo) for the nuclei. The cells were imaged using a fluorescent microscope (Axio Imager 2, Carl Zeiss, Jena, Germany).

5.2.6. β-hexosaminidase secretion assay

β-hexosaminidase, or N-Acetylglucosaminidase (NAG) is a lysosomal enzyme in the tear fluid secreted by lacrimal glands after carbachol stimulation, and 4-Nitrophenyl N-acetyl-β-D-glucosaminide (NP-GlcNAc) was used as the substrate for NAG. Secretion assay was carried out with four replicates in each group. The culture medium was replaced with DMEM/F12 (Thermo Fisher Scientific) and incubated at 37°C for 2 hours. After removing a baseline sample, carbachol (Sigma-Aldrich) was added to the medium to a final concentration of 100 μM, and incubated at 37°C for 30 minutes. The culture medium was collected and centrifuged at 700 rpm for 5 minutes. The resulting supernatants were analyzed for NAG catalytic activity with a NAG assay Kit (Sigma-Aldrich), per the protocol. The absorbance at 405 nm was measured using a microplate reader (BioTek, Winooski, VT).

5.2.7. Confocal microscopy measurement of secreted mucin *in vitro*

Similarly, after seven days of air-lifting culture, CECs cultured on Transwell® (Corning) were exposed to IL-1β (20 ng/ml) and each ECM particles for 48 hours. Texas Red-dextran (10 kDa, 2 mM in PBS; Thermo Fisher Scientific) solution was loaded onto upper chamber of Transwell® insert. Z-stack scanning was performed on the samples by a laser scanning confocal microscope (LSM 510, Carl Zeiss). The serial images were analyzed and stacked to generate 3-dimensional images for the measurement of mucin thin film thickness using ZEN imaging software (Carl Zeiss).

5.2.8. Animal surgeries and the application of ECM particles on corneal wound

New Zealand White rabbits, weighing between 2-3 kg, were used in the corneal wound healing study. The animals involved were housed and treated in accordance with the guidelines in the Association for Research in Vision and Ophthalmology (ARVO) Statement for the Use of Animals in Ophthalmic and Visual Research and also with the approval of the Animal Care and Use Committee at Johns Hopkins University at all time. They were anesthetized by intramuscular injection of ketamine (15 mg/kg) and xylazine (5 mg/kg). Corneal stromal injuries were introduced with superficial lamellar keratectomy (SLK) using an automated microkeratome (Bausch & Lomb, Rochester, NY). The dimension of the wound was 6 mm in diameter and 100 μm in depth on average. The corneal flaps were surgically removed, leaving the corneal stroma exposed (untreated; Figure 5.4A).

Fibrin glue (FG; Baxter, Deerfield, IL) sealant was used as a positive control treatment for wound healing, as well as the delivery agent of ECM particles. After SLK, 10 μL fibrinogen solution was first pipetted on top of the corneal wound, followed by the addition of 10 μL thrombin solution. The mixture was allowed to gel at room temperature for 5 min to form a layer covering the wounded area. LN-ECM powder was mixed with fibrinogen solution before adding to the corneal wound, and the final ECM concentration in FG gel was 30 mg/mL. A topical antibiotic ointment (0.5% erythromycin; Wilson, Mustang, OK) was applied after the procedures and every day afterwards, while no systemic and local immunosuppressive agents were used.

5.2.9. Clinical observations of re-epithelialization and corneal haze analysis

The epithelialization of cornea was evaluated by fluorescein staining under blue light every day in the first week post-surgery until completed healing. The area of cornea stained with fluorescein was measure using ImageJ software (National Institute of Health, NIH, Bethesda, MD), and normalized to the whole cornea and this value was used for comparison between groups (Figure 5.5A,C).

The eyes are also examined and photographed throughout the study by a slit lamp to assess corneal scar and haze formation. The amount of corneal haze was quantified with Photoshop software (Adobe Systems Inc., San Jose, CA) similarly as previously described (*98*). Front image of the corneas was converted to gray scale for better contrast. The “set black point” option in Photoshop was used for background correction, in which a point on the cornea above the pupil with no haze was set to be black. Hence the scarring area of each image was normalized to its respective unscarred regions, making the comparison more

accurate. The area above the pupil was selected using the "elliptical marquee tool" and the measurement was recorded (Figure 5.5B). The value of "integrated density" was used for analysis, as it is related to both brightness and area of the haze.

Scar tissue within corneal stroma was imaged at various time points by an *in vivo* confocal microscope (Nidek Confoscan 3, Fremont, CA, USA) similarly to a pervious study (*99*). Briefly, immediately after anesthesia, rabbits were placed on a customized platform and the heads were immobilized with one of the eyes facing towards the objective lens. Corneal stromal tissues of different layers (anterior, mid and posterior) were imaged using the Confoscan 3 software. Lubricant gel (Genteal; Novartis, East Hanover, NJ) was used throughout the imaging as an immersion fluid.

5.2.10. Quantitative real-time polymerase chain reaction (RT-qPCR)

Cornea samples *in vivo* were collected at one- and four-week post-surgery. After euthanasia, corneas were dissected off the eye and frozen at -80 °C in TRIzol® reagent (Sigma-Aldrich), and followed by cryogenically homogenization with mortar and pestle while immersed in liquid nitrogen. The homogenate was collected and used for total RNA isolation as follows.

Total RNA from cells growing *in vitro* and cornea samples *in vivo* was isolated using the RNeasy Mini Kit (Qiagen, Germantown, MD), according to manufacturer's protocol. The RNA concentration was measured using a NanoDrop Spectrophotometer (NanoDrop Technologies, Wilmington, DE). cDNA was synthesized from 1 μg of total RNA with the high-capacity cDNA reverse transcript kit (Thermo Fisher Scientific) on a MyCycler (Bio-Rad, Hercules, CA) thermal cycler. qPCR was conducted on the StepOnePlus System (Thermo

Fisher Scientific) using SYBR Green PCR Master Mix (Thermo Fisher Scientific) to quantify the expression level of target genes. Primer sequences are listed in Table 5.1. Relative quantification of the signals was carried out by the $\Delta\Delta C_T$ method with the expression level normalized to that of control samples. β-actin was used as internal reference.

Table 5.1. Primer sequences for RT-qPCR

Gene		Sequence	
conjunctiva specific	*MUC1*	forward	GAG TCA CAG TGC GTG ATG TT
		reverse	GGC CAG GGC TAT GAA ATA GAT G
	MUC5AC	forward	CGC CTT CTT CAA CAC CTT CA
		reverse	TGG GCA AAC TTC TCG TTC TC
lacrimal gland specific	*AQP5*	forward	CAA CGC GCT CAA CAA CAA
		reverse	GTG AGT CGG TGG AAG AGA AA
	LTF	forward	GAT GCC ATG ACC CTG GAT AG
		reverse	GTC TGT GGC TTC GCT TCT
inflammatory	*IL-6*	forward	GAA TAA TGA GAC CTG CCT GCT
		reverse	TTC TTC GTC ACT CCT GAA CTT G
	IL-8	forward	TGG ACC TCA CTG TGC AAA T
		reverse	GCT CAG CCC TCT TCA AGA AT
	TNF	forward	GTA GTA GCA AAC CCG CAA GT
		reverse	GGT TGT CCG TGA GCT TCA T
	MMP9	forward	AGT ACC GAG AGA AAG CCT ACT T
		reverse	TGC AGG ATG TCA AAG CTC AC
	iNOS	forward	CCA TCC CTG CAT CCT CAT T
		reverse	CCG GAG CCC TTT GTA CTC
	Arg1	forward	ACT CCA CTG ACA ACC ACA AG
		reverse	CCT GGT ACA TCA GGG ATC TTT C
fibrotic	*TGF*	forward	CCT GTA CAA CCA GCA CAA CC
		reverse	CGT AGT ACA CGA TGG GCA GT
	CTGF	forward	AGG AGT GGG TGT GTG ATG AG
		reverse	CCA AAT GTG TCT TCC AGT CG
	COL1	forward	TTC TGC AGG GCT CCA ATG AT
		reverse	TCG ACA AGA ACA GTG TAA GTG AAC CT
	αSMA	forward	AGA GCG CAA ATA CTC CGT CT
		reverse	CCT GTT TGC TGA TCC ACA TC
	IL-17a	forward	ATC TGT GTC ACT GCT GCT G
		reverse	GAG TCC AAG GTG AAG TAG ATC G
	IL-23a	forward	GAG GGA GAT GAA GAG ACT ACC A
		reverse	CAG GCA GAA CTG AGT GTT GT
internal reference	*β-actin*	forward	GCT ATT TGG CGC TGG ACT T
		reverse	GCG GCT CGT AGC TCT TCT C

5.2.11. Histology and immunohistochemistry (IHC)

Cornea samples *in vivo* were processed for histology and IHC as previously described (*21*). Briefly, samples were fixed in 4% PFA, dehydrated, embedded in paraffin (Tissue-Tek, Sakura Finetek, Torrance, CA) and sectioned at 5 μm thickness. Hematoxylin & Eosin (H&E; Sigma-Aldrich) staining was carried out per the protocol to examine corneal stromal and epithelial reconstruction. IHC (fluorescence) was performed to visualized the expression of wound healing related markers. Primary anti-CD11b antibody was purchased from BD Biosciences (BDB550282) and anti-alpha smooth muscle actin (αSMA) antibody was from Dako (Clone 1A4). Goat anti-mouse and anti-rat antibodies (conjugated with Alexa Fluor 594; Thermo Fisher Scientific) were used as secondary antibodies. The sections were either imaged with Axio Imager 2 or confocal laser scanning microscope (LSM 510; Carl Zeiss).

5.2.12. Statistical analysis

Data are expressed as mean values ± standard deviation, and quantitative experiments were performed with at least triplicates. Significance was analyzed by one-way analysis variance (ANOVA). Statistical comparisons were between IL-1β stimulated group and each dECM treated group, if not stated otherwise. Conventionally, *p* value less than 0.05 was considered significant.

5.3. RESULTS

5.3.1. The processing and morphology of particulate ECMs

Three different porcine tissues: lymph nodes (LN), cartilage (CA) and cornea (CO) (Figure 5.1A), were processed. As shown in the schematic, tissues were first decellularized to remove cellular components, and particulate ECM scaffolds were obtained by cryogenic pulverization. The morphology of the ECM particles was revealed by SEM imaging (Figure 5.1B). After processing, the ECM of lymph nodes mostly formed spherical particles. Cartilage ECM also formed some spherical particles, but it had elongated fibers and porous particles as well. While instead of separate spherical particles, cornea ECM formed microscopic lamellar sheets with fibrillar structures.

Similarly, the difference of particulate ECMs originated from various sources is also reflected on size distribution (Figure 5.1B). LN-ECM has a broad distribution that ranges from 68.06 to 6439 nm, with an average of 1502.3 nm. CA-ECM has a relatively narrower range, which is between 825 and 6439 nm, and the average is 2967.9 nm, the biggest particle size among all three. CO-ECM has a discontinuous distribution, and a much smaller average (231.5 nm).

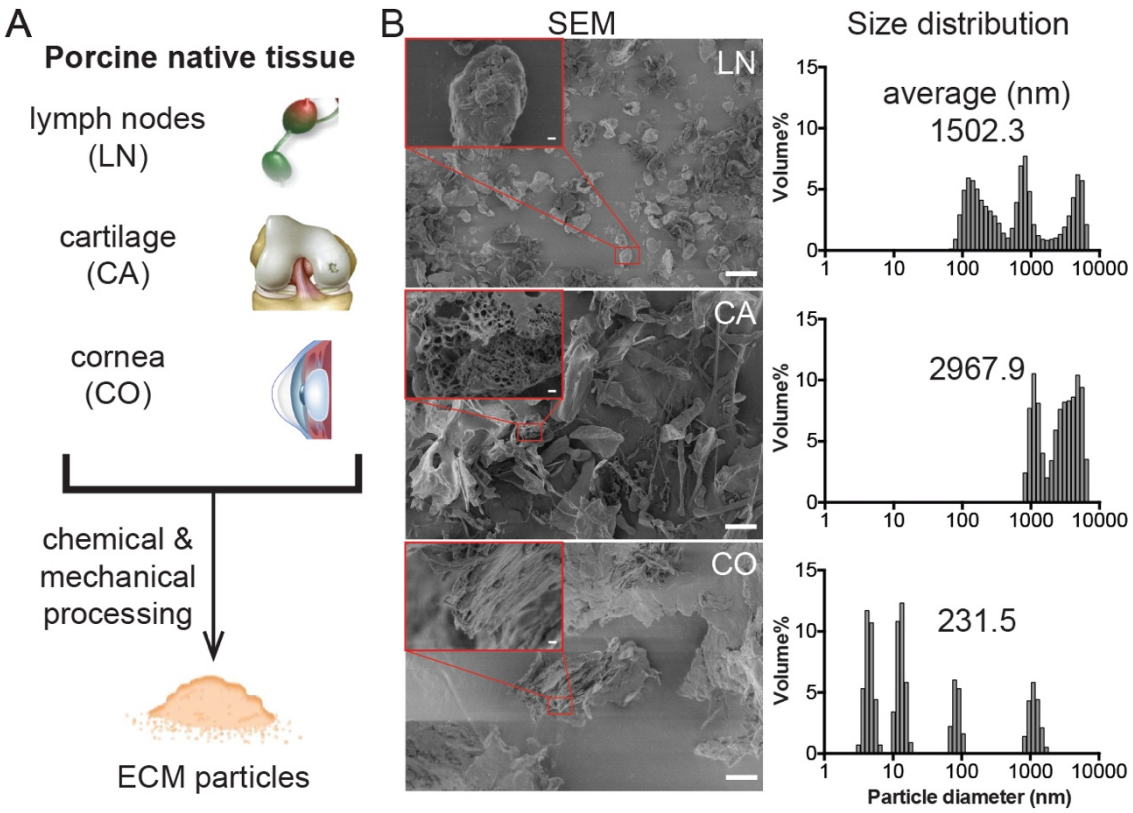

Figure 5.1. ECM processing and characterization.

(A) Porcine native tissues (lymph nodes, cartilage and cornea) were decellularized and pulverized into ECM particles. (B) SEM images and size distribution of ECM particles from different tissue sources. Scale bar: 10 μm (insert scale bar: 400 nm). Numbers on the graphs indicated average particle sizes.

5.3.2. The anti-inflammatory effect of ECM particles on keratocytes *in vitro*

Three types of ocular surface cells were isolated from rabbit tissues, including CECs, LGACs and corneal keratocytes. They were used for the study of the anti-inflammatory effect of ECM particles *in vitro* (Figure 5.2A). After keratocytes were exposed to IL-1β, inflammatory genes tumor necrosis factor alpha (TNFα), IL-6 and matrix metalloproteinase 9 (MMP9) all had drastic increase in mRNA level (Figure 5.2B). LN- and CO-ECM significantly decreased TNFα expression and CA-ECM reduced IL-6 expression. All three types of particulate ECMs lowered MMP9 expression, but it was still significantly higher than the level of control. Inflammatory environment and ECM supplements also have influence over the morphology of keratocytes *in vitro* as revealed by F-actin staining (Figure 5.2B). Under normal condition (control), keratocytes had a stellate shape with multiple processes (Figure 5.2B arrowheads). The keratocytes became more spread out with very few processes when IL-1β was present. Particulate ECMs increased the number of processes of keratocytes, however, the cells appeared more elongated, especially in the case of CO-ECM.

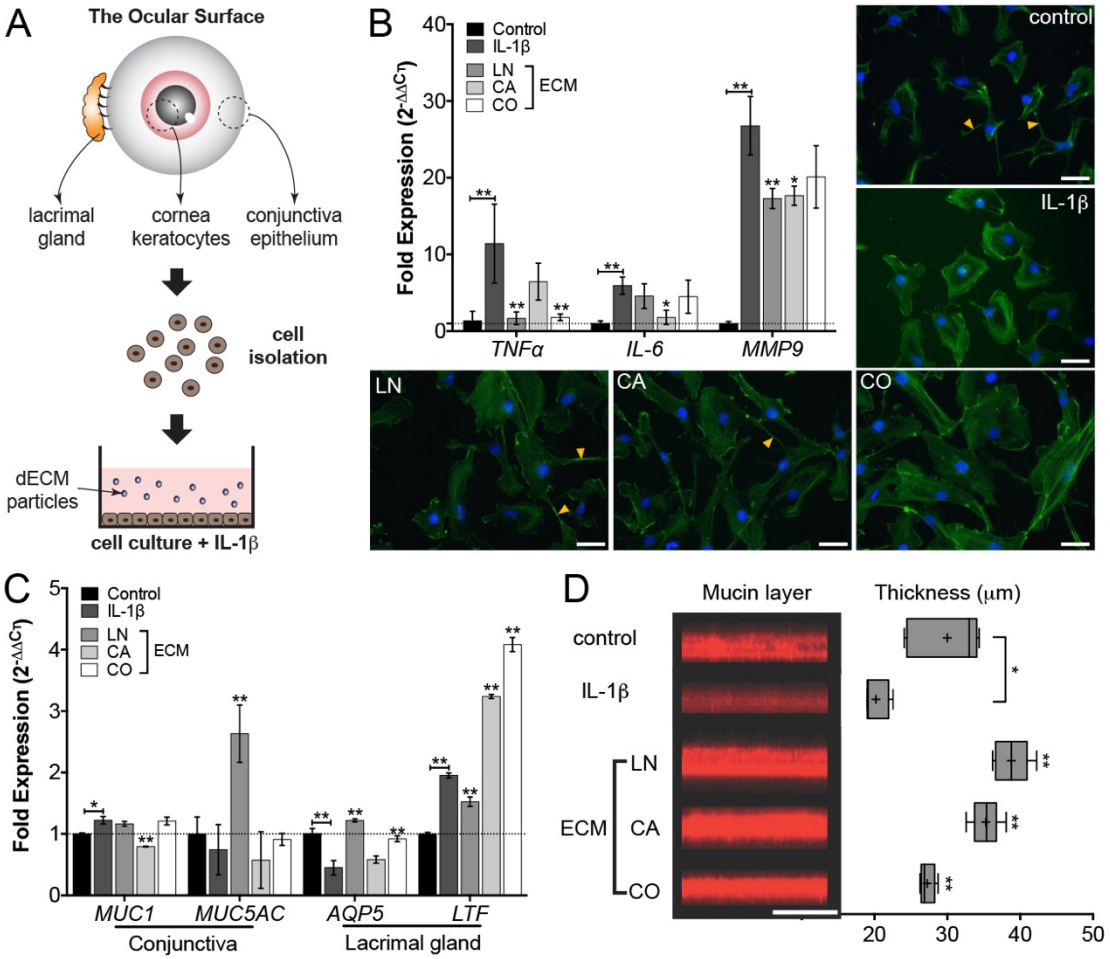

Figure 5.2. The anti-inflammatory effect of dECM on ocular surface epithelial cells *in vitro*.

(A) Ocular surface cells (lacrimal gland acinar cells, corneal keratocytes and conjunctival epithelial cells) were isolated and subject to IL-1β stimulation and ECM treatment. (B) Changes in gene expression (RT-qPCR) and morphology of keratocytes (F-acin staining) after exposure to IL-1β and ECM particles. F-actin was stained by phalloidin (green); cell processes were indicated with arrowheads. Scale bar: 50 μm. (C) RT-qPCR of tear film related gene expression of conjunctival epithelial and lacrimal gland acinar cells. (D) Mucin layer secreted by conjunctival epithelial cells in air-lifting culture was imaged by confocal microscope stained with Texas Red conjugated dextran. Images shown here were constructed from the x-z plane of a series of z-stacking images. Scale bar: 100 μm. Thickness values were measured from corresponding mucin layer images by Photoshop software and "+" indicated the mean values. *$p < 0.05$; **$p < 0.001$.

5.3.3. The influence of ECM particles on tear secretion of ocular surface cells *in vitro*

Gene and protein expressions related to tear secretion were examined for the *in vitro* experiments with CECs and LGACs, the two main components responsible for tear secretion. We found that IL-1β stimulation did not influence the level of mucin (MUC1) or mucin 5AC (MUC5AC), membrane bound mucin and secreted gel-forming mucin from the conjunctiva, respectively. However, the addition of LN-ECM increased MUC5AC expression by more than 2 folds. Regarding lacrimal gland related genes, inflammation environment resulted in fewer aquaporin 5 (AQP5) mRNA, and LN- and CO-ECM were able to restore the level back to normal. Lactotransferrin (LTF) mRNA was increased significantly when inflammation was induced by IL-1β, and ECM increased it even further (Figure 5.2C). The actual mucin film secreted by conjunctival goblet cells was stained with Texas Red conjugated dextran and imaged using confocal microscope with z-scanning, and the thickness was analyzed (Figure 5.2D). Texas Red-dextran has a good quantum yield and is relatively impermeable across the epithelia. Inflammation caused the mucin film thickness changed from about 30 μm to 20 μm, a much thinner layer as viewed under confocal microscope. When ECM particles were added to the medium, conjunctival goblet cells were able to secret more mucins even in an inflammatory environment.

Inflammatory gene expression and lysozyme (NAG) secretion were also examined for CECs and LGACs. In both type of cells, the stimulation of IL-1β induced significant increase the gene expression of multiple proinflammatory cytokines and chemokines, such as TNFα, IL-6, IL-8 and MMP9 (Figure 5.3A,B). The addition of LN-ECM was able to

reduce the expression of certain genes (IL-8 and MMP9 of CECs and MMP9 of LGACs, respectively), but the levels were still higher than control, and this effect on other genes was insignificant. The other two type of particulate ECMs, cartilage and cornea, had no significant influence on inflammatory gene expression. The NAG activity stimulated with carbachol is an easily measured function of LGACs (β-hexosaminidase assay). NAG secretion was slightly increased when IL-1β was added, and CA- and CO-dECM did not alter the secretion. However, LN-ECM doubled the secretion of NAG compared to control (Figure 5.3C).

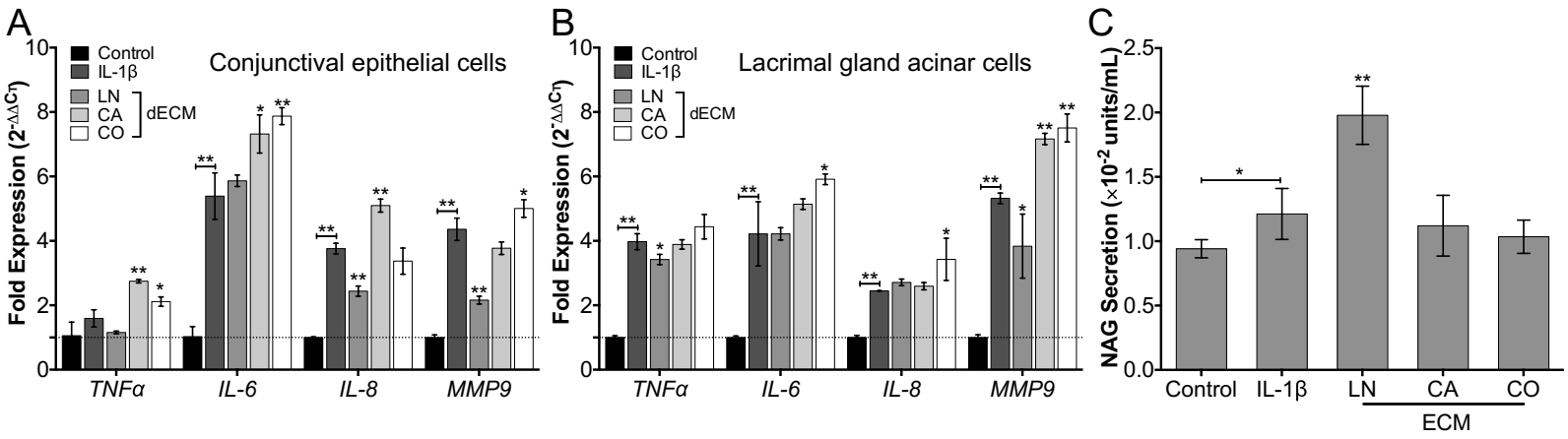

Figure 5.3. The anti-inflammatory effect of ECM on conjunctival epithelial and lacrimal gland acinar cells *in vitro*.

(A,B) RT-qPCR results of inflammatory gene expression of conjunctival epithelial and lacrimal gland acinar cells. (C) Lacrimal gland secretion measured by β-hexosaminidase assay for lysozyme (NAG). *$p < 0.05$; **$p < 0.001$.

5.3.4. ECM particle transplantation after SLK surgery

Because of its anti-inflammatory ability, LN-ECM particles were selected as the most potent one to be used in the application *in vivo*. SLK surgery (6.0 mm diameter and 100 μm depth) was performed with automated microkeratome and the flap was removed afterwards. About 20 μL of FG was applied on the wound as a positive control. ECM was mixed with FG during application. Outcomes from four groups (control, untreated, FG and FG+ECM) were compared (Figure 5.4A). The epithelialization of cornea after SLK was assessed by fluorescein staining (Figure 5.5). The healing process was completed in all three groups by day five, shown with no visible fluorescein staining. The re-epithelialization of the two treated groups (FG and FG+ECM) was slightly behind the untreated group at day two and three (Figure 5.5A,C). Slit lamp examination with diffused or focal illumination (Figure 5.4B,C) revealed that severe scar formed in untreated group after SLK. While there was some cornea haze developed in the two treated groups (FG and FG+ECM) at week one, the scar was significantly reduced and invisible at week four. Corneal haze after SLK was quantified at day 7, 14 and 28 (Figure 5.5B). The image was adjusted to gray scale, and the value of haze was expressed as integrated intensity of the area within the dashed line (Figure 5.5B insert). Without treatment, corneal haze kept increasing during the whole course of study. At week two and four, corneas treated with FG and/or ECM drastically reduced haze compared to the untreated group. Furthermore, at all three time points, FG+ECM reduced the haze formed within cornea stroma significantly more than FG alone.

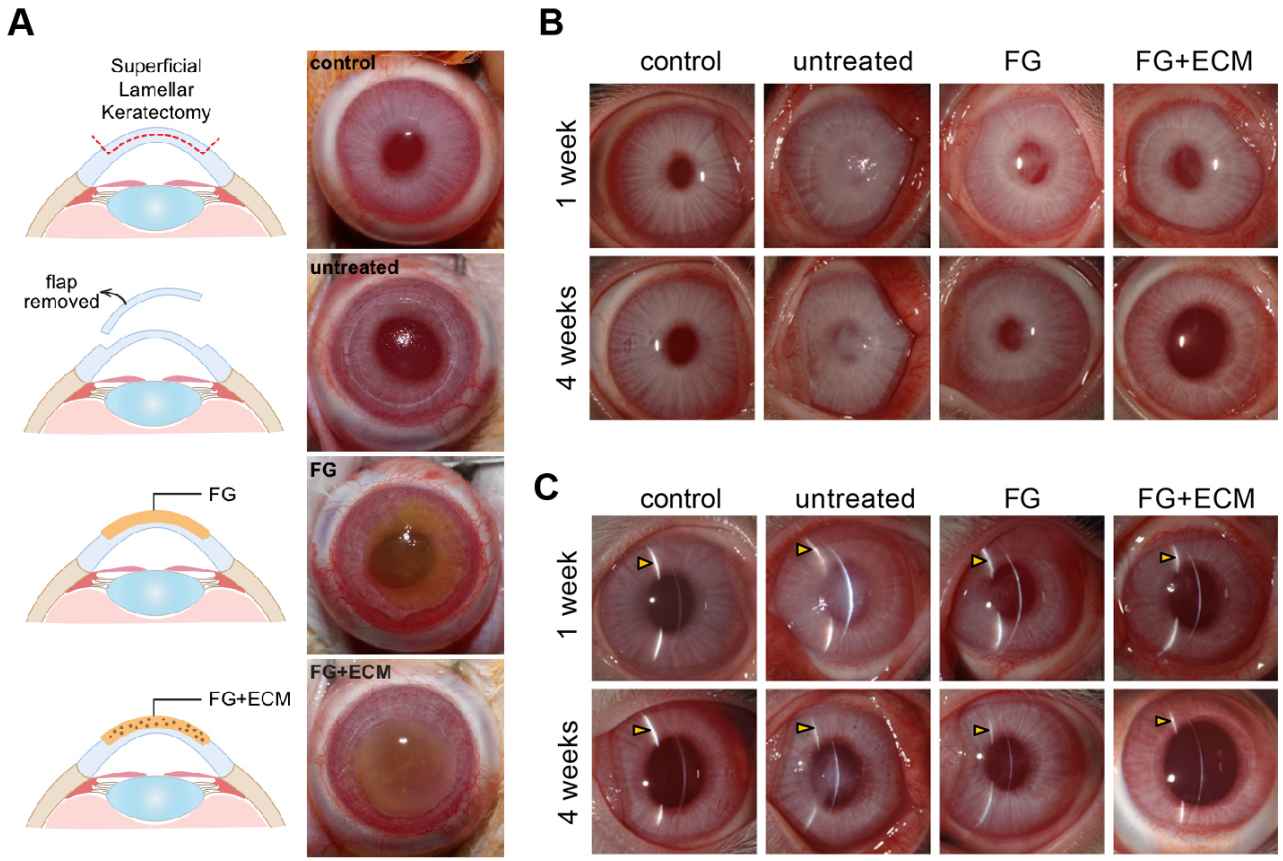

Figure 5.4. ***In vivo*** **application of ECM particles on cornea after lamellar keratectomy**.

(A) Surgery procedures. The flap was removed, and in the untreated group, corneal stroma was left exposed; FG sealant with or without ECM was applied on the wound. ECM particles were visible within the FG gel. Rabbit corneas examined at different stages by slit lamp using direct diffuse (B) and focal/beam (C) illumination.

The reduction in scar tissue and corneal opacity was also revealed by *in vivo* confocal imaging (Figure 5.6). Keratocytes in healthy cornea were clearly visible in all three parts of the stroma. SLK surgery without treatment resulted in severe scars (bright with high intensity) in anterior to mid stromal tissue at both one- and four-week time points. FG treatment alone reduced the amount of scar within the cornea at week four. However, there was still some scar tissue retained in the anterior part of the stroma. LN-ECM treated cornea only showed mild opacity in the anterior stroma at week one, and it became clear at week four.

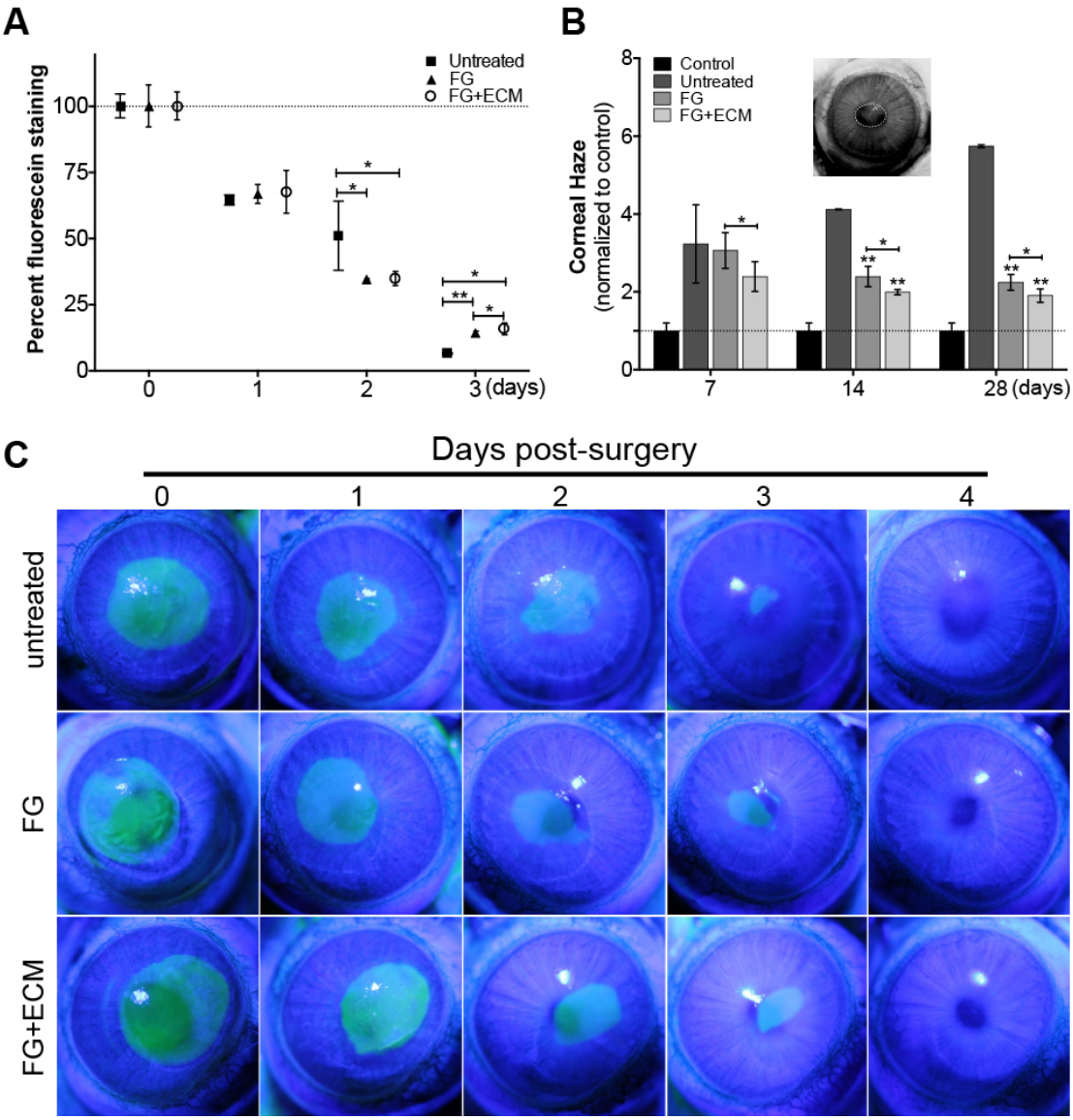

Figure 5.5. Corneal re-epithelialization and corneal haze in different groups after SLK.

(A) Re-epithelialization quantified from fluorescein staining images in (C) at different time points. Stained area (green) indicated injured cornea that is not fully covered by epithelium. Data was presented as percent stained with fluorescein, normalized to area of the whole cornea. (B) Corneal haze quantification. Images from (Figure 5.4B) were switched to gray scale and the background was adjusted too for consistence among groups. The dashed circle is right above the pupil and was analyzed for haze area and intensity (black and white insert). The "integrated intensity" value obtained from Photoshop was normalized to control (healthy cornea). *$p < 0.05$; **$p < 0.001$.

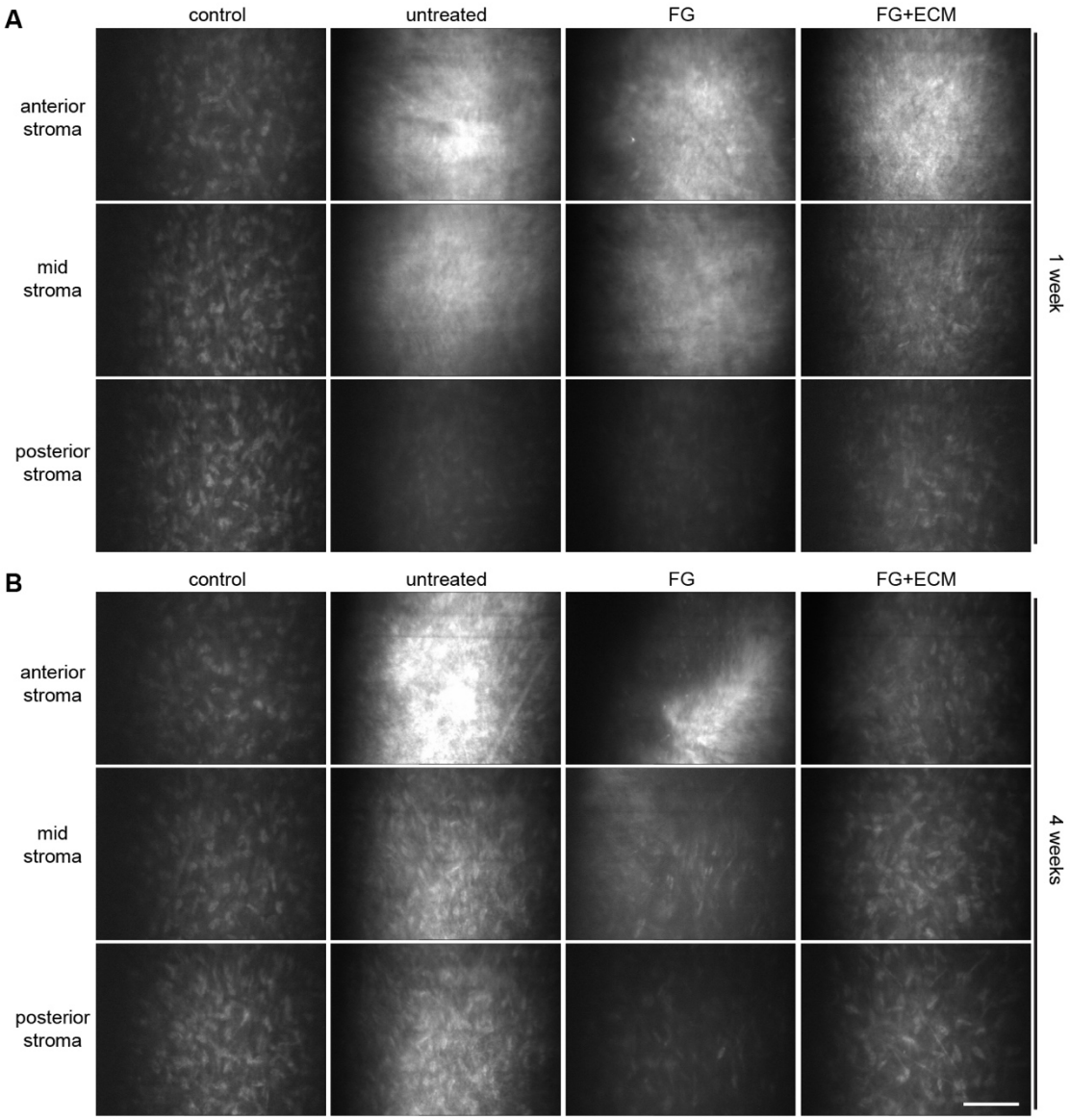

Figure 5.6. Corneal stromal tissue imaged by *in vivo* confocal microscope.

In control group, keratocytes were clearly imaged in all layers (anterior, mid and posterior) of stroma. High intensity (brighter) indicated the presence of scar tissue within the stroma. Images from both one-week (A) and four-week (B) time points were shown. Scar bar: 100 μm.

5.3.5. The immunoregulatory effect of ECM particles on corneal wound healing after SLK

The immunoregulatory effect of ECM particles was investigated throughout the animal study. Gene expression of proinflammatory cytokine TNFα was downregulated at both day 7 and 28 by FG and/or ECM treatment (Figure 5.7A). FG's reduction effect on the mRNA level of MMP9 was only significant at the later time point (day 28). FG+ECM decreased MMP9 expression at both time points. FG+ECM treatment also suppressed iNOS expression at week one, and arg1 was upregulated in all surgical groups at week one. By week four, iNOS expression in FG and/or ECM treated groups were higher than healthy and untreated corneas. However, arg1 expression went down in most groups except in FG treated cornea (Figure 5.7B).

Immunohistochemistry with CD11b showed macrophage/monocyte infiltration at early stage (one week) during the wound healing process (Figure 5.7C). We observed a significant amount of migrated immune cells in the wounded stromal area in the untreated group. There were fewer CD11b+ in FG treated group, and even fewer cells when ECM was added along with FG. Staining of Ki67 (Figure 5.7D), the marker for cell proliferation, demonstrated that at early time point (one week), SLK led to the proliferation of epithelial and stromal cells. Corneal cells stayed quiescent at four-week time point, and only a few epithelial cells in the FG treated cornea were positive for Ki67.

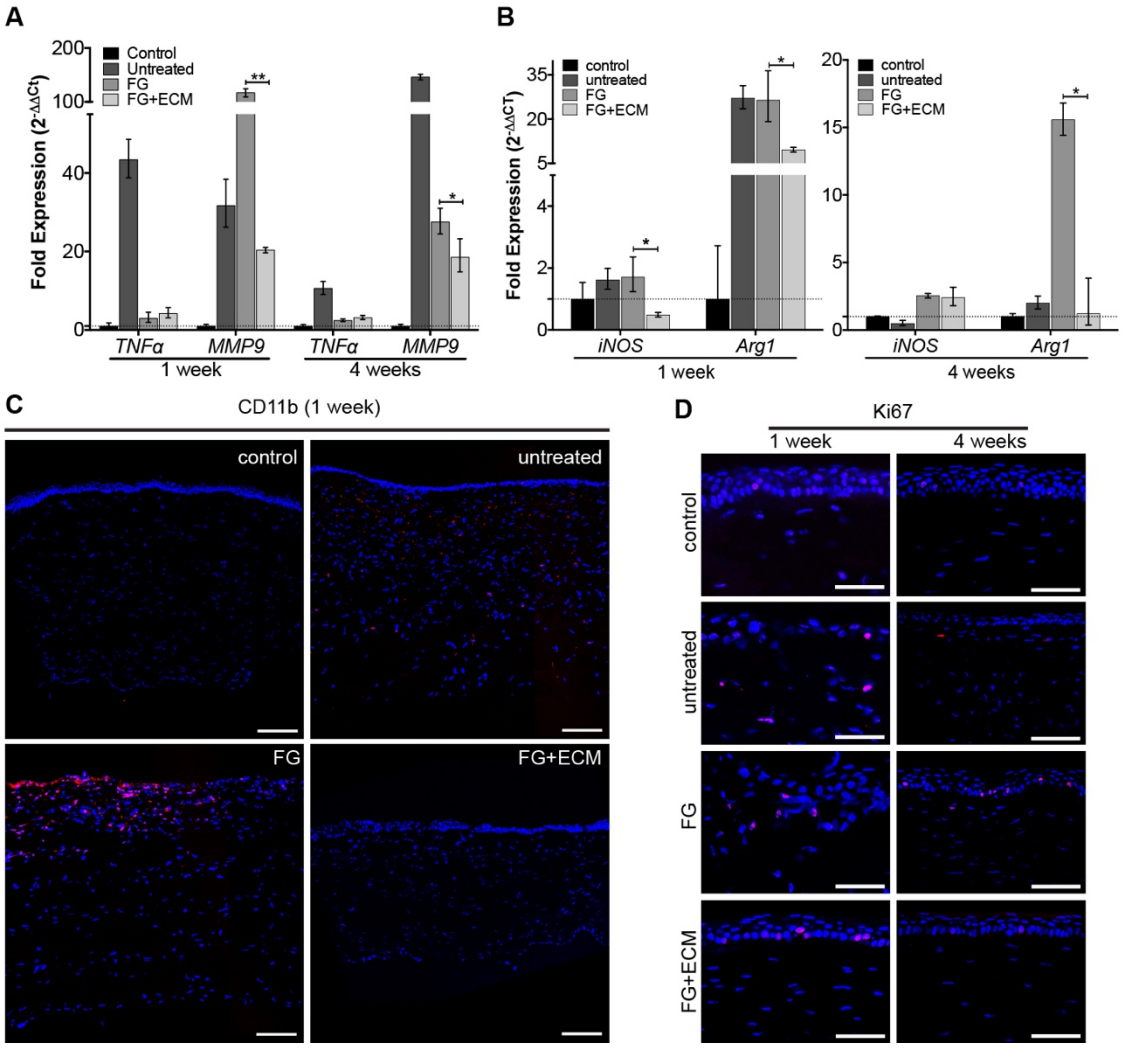

Figure 5.7. The anti-inflammatory effect of ECM on corneal wound healing *in vivo*.

(A,B) Inflammatory gene expression (TNFα, MMP9, iNOS and Arg1) of reconstructed cornea at day 7 and 28 in different groups, measured by RT-qPCR. (C) CD11b immunostaining (red) showing myeloid cell infiltration in the wounded area at week one. Scale bar: 200 μm. (D) Ki67 staining showing the presence of proliferating cells within the healing corneas at both week one and week four. Scale bar: 100 μm. *$p < 0.05$; **$p < 0.001$.

5.3.6. ECM influenced corneal fibrosis during wound healing

Markers associated with fibrosis were examined at week four during the wound healing exp. A decrease in the gene expression of TGFβ1, connective tissue growth factor (CTGF), Type I collagen (COL1) and αSMA was observed resulted from FG and/or ECM treatment, and FG+ECM's effect was more prominent than FG alone (Figure 5.8A). IL-17a was downregulated by FG and/or ECM treatments at week one, and its expression went down to the level of control at week four. FG and/or ECM treatments also increased IL-23a expression at early time point, but FG alone continued to upregulated IL-23a till week four (Figure 5.8B).

H&E staining was used to assess the fibrotic tissue within corneal stroma (Figure 5.8C; arrowhead). Dense fibrotic tissue formed in the stroma underneath the epithelium in the untreated group. FG treatment significantly reduced the severity of fibrosis. However, fibrotic tissue was reduced to minimum within corneal stroma in FG+ECM treated group. The addition of LN-ECM particles also affected the morphology of reconstructed corneal epithelium. Epithelial hyperplasia (thickened epithelium) was observed in untreated and FG-treated group, but absent in the FG+ECM treated group (Figure 5.8C; arrow). Immunostaining with αSMA at week four illustrated similar result (Figure 5.8D). Within the stroma of untreated cornea, large area was stained positive with αSMA, a marker for myofibroblasts. After FG treatment, the αSMA+ area was reduced within anterior stroma, and it was even more reduced by FG+ECM treatment.

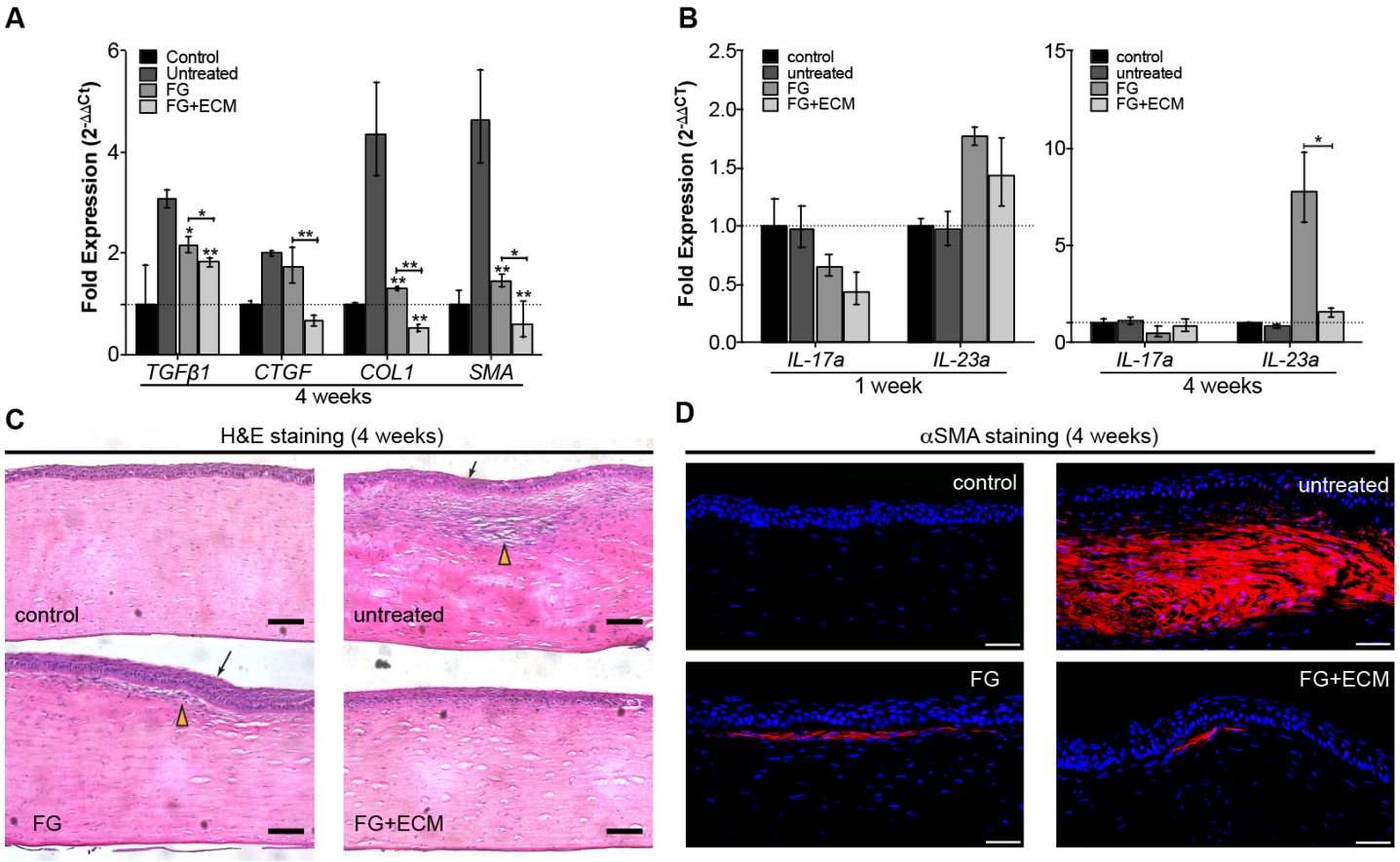

Figure 5.8. The anti-fibrotic feature of ECM on corneal wound healing *in vivo*.

(A,B) The expression of genes related to fibrosis (TGFβ1, CTGF, COL1, αSMA, IL-17a and IL-23a) was quantified by RT-qPCR at both week one and week four. (C) H&E staining of reconstructed corneal stroma and epithelium after SLK. Arrowheads are showing stromal scars formed after the surgery. The arrow indicated possible epithelial hyperplasia (thickening). Scale bar: 100 μm. (D) αSMA immunostaining (red) showing fibrotic tissue in the reconstructed corneal stroma at week 4. Scale bar: 50 μm. *$p < 0.05$; **$p < 0.001$.

5.4. DISCUSSION

Biomaterial derived from decellularized tissue ECM have been extensively studied and successfully applied in regenerative medicine for decades. As scaffolds for tissue repair, they offer many mechanical and structural advantages that are inherited from the native tissue. The extracellular signaling molecules and the residual intracellular content in ECM scaffolds also play an important role in supporting tissue remodeling and cell differentiation (*96*). After chemical, enzymatic and mechanical processing, ECM scaffolds could still retain structural features of the source tissue, and this is proved in our study as well. SEM images of dECM particles obtained from lymph nodes, cartilage and cornea show distinct features in morphology, and size distribution analysis also revealed difference in average particle size among the three particulate ECMs (Figure 5.1). For example, the long fibrils are unique to CA-ECM particles, which could also explain the wide range of the particle sizes. CO-ECM particles mainly contain lamellae-like structures and have a discontinuous particle distribution, which are indicators of the lamellar stacking within corneal stroma. Particulate ECM materials lose the load-bearing ability, however they become more versatile regarding delivery methods. They were used as media supplements *in vitro* and delivered to the ocular surface using FG sealant as a carrier. Considering the particle size (0.2 - 3.0 μm), they could also be injected via syringe to the target sites.

As more refractive surgeries are performed every year, corneal haze, dry eye and fibrosis are examples of complications that may happen after laser-assisted in situ keratomileusis (LASIK) and photorefractive keratectomy (PRK) surgeries. Cornea wound healing includes the crosstalk of many molecular mediators secreted by corneal and immune cells

(*100*). When the ocular surface epithelium is injured, IL-1 cytokine is released from damaged epithelial cells, consequently causing inflammatory cell infiltration into the ocular surface area (*86, 100*). Excessive inflammation could lead to acute or chronic dry eye and even neovascularization in the reconstructed corneal stroma (*100*). Many patients with severe cornea or ocular surface injuries often develop dry eye symptoms as well, and reduced level of anti-inflammatory components in the tear film could worsen the situation, making the wound healing process even more complicated as a vicious cycle (*91, 92*). Thus, the homeostasis of the entire ocular surface is crucial for optimal corneal wound healing. Effective regulation of the immunity within the wounded area as well as the other parts of the ocular surface is necessary for proper corneal wound healing and the prevention of fibrosis.

We first screened three kinds of ECM particles *in vitro*, regarding their anti-inflammatory ability for the ocular surface. Multiple ocular surface cells were used, which are CECs, LGACs, and corneal keratocytes. Goblet cells (included in CEC population) and LGACs are the major cell types for aqueous tear secretion. IL-1β, the proinflammatory cytokine, was used to induce inflammation. ECM particles, especially LN-ECM, significantly reduced the expression of proinflammatory mediators (TNFα, IL-6 and IL-8), and proteinase MMP9, one of the major indicators for the diagnosis of dry eye disease (*86*) (Figure 5.2B; Figure 5.3A,B). LN-ECM also affected the morphology and functions of ocular surface cells cultured *in vitro*. It prevented the morphological change of keratocytes from stellate shape (quiescent stage) to elongated shape (fibroblasts and myofibroblasts) (*101*) (Figure 5.2B). Furthermore, ECM particles are necessary in maintaining the normal secretion function of ocular surface cells under inflammatory conditions *in vitro*, regarding mucin and

lysozyme secretion, by goblet cells and LG acinar cells, respectively (Figure 5.2C,D; Figure 5.3C).

The different outcomes observed from the scaffolds are possibly due to the variation in ECM composition of the native tissues. Lymph nodes are filled with reticular networks that contains fibrillar collagens and basement membranes (*102*). As basement membrane components are beneficial for the growth and differentiation of epithelial cells, this could explain its effectiveness in regulating the inflammation in ocular surface epithelia. Cartilage and cornea are load bearing tissues, and their ECMs are composed of structural collagens in general (*85*). Therefore, despite the beneficial effects they offer to keratocytes, CA- and CO-ECM did not provide significant advantages as supplements for epithelial cells (CECs and LGACs) under inflammatory condition *in vitro*.

The experiments *in vitro* proved that LN-ECM was the most efficient in the regulation of ocular surface homeostasis. Therefore, it was delivered to wounded corneal stroma within FG sealant. FG itself has been used frequently before as a sealant or wound dressing during corneal surgeries (*103*). The corneal epithelial healing was more or less the same among all three group, which is completed at day five (Figure 5.5C). The value of corneal haze within the reconstructed stroma proved the efficacy of FG+ECM application (Figure 5.4B,C; Figure 5.5). It prevented the development of haze at early time point, and this effect persisted until the end of the study, and FG+ECM eliminated corneal haze even more than FG alone.

ECM/FG application ameliorated the immune response in cornea stroma after SLK surgery, which is comparable to the outcomes of previous cell therapies. Subconjunctival-injected

mesenchymal stem cells (MSCs) exerted anti-inflammatory mechanism during the acute phase of corneal chemical burn (*94*), such as reduction of TNFα expression and infiltrated inflammatory cells, and the paracrine effect of MSCs could also bring down the level MMPs after tissue injuries (*104*). These effects are similar to the results we observed in the early stage of corneal wound healing when LN-ECM was applied. Gene expression results showed that proinflammatory cytokine TNFα was downregulated at both early and late time points. MMP9, responsible for the degradation of ECM during corneal stromal remolding and the immune cell infiltration later on (*100*), was significantly reduced in the two treated groups, especially when LN-ECM was applied alongside FG (Figure 5.7A). LN-ECM also decreased the expression of IL-23a (Figure 5.8B) and Arg1 (Figure 5.7B). Consequently, the number of infiltrated CD11b+ cells was scarce in the reconstructed stroma in the LN-ECM treated group (Figure 5.7C). The resemblance of the anti-inflammatory effect could possibly due to the similarity between components in LN-ECM and paracrine factors secreted by MSCs. Unlike cell therapies, particulate ECM are more abundant, and can be prepared in advanced and stored for a long time before application. Hence ECM particles can be translated clinically with less complications.

Corneal epithelial wound healing is supported by the proliferation and migration of limbal stem cells residing in the corneoscleral junction (*105*), while corneal stroma healing is a more complicated process. The main signaling molecules involved are the TGF-β system. TGF-β1 induces the transition of keratocytes to fibroblasts, the emergence of myofibroblasts, and consequently scar formation and wound contracture. Suppressing the expression of profibrotic TGF-β growth factors has been a target for reducing corneal fibrosis and

haze. Gene therapy that declines TGF-β1 transcription and TGF-β inhibitors such as rosiglitazone and ROCK inhibitor are proved to be promising in managing corneal fibrosis (*98, 100*). In our study, at four-week time point, TGF-β1 was highly upregulated due to corneal epithelial and stromal injuries. LN-ECM particles reduced the gene expression of TGF-β1, as well as downstream corneal scar molecules, including CTGF, COL1 and α-SMA, and its effect is superior to the carrier FG sealant alone (Figure 5.8A). Therefore, the anti-fibrotic effect of LN-ECM in reducing scar formation is possibly acted upon the TGF-β system as well.

There is interaction between the epithelium and stroma while corneal wound healing is taking place. Injured epithelium could also secret TGF-β that induces the synthesis of irregular collagen fibrils and stromal haze. Therefore, optimal re-epithelialization could guarantee a better stromal remodeling. Biomaterial scaffolds with basement membrane compositions could be effective when used for corneal epithelial healing and stromal remodeling, such as amniotic membrane (AM), which induced faster epithelial healing and less keratocytes apoptosis (*106*). Similarly, LN-ECM/FG gel containing basement membrane components formed a barrier above the remodeling stroma, and prevented excessive infiltration of inflammatory cells, and eventually promoted the proper synthesis and assembly of collagen fibrils, and prevented corneal epithelial hyperplasia (Figure 5.8C,D).

Our previous study has shown that ECM scaffolds from various sources can be screened *in vitro*, and many of them have unique functions, such as guiding cell differentiation and inducing tissue matrix production (*96*). In this study, LN-ECM significantly ameliorated inflammation in the ocular surface both *in vitro* and *in vivo*, and reduced scar formation

after SLK surgery in the rabbit model. These benefits offered by LN-ECM resembles the paracrine effects observed from MSC therapy, and the mechanism is possibly the unique components originates from the lymph node reticular meshwork. Further proteomic analysis would be necessary for exact mechanism and for identifying the key signaling molecules. Besides ophthalmic application, LN-ECM particles could be utilized in other systems where both inflammation control and proper ECM remodeling are needed. At the same time, other types of ECM materials with similar compositions could be further explored as well. To improve the therapeutic outcomes of ECM scaffolds and delay degradation, particles could be loaded in the carrier at a higher concentration, applied as a compressed gel form or chemically crosslinked before application.

5.5. CONCLUSIONS

In summary, particulate ECM from lymph nodes, cartilage and cornea were processed into micro-particles and their anti-inflammatory function on the ocular surface was assessed. LN-ECM, the most potent scaffold was further examined in a corneal wound healing model. It successfully tuned down the inflammatory response in the reconstructed stromal area and prevented the formation of scar tissue and corneal haze. LN-ECM is proved to be efficient in mediating the homeostasis of cornea, as well as other parts of the ocular surface. Tissue derived ECM scaffolds are effective and accessible therapeutics for the management

of corneal reconstruction after traumatic injuries to the ocular surface and refractive surgeries. Overall, ECM scaffolds represent a new promising alternative for the modulating of immune response as well as matrix remodeling during the wound healing process.

Chapter 6. Summary and Future Research Directions

The main goal of this dissertation is to utilize several approaches, including biomaterials engineering, model system development and novel therapeutics, to optimize wound healing and prevent disease progression on the ocular surface (Figure 6.1). First, we discovered collagen vitrigel (CV) as an alternative graft material for conjunctival wound closure, which also supported goblet cell repopulation and possibly decreased the occurrence of dry eye disease. Next, we focused on dry eye disease, and developed a model system of the ocular surface *in vitro* for pathogenesis study and drug evaluation. Particulate ECM was studied as a new form of therapeutics for the reduction of inflammation and fibrosis during corneal wound healing. These three strategies targeted concerns on the ocular surface from different perspectives. In the future, each strategy presented here could be further investigated and a combinatory approach could also be explored.

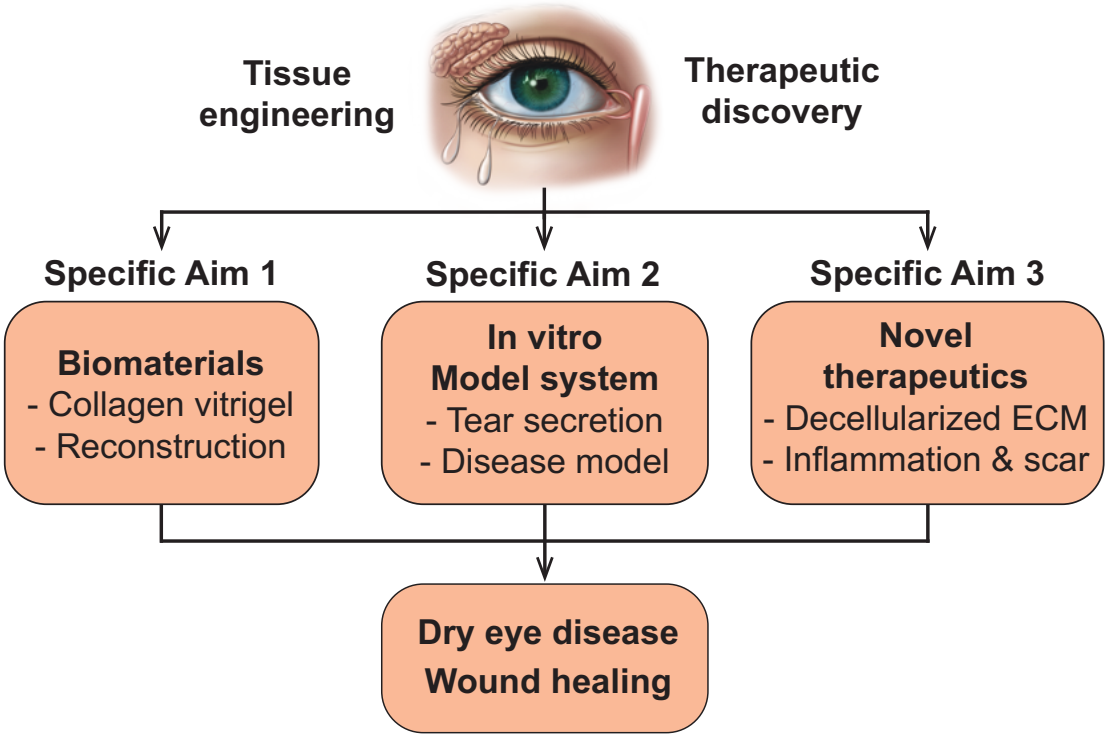

Figure 6.1. Summary of the dissertation.

6.1. CV AND PARTICULATE ECM FOR THE TREATMENT OF PTERYGIUM

In Chapter 3, we demonstrated that CV supported the growth of conjunctival cell and reconstruction of ocular surface defects (*21*). Previous study has shown that CV is an excellent substitute for engineering the cornea as well (*31*). Besides serving as a simple wound dressing, CV could also be used on other ocular surface diseases involving more complications.

Pterygium is the outgrowth of noncancerous conjunctival tissue onto the cornea, resulting in discomfort, decreased and obstructed vision, with a high recurrence rate (*107*). Graft transplantations with adjuvants have been shown to effectively reduce recurrence rate and complications after excision surgeries (*107-109*). CV as a biocompatible material supports both conjunctival and corneal cells. We have shown in Chapter 3 that conjunctival equivalent engineered with CV successfully repaired critical-sized defect. Therefore, CV is a promising candidate for wound closure after the excision of pterygia, which offers more advantages than amniotic membranes and other available materials as discussed in Chapter 2.

Over-proliferation of fibroblasts is associated with the recurrence of pterygium (*110*). Therefore, therapeutics that inhibit fibrosis and promote wound healing can be potentially beneficial after excision. Based on the results in Chapter 5, ECM particles significantly reduced inflammation and scar tissue. Thus, incorporating ECM materials together with CV for the treatment of pterygium could lower the reoccurrence rate even more. Similarly,

ECM particles can be mixed with fibrin glue sealant for the attachment of CV during application.

6.2. MICROFABRICATION OF THE OCULAR SURFACE MODEL SYSTEM

We developed the *in vitro* model system for the ocular surface in Chapter 4. The model system recapitulates the tear secretory function of a healthy ocular surface, and it can also be induced as a dry eye disease model for therapeutic evaluation. To improve the organization of the model system, and make it more tunable and efficient for high-throughput screening, techniques such as microfabrication and microfluidics can be applied to generate miniaturized versions of ocular surface model systems.

Organs-on-chips are microengineered systems which adapt microfabrication technique and mimic the physiological function on the organ level (*35*). Similarly, instead of Transwell insert, our ocular surface model system could be built on poly(dimethylsiloxane) (PDMS) chambers with microfluidic channels. Besides using proinflammatory cytokines, dry eye disease can also be induced by exposing the culture to desiccating stress, which could be more easily realized with PDMS chambers. CV could replace the porous membrane on the Transwell insert, for better ocular cell growth and differentiation. For the evaluation of multiple therapeutics, organ-on-chip systems can be linked together and the efficiency could be easily controlled and improved.

6.3. COMBINING CV AND ECM PARTICLES AS A NEW DELIVERY METHOD

Particulate ECM has shown promising results in reducing the inflammation and fibrosis associated with corneal wound healing in Chapter 5. To increase the initial loading dose of ECM particles and prolong the degradation time, several approaches could be studied in the future. CV could replace fibrin glue sealant or be applied additionally after corneal injuries. ECM particles could be combined with CV during the vitrification process. Thicker CV can be manufactured and several sheets of CV can be stacked together to improve the mechanical strength of the material composite. Particulate ECM can also be injected near the injury site. For ocular surface applications, subconjunctival injection of ECM particles may provide extra benefit in regulating the immune populations migrating towards the cornea through the conjunctival lymphatics, and is also a common procedure in the clinic. The degradation rate of ECM particles in the new material carrier must be investigated to match the progress of wound healing in the cornea, as materials that degrade too slowly and do not integrate well with the host tissue may cause delay in re-epithelialization, which could further disturb corneal stromal healing.

REFERENCES

1. I. K. Gipson, The ocular surface: the challenge to enable and protect vision: the Friedenwald lecture. *Invest Ophthalmol Vis Sci* **48**, 4390; 4391-4398 (2007).

2. K. M. Meek, C. Knupp, Corneal structure and transparency. *Prog Retin Eye Res* **49**, 1-16 (2015).

3. X. Cheng, S. J. Petsche, P. M. Pinsky, A structural model for the in vivo human cornea including collagen-swelling interaction. *J R Soc Interface* **12**, 20150241 (2015).

4. D. A. Dartt, Control of mucin production by ocular surface epithelial cells. *Exp Eye Res* **78**, 173-185 (2004).

5. C. D. Conrady, Z. P. Joos, B. C. Patel, Review: The Lacrimal Gland and Its Role in Dry Eye. *J Ophthalmol* **2016**, 7542929 (2016).

6. H. Obata, Anatomy and histopathology of the human lacrimal gland. *Cornea* **25**, S82-89 (2006).

7. T. Nakamura, T. Inatomi, C. Sotozono, N. Koizumi, S. Kinoshita, Ocular surface reconstruction using stem cell and tissue engineering. *Prog Retin Eye Res* **51**, 187-207 (2016).

8. S. Selvam, P. B. Thomas, S. C. Yiu, Tissue engineering: current and future approaches to ocular surface reconstruction. *Ocul Surf* **4**, 120-136 (2006).

9. S. Schrader *et al.*, Tissue engineering for conjunctival reconstruction: established methods and future outlooks. *Curr Eye Res* **34**, 913-924 (2009).

10. M. P. Hatton, P. A. Rubin, Conjunctival regeneration. *Adv Biochem Eng Biotechnol* **94**, 125-140 (2005).

11. D. T. Tan, S. P. Chee, K. B. Dear, A. S. Lim, Effect of pterygium morphology on pterygium recurrence in a controlled trial comparing conjunctival autografting with bare sclera excision. *Archives of ophthalmology* **115**, 1235-1240 (1997).

12. C. Mai, E. Bertelmann, Oral mucosal grafts: old technique in new light. *Ophthalmic research* **50**, 91-98 (2013).

13. C. Sotozono *et al.*, Visual improvement after cultivated oral mucosal epithelial transplantation. *Ophthalmology* **120**, 193-200 (2013).

14. J. Elisseeff, M. G. Madrid, Q. Lu, J. J. Chae, Q. Guo, Future perspectives for regenerative medicine in ophthalmology. *Middle East African journal of ophthalmology* **20**, 38-45 (2013).

15. J. Liu, H. Sheha, Y. Fu, L. Liang, S. C. Tseng, Update on amniotic membrane transplantation. *Expert Rev Ophthalmol* **5**, 645-661 (2010).

16. S. C. Tseng, Amniotic membrane transplantation for ocular surface reconstruction. *Bioscience reports* **21**, 481-489 (2001).

17. A. K. Riau, R. W. Beuerman, L. S. Lim, J. S. Mehta, Preservation, sterilization and de-epithelialization of human amniotic membrane for use in ocular surface reconstruction. *Biomaterials* **31**, 216-225 (2010).

18. R. Arora, D. Mehta, V. Jain, Amniotic membrane transplantation in acute chemical burns. *Eye (Lond)* **19**, 273-278 (2005).

19. S. C. Tseng *et al.*, How does amniotic membrane work? *Ocul Surf* **2**, 177-187 (2004).

20. H. S. Dua, I. Rahman, A. Miri, D. G. Said, Variations in amniotic membrane: relevance for clinical applications. *Brit J Ophthalmol* **94**, 963-964 (2010).

21. H. Zhou *et al.*, Vitrified collagen-based conjunctival equivalent for ocular surface reconstruction. *Biomaterials* **35**, 7398-7406 (2014).

22. S. Y. Lee *et al.*, In vivo conjunctival reconstruction using modified PLGA grafts for decreased scar formation and contraction. *Biomaterials* **24**, 5049-5059 (2003).

23. L. P. Ang *et al.*, The development of a serum-free derived bioengineered conjunctival epithelial equivalent using an ultrathin poly(epsilon-caprolactone) membrane substrate. *Invest Ophthalmol Vis Sci* **47**, 105-112 (2006).

24. W. C. Hsu, M. H. Spilker, I. V. Yannas, P. A. Rubin, Inhibition of conjunctival scarring and contraction by a porous collagen-glycosaminoglycan implant. *Invest Ophthalmol Vis Sci* **41**, 2404-2411 (2000).

25. S. Reichl, M. Borrelli, G. Geerling, Keratin films for ocular surface reconstruction. *Biomaterials* **32**, 3375-3386 (2011).

26. T. Takezawa, K. Ozaki, A. Nitani, C. Takabayashi, T. Shimo-Oka, Collagen vitrigel: A novel scaffold that can facilitate a three-dimensional culture for reconstructing organoids. *Cell Transplantation* **13**, 463-473 (2004).

27. T. Takezawa, K. Nishikawa, P. C. Wang, Development of a human corneal epithelium model utilizing a collagen vitrigel membrane and the changes of its barrier function induced by exposing eye irritant chemicals. *Toxicology in vitro : an international journal published in association with BIBRA* **25**, 1237-1241 (2011).

28. X. Calderon-Colon *et al.*, Structure and properties of collagen vitrigel membranes for ocular repair and regeneration applications. *Biomaterials* **33**, 8286-8295 (2012).

29. Z. Y. Xia, X. Calderon-Colon, M. Trexler, J. Elisseeff, Q. Y. Guo, Thermal denaturation of type I collagen vitrified gels. *Thermochim Acta* **527**, 172-179 (2012).

30. Q. Guo *et al.*, Modulation of keratocyte phenotype by collagen fibril nanoarchitecture in membranes for corneal repair. *Biomaterials* **34**, 9365-9372 (2013).

31. W. McIntosh Ambrose *et al.*, Collagen Vitrigel membranes for the in vitro reconstruction of separate corneal epithelial, stromal, and endothelial cell layers. *J Biomed Mater Res B Appl Biomater* **90**, 818-831 (2009).

32. S. C. Pflugfelder *et al.*, Management and therapy of dry eye disease: Report of the Management and Therapy Subcommittee of the international Dry Eye WorkShop (2007). *Ocul Surf* **5**, 163-178 (2007).

33. J. A. Smith *et al.*, The epidemiology of dry eye disease: Report of the Epidemiology Subcommittee of the international Dry Eye WorkShop (2007). *Ocul Surf* **5**, 93-107 (2007).

34. I. K. Gipson *et al.*, Research in dry eye: Report of the Research Subcommittee of the international dry eye WorkShop (2007). *Ocul Surf* **5**, 179-193 (2007).

35. D. Huh *et al.*, Microfabrication of human organs-on-chips. *Nature protocols* **8**, 2135-2157 (2013).

36. S. N. Bhatia, D. E. Ingber, Microfluidic organs-on-chips. *Nature biotechnology* **32**, 760-772 (2014).

37. D. Huh *et al.*, Reconstituting organ-level lung functions on a chip. *Science* **328**, 1662-1668 (2010).

38. C. Luni, E. Serena, N. Elvassore, Human-on-chip for therapy development and fundamental science. *Current opinion in biotechnology* **25**, 45-50 (2014).

39. H. J. Kim, D. E. Ingber, Gut-on-a-Chip microenvironment induces human intestinal cells to undergo villus differentiation. *Integrative biology : quantitative biosciences from nano to macro* **5**, 1130-1140 (2013).

40. S. A. Lee *et al.*, Spheroid-based three-dimensional liver-on-a-chip to investigate hepatocyte-hepatic stellate cell interactions and flow effects. *Lab on a chip* **13**, 3529-3537 (2013).

41. L. G. Rigat-Brugarolas *et al.*, A functional microengineered model of the human splenon-on-a-chip. *Lab on a chip* **14**, 1715-1724 (2014).

42. Y. S. Torisawa *et al.*, Bone marrow-on-a-chip replicates hematopoietic niche physiology in vitro. *Nature methods* **11**, 663-669 (2014).

43. S. H. Chung, J. H. Lee, J. H. Yoon, H. K. Lee, K. Y. Seo, Multi-layered culture of primary human conjunctival epithelial cells producing MUC5AC. *Exp Eye Res* **85**, 226-233 (2007).

44. M. Hirayama *et al.*, Functional lacrimal gland regeneration by transplantation of a bioengineered organ germ. *Nature communications* **4**, 2497 (2013).

45. C. K. Marko *et al.*, Spdef null mice lack conjunctival goblet cells and provide a model of dry eye. *The American journal of pathology* **183**, 35-48 (2013).

46. J. Elisseeff, A. Ferran, S. Hwang, S. Varghese, Z. Zhang, The role of biomaterials in stem cell differentiation: applications in the musculoskeletal system. *Stem Cells Dev* **15**, 295-303 (2006).

47. P. Rama *et al.*, Autologous fibrin-cultured limbal stem cells permanently restore the corneal surface of patients with total limbal stem cell deficiency. *Transplantation* **72**, 1478-1485 (2001).

48. P. Vinciguerra, E. Albe, P. Rosetta, E. Di Iorio, G. Pellegrini, Custom phototherapeutic keratectomy and autologous fibrin-cultured limbal stem cell autografting: a combined approach. *J Refract Surg* **24**, 323-324 (2008).

49. M. A. Shatos *et al.*, Isolation, characterization, and propagation of rat conjunctival goblet cells in vitro. *Invest Ophthalmol Vis Sci* **42**, 1455-1464 (2001).

50. K. J. Livak, T. D. Schmittgen, Analysis of relative gene expression data using real-time quantitative PCR and the 2(-Delta Delta C(T)) Method. *Methods* **25**, 402-408 (2001).

51. I. Wu, Z. Nahas, K. A. Kimmerling, G. D. Rosson, J. H. Elisseeff, An injectable adipose matrix for soft-tissue reconstruction. *Plast Reconstr Surg* **129**, 1247-1257 (2012).

52. D. Meller, V. Dabul, S. C. Tseng, Expansion of conjunctival epithelial progenitor cells on amniotic membrane. *Exp Eye Res* **74**, 537-545 (2002).

53. D. Meller, S. C. Tseng, Conjunctival epithelial cell differentiation on amniotic membrane. *Invest Ophthalmol Vis Sci* **40**, 878-886 (1999).

54. L. P. Ang *et al.*, Cultivated human conjunctival epithelial transplantation for total limbal stem cell deficiency. *Invest Ophthalmol Vis Sci* **51**, 758-764 (2010).

55. R. Lu *et al.*, Conjunctival reconstruction with progenitor cell-derived autologous epidermal sheets in rhesus monkey. *PLoS One* **6**, e25713 (2011).

56. I. G. Fostad *et al.*, Biopsy harvesting site and distance from the explant affect conjunctival epithelial phenotype ex vivo. *Exp Eye Res* **104**, 15-25 (2012).

57. M. Rolando, M. Zierhut, The ocular surface and tear film and their dysfunction in dry eye disease. *Surv Ophthalmol* **45**, S203-S210 (2001).

58. M. A. Lemp *et al.*, The definition and classification of dry eye disease: Report of the Definition and Classification Subcommittee of the international Dry Eye WorkShop (2007). *Ocul Surf* **5**, 75-92 (2007).

59. M. E. Stern, J. Gao, K. F. Siemasko, R. W. Beuerman, S. C. Pflugfelder, The role of the lacrimal functional unit in the pathophysiology of dry eye. *Exp Eye Res* **78**, 409-416 (2004).

60. M. E. Stern, C. S. Schaumburg, S. C. Pflugfelder, Dry eye as a mucosal autoimmune disease. *Int Rev Immunol* **32**, 19-41 (2013).

61. W. Stevenson, S. K. Chauhan, R. Dana, Dry eye disease: an immune-mediated ocular surface disorder. *Archives of ophthalmology* **130**, 90-100 (2012).

62. D. Huh *et al.*, A human disease model of drug toxicity-induced pulmonary edema in a lung-on-a-chip microdevice. *Sci Transl Med* **4**, 159ra147 (2012).

63. X. Zhong *et al.*, Generation of three-dimensional retinal tissue with functional photoreceptors from human iPSCs. *Nature communications* **5**, 4047 (2014).

64. A. C. McUsic, D. A. Lamba, T. A. Reh, Guiding the morphogenesis of dissociated newborn mouse retinal cells and hES cell-derived retinal cells by soft lithography-patterned microchannel PLGA scaffolds. *Biomaterials* **33**, 1396-1405 (2012).

65. Y. K. Chan *et al.*, In Vitro Modeling of Emulsification of Silicone Oil as Intraocular Tamponade Using Microengineered Eye-on-a-Chip. *Invest Ophthalmol Vis Sci* **56**, 3314-3319 (2015).

66. C. M. Puleo, W. McIntosh Ambrose, T. Takezawa, J. Elisseeff, T. H. Wang, Integration and application of vitrified collagen in multilayered microfluidic devices for corneal microtissue culture. *Lab on a chip* **9**, 3221-3227 (2009).

67. H. Lin *et al.*, Three-Dimensional Culture of Functional Adult Rabbit Lacrimal Gland Epithelial Cells on Decellularized Scaffold. *Tissue Eng Part A* **22**, 65-74 (2016).

68. K. Spaniol *et al.*, Engineering of a Secretory Active Three-Dimensional Lacrimal Gland Construct on the Basis of Decellularized Lacrimal Gland Tissue. *Tissue Eng Part A* **21**, 2605-2617 (2015).

69. S. Selvam *et al.*, Tissue-engineered tear secretory system: functional lacrimal gland acinar cells cultured on matrix protein-coated substrata. *J Biomed Mater Res B Appl Biomater* **80**, 192-200 (2007).

70. L. Goers, P. Freemont, K. M. Polizzi, Co-culture systems and technologies: taking synthetic biology to the next level. *J R Soc Interface* **11**, (2014).

71. C. S. Wallace, G. A. Truskey, Direct-contact co-culture between smooth muscle and endothelial cells inhibits TNF-alpha-mediated endothelial cell activation. *Am J Physiol-Heart C* **299**, H338-346 (2010).

72. C. A. Dinarello, The IL-1 family and inflammatory diseases. *Clin Exp Rheumatol* **20**, S1-13 (2002).

73. T. J. Nagelhout, D. A. Gamache, L. Roberts, M. T. Brady, J. M. Yanni, Preservation of tear film integrity and inhibition of corneal injury by

dexamethasone in a rabbit model of lacrimal gland inflammation-induced dry eye. *J Ocul Pharmacol Th* **21**, 139-148 (2005).

74. S. Viau *et al.*, Time course of ocular surface and lacrimal gland changes in a new scopolamine-induced dry eye model. *Graefes Arch Clin Exp Ophthalmol* **246**, 857-867 (2008).

75. P. Argueso *et al.*, Decreased levels of the goblet cell mucin MUC5AC in tears of patients with Sjogren syndrome. *Invest Ophthalmol Vis Sci* **43**, 1004-1011 (2002).

76. S. J. Spurr-Michaud, I. K. Gipson, Methods for culture of human corneal and conjunctival epithelia. *Methods Mol Biol* **945**, 31-43 (2013).

77. S. Schrader, C. Kremling, M. Klinger, H. Laqua, G. Geerling, Cultivation of lacrimal gland acinar cells in a microgravity environment. *Brit J Ophthalmol* **93**, 1121-1125 (2009).

78. H. K. Kleinman, G. R. Martin, Matrigel: basement membrane matrix with biological activity. *Semin Cancer Biol* **15**, 378-386 (2005).

79. R. O. Hynes, The extracellular matrix: not just pretty fibrils. *Science* **326**, 1216-1219 (2009).

80. I. T. Swinehart, S. F. Badylak, Extracellular matrix bioscaffolds in tissue remodeling and morphogenesis. *Dev Dyn* **245**, 351-360 (2016).

81. S. Badylak, K. Kokini, B. Tullius, A. Simmons-Byrd, R. Morff, Morphologic study of small intestinal submucosa as a body wall repair device. *J Surg Res* **103**, 190-202 (2002).

82. T. W. Gilbert *et al.*, Collagen fiber alignment and biaxial mechanical behavior of porcine urinary bladder derived extracellular matrix. *Biomaterials* **29**, 4775-4782 (2008).

83. J. M. Aamodt, D. W. Grainger, Extracellular matrix-based biomaterial scaffolds and the host response. *Biomaterials* **86**, 68-82 (2016).

84. J. M. Fishman *et al.*, Immunomodulatory effect of a decellularized skeletal muscle scaffold in a discordant xenotransplantation model. *Proc Natl Acad Sci U S A* **110**, 14360-14365 (2013).

85. S. F. Badylak, D. O. Freytes, T. W. Gilbert, Extracellular matrix as a biological scaffold material: Structure and function. *Acta Biomater* **5**, 1-13 (2009).

86. S. Barabino, Y. Chen, S. Chauhan, R. Dana, Ocular surface immunity: homeostatic mechanisms and their disruption in dry eye disease. *Prog Retin Eye Res* **31**, 271-285 (2012).

87. S. E. Wilson *et al.*, The corneal wound healing response: cytokine-mediated interaction of the epithelium, stroma, and inflammatory cells. *Prog Retin Eye Res* **20**, 625-637 (2001).

88. M. V. Netto *et al.*, Wound healing in the cornea: a review of refractive surgery complications and new prospects for therapy. *Cornea* **24**, 509-522 (2005).

89. J. W. Streilein, Ocular immune privilege: therapeutic opportunities from an experiment of nature. *Nat Rev Immunol* **3**, 879-889 (2003).

90. O. Yamanaka, T. Sumioka, S. Saika, The role of extracellular matrix in corneal wound healing. *Cornea* **32 Suppl 1**, S43-45 (2013).

91. S. E. Wilson, Laser in situ keratomileusis-induced (presumed) neurotrophic epitheliopathy. *Ophthalmology* **108**, 1082-1087 (2001).

92. F. Bian *et al.*, Desiccating Stress-Induced MMP Production and Activity Worsens Wound Healing in Alkali-Burned Corneas. *Invest Ophthalmol Vis Sci* **56**, 4908-4918 (2015).

93. Z. Vereb *et al.*, Role of Human Corneal Stroma-Derived Mesenchymal-Like Stem Cells in Corneal Immunity and Wound Healing. *Sci Rep* **6**, 26227 (2016).

94. L. Yao *et al.*, Role of mesenchymal stem cells on cornea wound healing induced by acute alkali burn. *PLoS One* **7**, e30842 (2012).

95. S. Basu *et al.*, Human limbal biopsy-derived stromal stem cells prevent corneal scarring. *Sci Transl Med* **6**, 266ra172 (2014).

96. V. Z. Beachley *et al.*, Tissue matrix arrays for high-throughput screening and systems analysis of cell function. *Nature methods* **12**, 1197-1204 (2015).

97. S. V. Andersson, S. F. Hamm-Alvarez, J. P. Gierow, Integrin adhesion in regulation of lacrimal gland acinar cell secretion. *Exp Eye Res* **83**, 543-553 (2006).

98. S. Sriram *et al.*, Assessment of anti-scarring therapies in ex vivo organ cultured rabbit corneas. *Exp Eye Res* **125**, 173-182 (2014).

99. E. C. Kim, H. Meng, A. S. Jun, N-Acetylcysteine increases corneal endothelial cell survival in a mouse model of Fuchs endothelial corneal dystrophy. *Exp Eye Res* **127**, 20-25 (2014).

100. A. V. Ljubimov, M. Saghizadeh, Progress in corneal wound healing. *Prog Retin Eye Res* **49**, 17-45 (2015).

101. M. E. Fini, Keratocyte and fibroblast phenotypes in the repairing cornea. *Prog Retin Eye Res* **18**, 529-551 (1999).

102. C. L. Willard-Mack, Normal structure, function, and histology of lymph nodes. *Toxicol Pathol* **34**, 409-424 (2006).

103. A. Panda, S. Kumar, A. Kumar, R. Bansal, S. Bhartiya, Fibrin glue in ophthalmology. *Indian J Ophthalmol* **57**, 371-379 (2009).

104. M. Gnecchi, Z. Zhang, A. Ni, V. J. Dzau, Paracrine mechanisms in adult stem cell signaling and therapy. *Circ Res* **103**, 1204-1219 (2008).

105. P. Rama *et al.*, Limbal stem-cell therapy and long-term corneal regeneration. *N Engl J Med* **363**, 147-155 (2010).

106. H. M. Woo *et al.*, Effects of amniotic membrane on epithelial wound healing and stromal remodelling after excimer laser keratectomy in rabbit cornea. *Brit J Ophthalmol* **85**, 345-349 (2001).

107. B. J. Janson, S. Sikder, Surgical management of pterygium. *Ocul Surf* **12**, 112-119 (2014).

108. T. Nakamura *et al.*, Novel clinical application of sterilized, freeze-dried amniotic membrane to treat patients with pterygium. *Acta Ophthalmol Scand* **84**, 401-405 (2006).

109. G. S. Noureddin, S. N. Yeung, The use of dry amniotic membrane in pterygium surgery. *Clin Ophthalmol* **10**, 705-712 (2016).

110. K. W. Kim, S. H. Park, J. C. Kim, Fibroblast biology in pterygia. *Exp Eye Res* **142**, 32-39 (2016).

VITA

Name Qiaozhi Lu (Nicole)

Address Nicole may be contacted through Prof. Jennifer H. Elisseeff at Translational Tissue Engineering Center (TTEC)

Smith Building 5001, 400 N Broadway
Wilmer Eye Institute, Johns Hopkins School of Medicine
Baltimore, MD 21231

Email luqiaozhi@gmail.com

Education Biological Science, BS – 2009 Zhejiang University, China
Biomedical Engineering, MS – 2011 Johns Hopkins University
Materials Science and Engineering, PhD – 2016 Johns Hopkins University

Nicole was born in China in 1987 to Hong Lu and Liya Sun. Ever since the 4th grade, she discovered her enthusiasm in science and engineering. After graduating from Zhejiang University in 2009, she attended the master program in Biomedical Engineering at Johns Hopkins University. She further developed her interest in tissue engineering research and continued to pursue doctoral study in the fields of biomaterials at 2011.

She started worked in the laboratory of Prof. Jennifer H. Elisseeff on tissue engineering since 2009. At first, she worked on using small molecules (carnitine) to influence the musculoskeletal differentiation of mesenchymal stem cells. Afterwards, she optimized an ocular surface tissue adhesive for wound closure and drug release and started to work in the ocular field since then. Under the guidance of Dr. Elisseeff, she investigated multiple biomaterials for tissue reconstruction and immunoregulation, and developed a model system

for the ocular surface and tear film. She also studied and tested a novel eye drop formulation for dry eye patients.

Other than work and research, she really enjoys cooking and discovering new recipes. She likes exercising, calligraphy, dancing and spending time with family, friends and her two lovely cats.